THE IMPACT OF OVERTOPPING ON THE FAILURE PROBABILITY OF SLIPPED RIVER DIKES

V.A. Verdonk

MSc-thesis – Civil Engineering and Management

UNIVERSITY OF TWENTE.

Risk

THE IMPACT OF OVERTOPPING ON THE FAILURE PROBABILITY OF SLIPPED RIVER DIKES

Cover: panorama of a bicycle path along the river Waal by Marc Venema

Document type:	Master thesis	
Version	1.0	
Date	July 18th, 2020	
Location	Enschede, the Netherlands	
Author	V.A. Verdonk (Vincent)	
Student number	s1599682	
E-mail address	v.a.verdonk@alumnus.utwente.nl	
Institute	University of Twente	
Graduation committee	Prof. dr. S.J.M.H. Hulscher	University of Twente
	Dr. J.J. Warmink	University of Twente
	V.M. van Bergeijk MSc.	University of Twente

UNIVERSITY OF TWENTE. Risk

Summary

Current Dutch WBI safety standards are strict and result in substantial investments in dike reinforcement projects until 2050. Normative standards prescribe a single failure mechanism to determine dike failure. However, in the event of a slipped profile, follow-up mechanisms are often required before a dike breach occurs. Wave overtopping on the inner slope of a river dike profile is one possible follow-up mechanism that results in dike failure after a certain depth has eroded. The extent of failure development by this follow-up mechanism has not yet been examined and may result in more accurate standards. Previous studies have proposed a method to account for the residual strength for subsequent slope instabilities, but the effects of erosion by wave overtopping are not included for this.

The goal of this study is to quantify the residual dike strength for the follow-up mechanism of wave overtopping for slipped dikes that result from macro-instability. This is performed by developing a method to include the effect of overtopping on slipped profiles and by developing a new framework to derive the failure probability of overtopping by erosion on the inner dike slope. Simulations for this study have been performed by evaluating the failure erosion conditions for both the Hoffmans and Transition erosion model by using analytical flow equations. An approximation of the jet impact of a slipped profile for both erosion models is based on wave overtopping experiments and cover conditions from literature. Failure probabilities are next derived by performing a Monte Carlo analysis at varying water levels to obtain fragility curves after which the failure probabilities for a regular dike profile and a slipped dike profile are obtained.

Results from wave overtopping experiments indicate that the jet impact at a dike can be approximated by a maximum turbulence parameter ω = 2.8 corresponding to a turbulence intensity r_0 = 0.26. This turbulence parameter was found to vary for different grass cover qualities. The slipped river dike profiles evaluated for Millingen aan de Rijn fail at a wave overtopping discharge of 3 l/m/s for both the Hoffmans and Transition model during a 6-hour storm. Failure is first predicted just after the dike crest for the Transition model and in the middle of the inner dike slope for the Hoffmans model. The Hoffmans model also evaluates failure for similar conditions just after the dike crest. Moreover, conservative model runs indicated that a slipped dike is expected to increase the failure occurrence by overtopping by a factor 2–10 compared to a regular dike for which failure by erosion occurs near the dike toe.

This research describes a new framework that indicates that a residual strength occurs by wave overtopping. This residual strength can be included in more extensive probabilistic analyses for the assessment of safety standards for river dikes. The provided approach improves on current model approaches by considering local characteristics both in front of and at the inner slope of the dike to derive a probability of failure for erosion by wave overtopping using basic models. It is recommended to carry out overtopping experiments at slipped dikes to validate derived relationships. The resulting data can be used to test whether current erosion models approximate the impact of a slipped profile at varying dike locations accurately. Moreover, it is useful to examine the erosion process at a slipped profile more thoroughly by using advanced RFEM shear and CFD overtopping models as extensive research enables validation of findings.

Preface

Before you, I present the research report “The impact of overtopping on the failure probability of slipped river dikes”. This report was written to fulfil the graduation needs of the River and Coastal engineering master’s programme in Civil Engineering and Management at the University of Twente. During this research, I have had the help of several people, whom I would like to give my gratitude.

Firstly, I would like to express my gratitude to Suzanne Hulscher, Jord Warmink and Vera van Bergeijk for their supervision and useful feedback during this project. Your enthusiasm and support enabled me to write this thesis academically. I am also very thankful for the All-Risk participants Joost Pol, Guido Remmerswaal and Mark van der Krogt from the TU Delft for providing me with key insights during this thesis. Finally, I would like to thank my family, friends, and peers for their encouragement during this research. With special thanks to Britte, Romy, Jan and Jaume for the support at home in Enschede.

I hope that you enjoy reading my thesis report!

Vincent Verdonk

Enschede, July 2020

Index

1 Introduction

1.1 Background

The Netherlands is a large delta through which the European rivers Rhine and Meuse flow. During periods of high discharge, dikes located along the rivers protect the hinterlands from flooding. Historic extreme discharge events have severely impacted society, resulting in economic damage and loss of life. Moreover, future challenges such as land subsidence and population growth are expected to increase flooding vulnerability. The establishment and enforcement of this acceptable degree of vulnerability through assessment and maintenance of flood defences is of great importance to society. Dikes continuously need to be maintained and monitored as dike failures result in major losses.

To ensure the functionality of dikes, the Dutch WBI assessment protocol (*Wettelijk Beoordelingsinstrumentarium*) defines protection standards in terms of maximum allowable flooding probabilities for a variety of failure mechanisms. By law, the dike assessment must be carried out at least once every twelve years by the authorised local water authorities following the WBI. Accurate failure probabilities are necessary to quantify the occurrence of failure and, subsequently, the risk of flooding. Better understanding of the occurring failure mechanisms can potentially reduce projected costs for future dike reinforcement projects by using more precise calculation methods. In this study the two failure mechanisms of wave overtopping and macro instability are investigated.

Wave overtopping during a storm can be characterised as a combination of many small overtopping waves and some larger waves, where the largest waves often result in damage (Van der Meer, 2011). Processes related to wave overtopping are shown in Figure 1.1. During events with high water levels and high wind speeds, waves approaching the dike can break and run up the dike. The highest waves reaching the top of the dike flow over the crest and reach the inner slope of the dike. These overtopping waves result in an overtopping velocity on the crest and the inner slope.

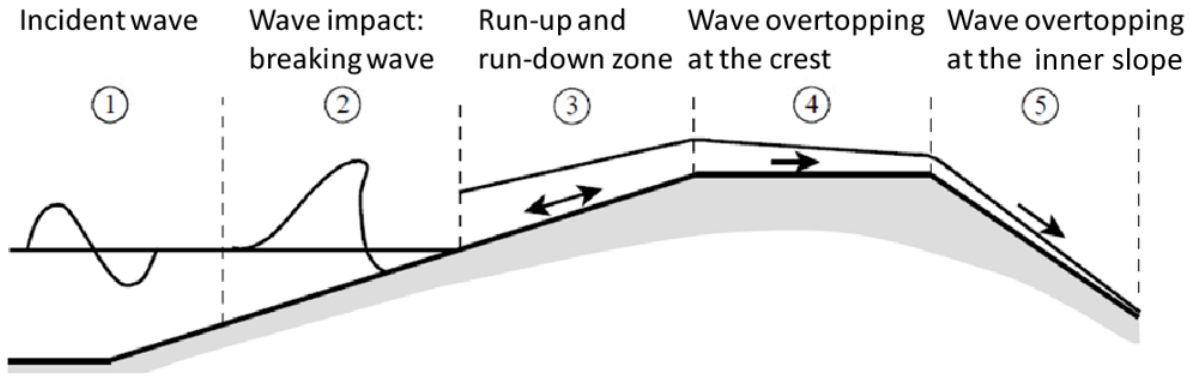

Figure 1.1: Process of wave breaking, run up and overtopping for a dike adopted from Schüttrumpf (2001).

As a result of high overtopping velocities, it is possible that erosion (Figure 1.2a) will occur on the crest and the inner slope of a grass-covered dike. This erosion process is defined as a critical failure mechanism within the WBI legal assessment for which failure is regarded at an erosion depth of 20 cm. The potential erosion damage is currently evaluated within the WBI by using the cumulative overload method (Steendam et al., 2010). This method results in a

damage number *D* with three damage criteria: (1) first damage, (2) various damage, and (3) failure (Van der Meer et al., 2011). Other methods for calculating the amount of erosion consist of calculating the depth of erosion along a dike profile. For this purpose, erosion models are often reliable up to a depth of 10–20 cm after which failure is regarded (Bomers et al., 2018).

After the initial grass layer has been eroded along the slope, an erosion pit will continue to develop until headcut erosion initiates (Figure 1.2b). During this process, the clay layer under the top layer erodes through progressive erosion, exposing the underlying cover layers to wave overtopping (Van der Meer et al., 2015b). As a result of progressive erosion, the exposed clay or sand layer will further erode up the dike. Once this erosion occurs upwards, the grass layer at the top of the scour hole will collapse.

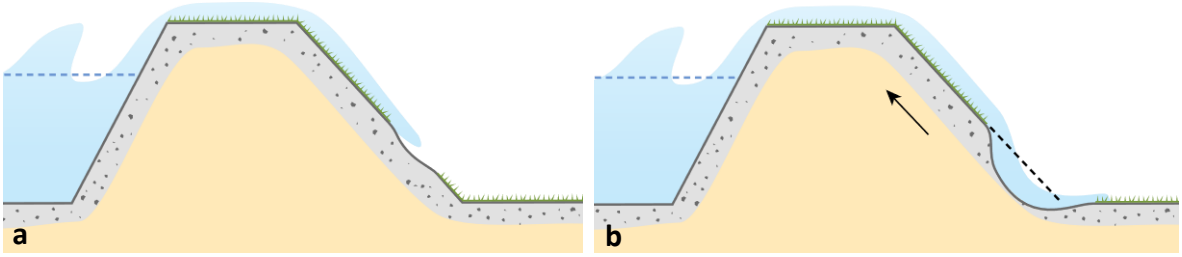

Figure 1.2: Failure processes by wave overtopping: (a) wave overtopping with initial erosion of the grass cover and (b) initiation and progression of headcut erosion. The figure illustrates an overtopping wave with grass layer (green), dike clay cover (grey), and a sand composition (brown).

In addition to wave overtopping, a dike can fail by other mechanisms such as macro-instability. Macro-instability is caused by the imbalance (loss of stability) of a soil mass along a slip plane which can be caused by a high load (i.e. water level) on a dike. This mechanism results in an instability where a large volume of soil slips away along a slip surface until a new equilibrium condition is reached. The WBI legal assessment defines failure by macro-instability as occurring when a dike profile slips (Figure 1.3a).

When the remaining profile following macro-instability remains high enough to withstand the water, the dike will not breach. In these situations, it is possible that critical damage can only occur by successive failure mechanisms such as wave overtopping. Figure 1.3 (b) illustrates the expected development of this critical erosion by overtopping waves. After sufficient erosion due to wave overtopping, dike failure due to headcut erosion as in Figure 1.2b is expected to occur.

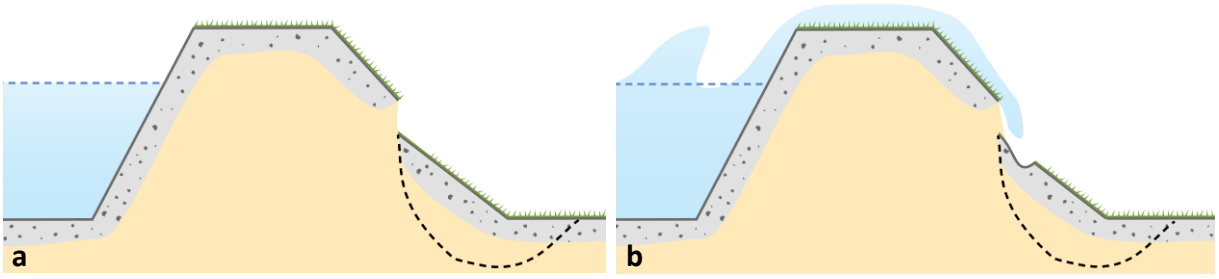

Figure 1.3: Failure processes by macro-instability with wave overtopping: (a) slipped profile occurring as a result of a high water level and (b) erosion of the grass cover on the slipped dike profile. The figure illustrates an overtopping wave with grass layer (green), dike clay cover (grey), a sand composition (brown), and a slipped profile (dashed black).

Cover failure is considered at 15 cm (0.5 ft) of erosion for the (vegetated) earthen dams (US) (Temple et al., 2007). After the initial failure of the cover layer, the erosion will develop downward, resulting in the formation of a vertical or near-vertical headcut which will migrate upwards, causing the topsoil to become unstable. It is not precisely known at what height upward migration occurs based on the soil composition. It may also be possible that headcut erosion is initiated immediately by exposure of the underlying sand (’t Hart et al., 2016). In this case, it is expected that the dike will erode almost immediately.

1.2 Problem context

Within the Flood Protection Programme, 900 km of dikes will be reinforced up to 2050 at an estimated cost of €7–9 million per kilometre to comply with new standards (Hoogwaterbeschermingsprogramma, 2019). Projected costs are high, and efforts are aimed at reducing costs through more efficient designs, reinforcement, and testing. Possibly costs can be reduced by taking into account the residual strength of a dike, which is an aspect that is examined within the All-Risk research programme.

Dike failure is currently defined within WBI by the primary failure mechanism, such as macro-instability. However, in the event of failure according to this definition, a dike is often not yet breached and continues to perform its water-retaining function. In this case, a residual profile after sliding is still present, and immediate failure cannot be considered (De Visser et al., 2018). The WBI thus considers failure based on a conservative assumption. To extend this assumption, it is necessary to understand the extent to which interaction with other failure mechanisms can occur. Three interaction mechanisms that result in failure have been defined for this purpose by Zwanenburg et al. (2018) where (1) a critical erosion depth is caused by overtopping waves, (2) secondary and follow-up slipping occurs, resulting in a dike profile below the water level, and (3) micro-stability occurs for a non-cohesive permeable material for which the exit point is above the slipped profile. Within the WBI’s failure definition, possible follow-up mechanisms as defined by Zwanenburg et al. such as wave overtopping are not considered after macro-stability for the approximation of the (residual) dike strength. Recent research has provided insight into the failure probabilities in the event of a follow-up slipped profile (Van Der Krogt et al., 2019). To assess the residual dike strength after a first macro-instability, it is necessary to gain an understanding of the probability of wave overtopping as a follow-up mechanism of slipped dike profiles. It is however not known how the wave overtopping process proceeds after macro instability and to which extent overtopping by erosion causes failure of a dike.

Within the European Comcoast research programme, the first series of tests with wave overtopping simulators (WOS) were carried out on a dike near Delfzijl for which 20 cm of the grass cover had been removed (Figure 1.4b). The extent to which headcut erosion occurred during wave overtopping experiments was later investigated within the framework of the WTI2017 by considering the USDA-NRCS sites spillway erosion analysis headcut model (Van Hoven et al., 2014). This study recalculated erosion parameters from the headcut observed at Delfzijl and Bergambacht and concluded that values were inconsistent with correlations from NRCS. It was noted from this that headcut parameters based on the Delfzijl case would be too conservative due to the removed cover layer whereas erosion values for Bergambacht

were found to be an order of magnitude lower. Regarding residual strength, it was concluded that for clay dikes an additional safety margin could be considered for overtopping of 1 l/s/m resulting in a maximum erosion length of 1.5 m. Although for both Delfzijl and Bergambacht, no significant erosion was observed at a discharge of 1 l/s/m, no conclusions were drawn for higher overtopping discharges due to uncertainties of the headcut model.

Figure 1.4: (a) Slipped profile at the Zuiderlingedijk Spijk, the Netherlands and (b) headcut erosion at Delfzijl following wave overtopping experiments adopted from Van Hoven et al. (2014).

From the current findings, it can be concluded that the residual dike strength is expected to be limited in the absence of a grass cover layer. A limitation of the WTI2017 study is that it did not consider the initial failure of the vegetal cover as can be expected for Dutch river dikes. As the evaluation of grass-covered slipped profile transitions has not been performed with wave overtopping tests, the strength of the vegetated cover of a slipped profile is unknown. Nevertheless, the extent to which the grass cover strength can be neglected is questionable for slipped dike profiles such as those shown in Figure 1.4 (a). For these reasons, it is interesting to study the initial failure phase of the grass cover layer after sliding of the dike profile to determine the residual strength of a slipped profile, including the grass cover layer, for wave overtopping. The grass cover especially can lead to additional strength, and therefore, it could be an important parameter in assessing the residual dike strength.

1.3 Study objective

The goal of this study is to assess the erosion failure vulnerability of a dike cover layer to wave overtopping for regular and slipped dike profiles. An assessment is therefore performed to quantify the potential residual strength that prevents a dike from failure. Additionally, overtopping conditions for which dike failure occurs are investigated for two erosion models. Next, the failure probabilities are calculated at varying water levels to determine to what extent slipped dike profiles are more at risk of overtopping than regular dike profiles. By comparing fragility curves for both scenarios, differences in the failure occurrence are established.

The following research objective is defined:

How does wave overtopping affect the failure vulnerability by erosion of regular and slipped river dike profiles?

For this the research objective, the following research questions are addressed:

1. *What are the wave volumes that can overtop a dike crest for varying return periods?*
2. *How is the erosion depth in erosion models along the crest and landward slope affected by the outer dike slope, cover type, hydraulic load and grass cover characteristics?*
3. *For which overtopping conditions are the critical erosion depth reached for different slip locations and characteristics?*
4. *What are the failure probabilities of wave overtopping of a dike with and without slope instability?*

1.4 Method

This thesis uses certain approaches according to each of the research questions. Considered approaches are described below.

For the first research question, a river dike is considered for which the wind speeds and local geometry are combined to obtain wave properties in front of a dike. Next, a volume load distribution is determined. Further, the distribution of volumes is analysed for varying water levels and wind conditions.

For the second research question, overtopping wave volumes are converted into wave velocities and into overtopping periods at the start of the dike crest. Next, the flow velocity along a dike profile is calculated for individual overtopping waves during a storm using analytical formulas. These flow velocities along the dike profile are used as input for two erosion models to approximate the erosion depth across the dike by overtopping. Insight into the sensitivity of the erosion depth for varying properties is gained by varying volume load distributions for different grass strengths, soil types, outer dike slope, and water levels.

For the third research question, failure conditions for the grass cover layer on a slipped dike profile are investigated. Failure conditions are identified by analysing failed dike sections that showed significant damage near the inner dike slope during wave overtopping experiments. Next, a turbulence parameter for both erosion models is calibrated to approximate critical conditions for slipped dike profiles. Scenarios for interaction between failure mechanisms are identified, after which slipped profile conditions are evaluated for the two erosion models.

For the fourth research question, a fully probabilistic approach is implemented. By calculating the failure probability for different water levels from the dominant wind direction, the development of the failure probability over the water depth can be constructed. On this basis, a fragility curve is obtained for a selection of dike scenarios for which parameters of the clay quality are varied.

The design methodology is schematically illustrated in Figure 1.5 and includes the aspects needed to meet the objective of this study. Within this framework, the four research questions are divided into four sections, from top to bottom.

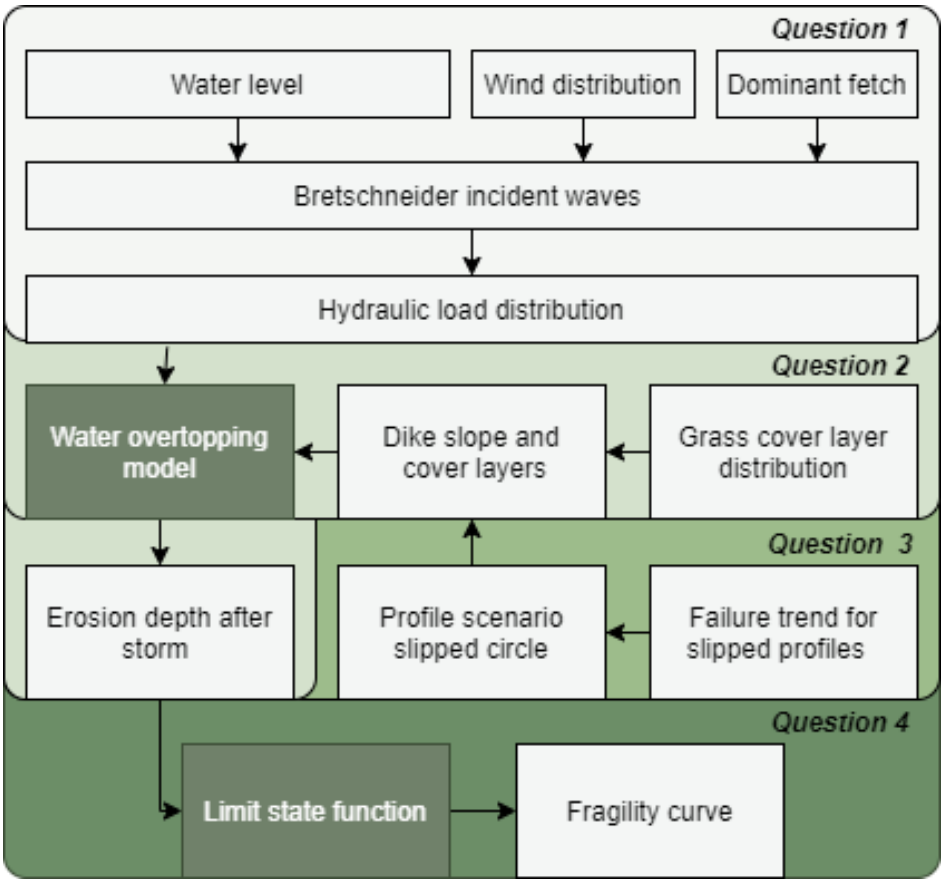

Figure 1.5: Method tree including the research design with key stages for each research question.

1.5 Study area

This study investigates river dikes that border a body of water with a large water surface. Across this surface, waves can form by a high wind speeds that build up over a long distance (fetch length). For this research, the dike profile of Millingen aan de Rijn at the Rijndijk is investigated located at the ME024 'Dijkpaal'. This dike has a crest height of 17.93 m + N.A.P., a crest width of 4.20 m, and both an inner and outer slope steepness of approximately 1:3 (height to width) or a cot(α) of 3.0 (Hoffmans, 2015). This clay river dike with a grass cover is situated at the junction of the Rhine, the Pannerdensch canal, and the Waal, causing the fetch length over which waves can build up from several directions to be almost 3 km. The dike ring area of Millingen on the Rhine is shown in Figure 1.6. The location of the research area is circled. For this study, the small pond located south of the dike section is disregarded.

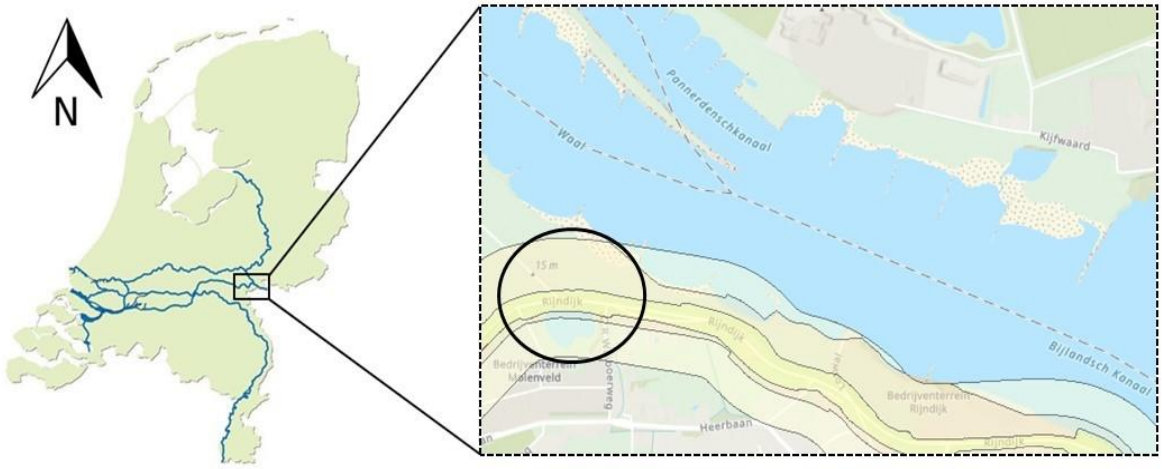

Figure 1.6: The study area near Millingen aan de Rijn where the crest of the dike is illustrated by the yellow line along which the outer slope is to the north and the inner slope is near a small pond. Figure obtained from the Waterschap Rivierenland ArcGIS Hub.

1.6 Thesis outline

The thesis is organised into the following chapters. Chapter 2 introduces the theoretical background of erosion processes, erosion models, and wave overtopping tests. Moreover, it addresses probabilistic methods that can be used to derive failure probabilities. Chapter 3 defines the methodology; it describes the methods and frameworks that are used to approximate the erosion depth along dikes based on a variety of model configurations and simulations. Chapter 4 describes the results obtained for the applied erosion models for the evaluated scenarios. Chapter 5 discusses the results, after which Chapter 6 presents conclusions and recommendations.

2 Theoretical background

2.1 Cover layer

The cover of inner dike slopes of Dutch dikes can be characterised by a specific dike structure and layout consisting of a cover layer in which grass vegetation is rooted. As shown in Figure 2.1, the topsoil and the subsoil are distinguished for assessment of the erosion resistance of the layer. The topsoil consists of a layer also known as the turf layer of a grass sod with a thickness ranging from 5–10 cm (’t Hart et al., 2016). In the topsoil below the turf layer, the roots can still have a significant influence on the erosion resistance of the soil. Erosion resistance is low in the subsoil because here roots are practically non-existent.

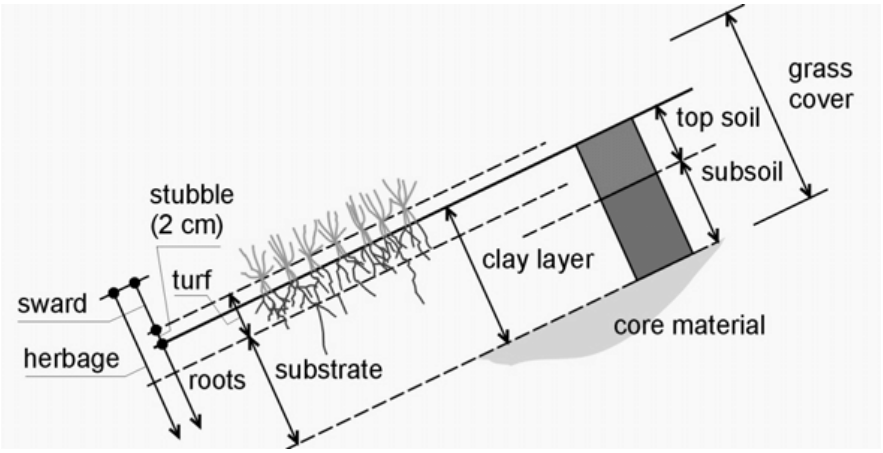

Figure 2.1: Cross drawing of the grass cover layer design (Muijs, 1999).

The resistance of a dike against erosion varies by the strength of the topsoil layer. Hoffmans (2012) states that the topsoil strength in clay varies by the soil structure compositions for which the suction pressures depend on clay characteristics and factors in the surroundings. The strength of the topsoil can increase in layers containing sand or silt particles as a result of cemented soils (cohesive bonds) in unsaturated conditions (Van der Meer et al., 2011; Steendam et al., 2010). The stability of a grass cover depends on the amount of roots, the critical root tension, and the cohesion that can arise between the roots and the soil (Hoffmans, 2012). Without the presence of roots, the soil will quickly erode due to less effective reinforcement of the soil.

2.2 Dike cover erosion mechanisms

The results of various overtopping experiments have led to the classification of several damage mechanisms for grass cover layers (Van der Meer et al., 2015b). It has been found from experiments that erosion is typically initiated at the weak spots along the slope (Steendam et al., 2010, 2014). This erosion damage tend to occur in areas with weak grass layers (Aguilar Lopez et al., 2018) and transitions (Bomers et al., 2018; Van Bergeijk et al., 2019a). Mechanisms for which initial erosion occurs at the grass layer on the inner slope are briefly discussed here.

Pull-up erosion: As a result of a high-turbulence flow under pressure at the top of the cover layer, grass sod can be lifted and loosened from its structure. The pressure changes the vertical balance of the sod. If this vertical force is large enough, a piece of turf can be pulled out from the cover layer (Figure 2.2a). Bulging is also considered part of this mechanism for a strong cover. In this case, the cover is not directly eroded, but a bulge is formed (Figure 2.2b) which can cause the turf layer to be completely washed away by large, successive overtopping waves.

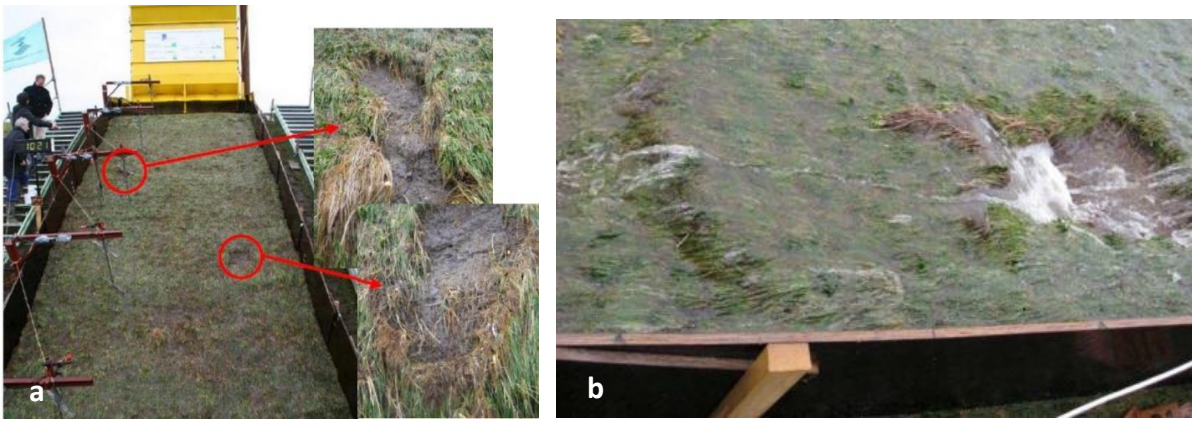

Figure 2.2: Pull-up erosion mechanisms observed: (a) pulled-out sod at two locations at St. Philipsland and (b) bulging mechanism observed at the Boonweg (Bakker et al., 2011).

Jet erosion: Jet erosion occurs at geometrical transitions such as the transition from a slope to a horizontal part of the dike as shown in Figure 2.3 (Valk, 2009; Van der Meer et al., 2015b) or the transition of the dike crest to the inner slope as shown in Figure 2.4 (Ponsioen et al., 2019). At these locations, the flow direction and velocities often change abruptly which results in an increased load on the grass cover. The load from a jet is expected to vary due to

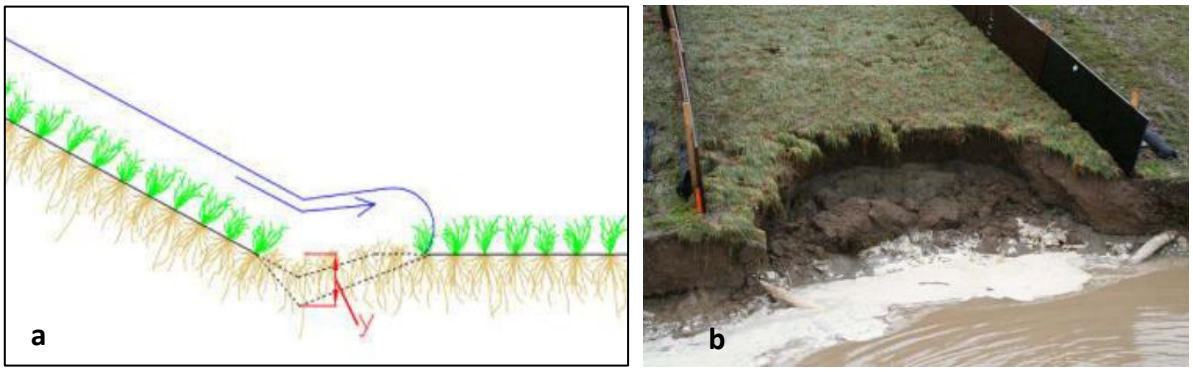

Figure 2.3: Jet scour at the dike toe: (a) according to Valk (2009) for which a scour hole develops from $y = 0$ *to* $y = y(t)$ *after an overtopping time* t *and (b) observed at the dike toe after wave overtopping experiments at the Kattendijke (Bakker et al., 2008).*

the impact angle and the initial speed (Valk, 2009) and its location can change over time for a single overtopping wave (Ponsioen et al., 2019).

Scour/wear erosion: Wear erosion can take place on top of a layer of grass where it often initiates in weaker areas, causing small sand and clay particles to erode from the surface layer. The gradual erosion caused by overtopping waves characterises wear erosion. The mechanism itself often is not to be a critical failure mechanism. During experiments, this form of erosion mainly occurred at weaker areas across the dike for materials with limited cohesion between the soil particles and the roots (Van der Meer et al., 2015b).

In addition to the mechanisms listed above, other erosion mechanisms may be triggered because of the initiation mechanisms described above. These could be, for instance, roll-up mechanisms in which in which the grass layer is lifted and tilted or headcut, as discussed previously. Moreover, aspects such as the fatigue of the grass layer can play a role, after which a turf layer can suddenly crack, causing a piece of the sod to come loose. Furthermore, there is a wide variability of damage that can occur to a turf cover as some roots break; some roots are pulled out due to a lack of anchoring, whereas other roots are not pulled out at all (Pollen & Simon, 2003). Experiments have highlighted that dike profiles can fail for varying loads and locations. The extent to which these combined mechanisms result in failure for varying dike profiles is, however, largely unknown.

To evaluate the extent of erosion that occurs by overtopping, erosion models are defined for different failure mechanisms. For erosion models based on the scouring and jet mechanisms, research has shown that there is a similarity between the erosion depths observed during experiments (Valk, 2009; Bomers et al., 2018; Frankena, 2019; Van Bergeijk et al., 2019a). Figure 2.4 shows an overview of models that can be used to determine a damage number or an erosion depth across a dike profile for scour or jet erosion. Although modelled mechanisms may not correspond with the exact mechanisms, these models can provide insight into the depth of erosion during an overtopping event across a dike.

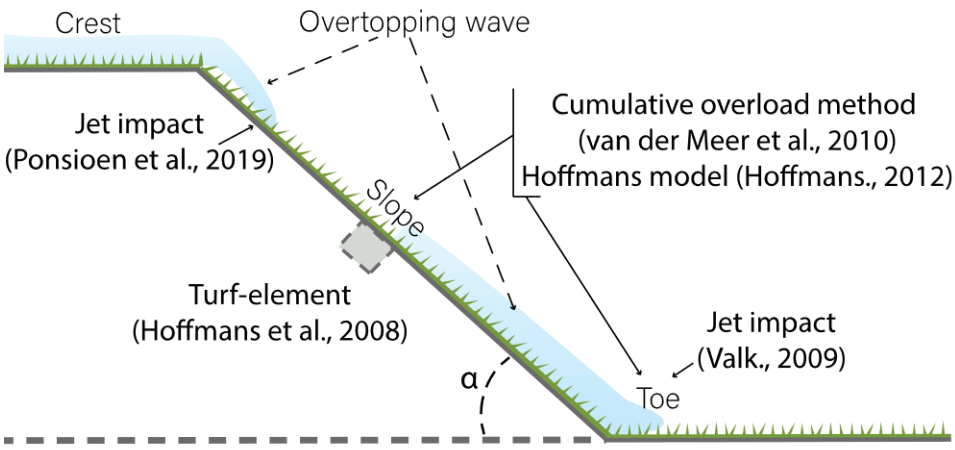

Figure 2.4: Erosion models used for approximation of dike erosion across a dike slope and for jet erosion at the transition from the crest to the dike slope and from the dike slope to the dike toe.

2.3 Erosion models

Erosion models can be used to evaluate the erosion depth across a dike profile. Model approaches, however, vary in their assessment of the amount of erosion either on the basis of a damage number or the depth of erosion. For this study, the erosion depth is evaluated for two depth-dependent models. These models are based on scouring mechanisms in which adjustments can be made to include erosion impacts by jets. Such models can be suitable for evaluating conditions for critical jet impacts for a slipped profile. First, the Cumulative Overload method, (the normative method) described by the WBI is addressed, after which the depth-dependent models of Hoffmans and Valk are described.

Cumulative overload method

The cumulative (hydraulic) overload method is the normative method within the WBI to assess whether a dike is safe for wave overtopping. This method shown in Equation 1 and 2 calculates the sum of waves *N* with a front velocity on the crest U_i [m/s] that exceed a critical velocity U_c [m/s] (Van der Meer et al., 2011). Along the dike profile, factors for the load α_M, strength α_s, and acceleration α_a can be included for this method. In this context, dike failure is considered at a damage number of 7,000 m^2/s^2 (Steendam et al., 2014; Rijkswaterstaat, 2017b; Hoffmans et al., 2018; Zwanenburg et al., 2018).

$$D = \sum_{i=1}^{N} (U_i^2 - U_c^2) \tag{1}$$

$$\text{for } U_i > U_c \tag{2}$$

Hoffmans model

The Hoffmans erosion model is based on the turf-element model that considers the forces acting on a turf element for a length scale of 10 cm (Hoffmans et al., 2008; Hoffmans, 2012). This model in Equation 3 and 4 can be used to calculate the erosion depth *d* [m] of an individual wave across a dike profile. For this study, the Hoffmans model is used to evaluate the erosion depth across the dike and at impact locations. A squared turbulence coefficient ω [-] is used to account for the additional load at transitions based on a depth-averaged turbulence intensity r_0 following Equation 5. The erosion depth across a dike profile during a storm can be defined as:

$$d(x) = \sum_{i=1}^{N} \left((\omega^2 U_i^2 - U_c^2) T_0 CE \right) \tag{3}$$

$$\text{for } \omega U_i \geq U_c \tag{4}$$

$$\omega = 1.5 + 5 r_0 \tag{5}$$

The model approximates erosion for loads that are greater than the grass cover strength. The squared difference between this load and the strength of the grass layer is multiplied by the characteristic overtopping period T_o [s]. This is multiplied by the inverse strength parameter *CE* [s/m] to obtain the erosion depth of an individual wave. Thus, more erosion will occur within this model at higher flow velocities.

Transition model

Valk (2009) designed a Transition model to approximate the erosion depth caused by jet formation. The model as shown in Equation 6 and 7 is designed to calculate the erosion depth *d* [m] of individual waves at the dike toe. At this location, shear stresses are expected to be higher than on the dike slope. Like the Hoffmans model, the Transition model contains a squared turbulence parameter ω [-]. The model contains a depth-dependent shear stress τ and a depth-dependent critical shear stress τ_c which is linked to the depth-dependent strength parameter *CE* [s/m] by the depth-dependent factor for the profile strength τ_{total} [N/m^2]. The erosion depth at a transition during a storm with the number of waves *N* can be defined as:

$$d(x) = \sum_{i=1}^{N} \left(\omega^2 \tau(d) - \tau_c(d)\right) T_0 CE(d) \tag{6}$$

$$\text{for} \quad \omega\tau(d) > \tau_c(d) \tag{7}$$

with a depth-dependent load:

$$\tau(d) = \frac{1}{2}\rho_w \left(\frac{1}{(1+\varepsilon)} U_i\right)^2 0.016\mathrm{e}^{-\mathrm{wd}} \tag{8}$$

With a water density ρ_w of 1,000 kg/m^3. Valk obtained a single value for the load coefficient of 0.016 for a jet impact angle of 1:2.5 following the experiments of Beltaos (1976). For the approximation of erosion across a dike, the velocity reduction coefficient is neglected for the air-water content ε [-] as a conservative estimate. Furthermore, the depth-dependent factor e^{-wd} in which *w* approximates dampening of the jet impact for a varying clay quality is disregarded because, for a (slipped) dike profile, it is unknown to what extent a single crack, once formed, will evolve. By replacing the load coefficient of a jet (0.016) with a friction factor f_{bf} [-], the following relation for the shear stress caused by an overtopping wave is considered (Van Bergeijk et al., 2019b):

$$\tau = \frac{1}{2}\rho_w U_i^2 f_{bf} \tag{9}$$

The Transition model contains a depth-dependent critical shear stress τ_c*:*

$$\tau_c(d) = \alpha_\tau\left((\rho_s - \rho_w) g d_a + \tau_{total}(d)\right) \tag{10}$$

which includes a pressure fluctuation parameter 1/18 α_τ [-], soil density ρ_s of 2,000 kg/m^3, and a gravitational constant of 9.81 m/s^2 with an aggregate diameter d_a = 0.004 m (Hoffmans et al., 2008). Moreover, the turf-element model (Hoffmans et al., 2008) can be used as an indication of the cover layer strength by taking into account the forces that act on a cubical turf aggregate. The inverse strength parameter of Equation 11 can be used for hydraulic rough conditions (Hoffmans et al., 2008). Based on this equation, a depth-dependent inverse strength parameter was derived by Valk, as shown in Equation 12**:**

$$CE = \alpha_E \frac{g^2 d_a}{v U_c^2} \tag{11}$$

$$CE(d) = \alpha_E \frac{g^2 d_a}{v\left(\frac{\alpha_0}{r_0}\sqrt{\left((\rho_s - \rho_w)/\rho_w\right) g d_a + \frac{\tau_{total}(d)}{\rho_w}}\right)^2} \tag{12}$$

For this equation, the parameter values consist of the kinematic viscosity v as 10^{-6} [m^2/s] and the dimensionless coefficients of $\alpha_E = 10^{-10}$ and $\alpha_0 = 0.29$ (Hoffmans et al., 2008). Additionally, the depth-dependent profile strength τ_{total} consists of a depth-dependent component for the strength of the clay layer and a depth-dependent strength of the cover layer:

$$\tau_{total}(d) = f\,\tau_{clay,0}(1 + a_{cs} d) + \sigma_{roots,0} e^{-\beta d} \tag{13}$$

Valk recommended a value for the clay cohesion factor and for the depth-dependent cohesion factor of clay of f = 0.21 [-] and a_{cs} = 20 [-], respectively. For the decrease in root density over depth β, a value of 22.32 was found by Sprangers (1999). This parameter is required as input for both the depth-dependent critical shear stress τ_c and the depth-dependent strength parameter *CE*.

2.4 Profile analysis of model cases

The results of various overtopping experiments have led to the classification of several damage mechanisms for grass cover layers (Van der Meer et al., 2015b). These profiles were often damaged near weak spots, such as mole hills or bald spots, or were damaged just below the crest. Failed dike profiles are analysed for which damage occurred on the inner slope of the dike. A total of eight sections are selected to obtain insight into the wave load by jet impact that can affected the dike slope of a slipped dike.

Afsluitdijk 2

For the Afsluitdijk, overtopping experiments were performed with average overtopping discharges of 1 l/s/m and 10 l/s/m (Bakker et al., 2009). During the first event, the damage was observed at the 3-m line of the slope which is measured from the transition of the crest to the slope. This damage developed downwards, causing severe damage to the paving at the bottom of the dike. The section failed due to damage at the toe, after which the tests ended. On the slope, 13 cm of erosion was measured after the 10 l/s/m event, as can be seen in Figure 2.5.

Kattendijke 2

The wave overtopping experiments at the Kattendijke dike started with a high initial wave overtopping discharge. Due to significant damage resistance during prior experiments, only overtopping rates of 30 l/s/m and 50 l/s/m were executed. Along the profile of the section, a pole was placed at 7 m from the crest line (Bakker et al., 2008). During the 50 l/s/m event, this pole was washed out by a wave which, in combination with the mole activity, resulted in a slice of clay separating from the cover layer, as shown in Figure 2.5a. As the damage was expected to increase drastically at 75 l/s/m, the tests were stopped.

Figure 2.5: Grass cover erosion at the slope at test sections (a) Afsluitdijk 2 and (b) Kattendijke 2 after wave overtopping tests with mean overtopping discharges of 10 l/s/m and 50 l/s/m, respectively (Bakker et al., 2008, 2009).

St Philipsland

The dike section of St Philipsland was tested with overtopping events with an average overtopping discharge q of 0.1, 1, 10, 30, and 50 l/s/m. For all events before the 50 l/s/m event, gradual erosion of the molehills was noticed. This was followed by significant erosion at two locations near the 4- and 7-m line from the crest (Bakker et al., 2008). In contrast to the experiments at the Kattendijke dike, the development of this initial damage continued at

7 m from the crest line, as shown in Figure 2.6b. The 50 l/s/m event caused the clay layer to erode after which the sand core was reached.

Figure 2.6: Grass cover erosion on the slope at the test section of St Philipsland (a) during and (b) after the wave overtopping event with a mean overtopping discharge of 50 l/s/m (Bakker et al., 2008).

Tholen 3

At Tholen 3, the tests were stopped after the experiments with average wave overtopping discharges of 1 and 5 l/s/m. Local subsidence was observed during the second event with a wave overtopping discharge of 5 l/s/m, resulting in water bulging up from underground as shown in Figure 2.7. This bulging resulted in the development of a hole which quickly evolved into failure. Although the test was continued after repairs, the dike failed near the 9–10-m line from the overtopping machine during the second third of the 5 l/s/m event (Bakker et al., 2011). Although this test was aimed at investigating the impact of fencing, the fencing effect was concluded to be limited.

Figure 2.7: Grass cover erosion on the slope at Tholen 3 at (a) 40 min and (b) after stopping the wave overtopping event with a mean overtopping discharge of 5 l/s/m (Bakker et al., 2011).

Tielrodebroek 1 & 2

Wave overtopping experiments were carried out at Tielrodebroek to examine the erosion resistance of a river dike. For overtopping conditions at both sections, a high river tide of 2 hour was used with a significant wave height H_s 0.75–1.00 m and a mean wave period T_m 3.1–3.6 s (Peeters et al., 2012). For the tests, wave overtopping rates of 1, 10, and 30 l/s/m were simulated; reproduced overtopping conditions are provided in Appendix B.

At section 1, increasingly more small holes and bare places gradually appeared during the first two events. During the third overtopping event of 30 l/s/m, the turf collapsed, after which a cliff was formed which quickly eroded (Figure 2.8). At section 2, bald spots in the grass cover were the result of local mole activity. Small cliffs formed during the 10 l/s/m event that resulted in the washout of soil. Both sections failed early at two sixths and one sixth of the way through the 30 l/s/m event at the 2-m line from the crest (Peeters et al., 2012).

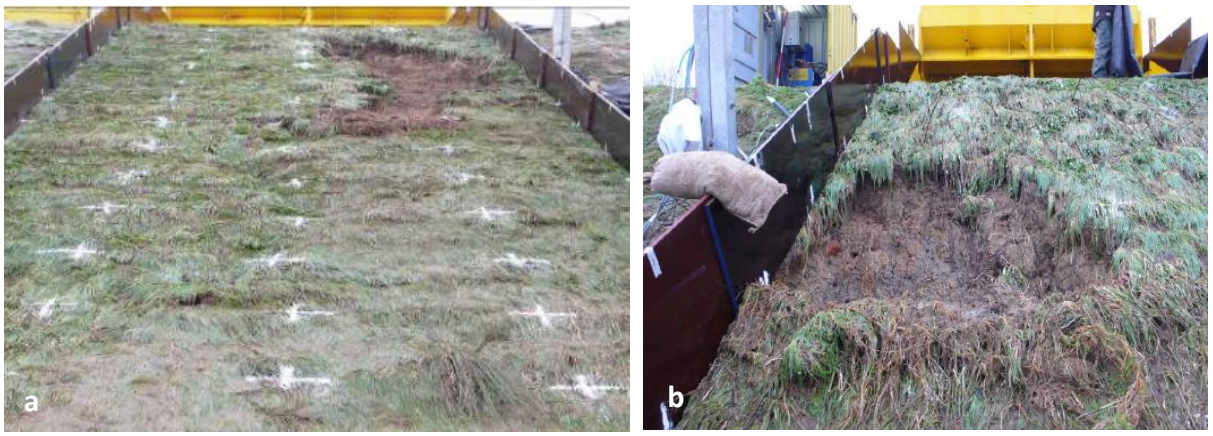

Figure 2.8: Grass cover erosion on the slope at test sections (a) Tielrodebroek 1 and (b) Tielrodebroek 2 after 20 and 40 min of testing with a mean overtopping discharges of 30 l/s/m (Peeters et al., 2012).

Wijmeers 1 & 3

Similar to Tielrodebroek, for Wijmeers, wave overtopping experiments were performed for a 2-hour storm. Separate control lists were developed, which are replicated in Appendix B, based on an increasing significant wave height H_s 0.4–1.3 m and a mean wave period T_m 2.11–3.80 s (Pleijter et al., 2018).

The experiments at Wijmeers 1 were carried out with average wave overtopping discharges of 1, 5, 25, and 50 l/s/m. At the first section, significant damage occurred during the 10 l/s/m event near a rabbit hole, leading to the washout of sand. The damage further developed during the first hour of the 25 l/s/m event, forming a downward erosion path. During the second hour, the erosion progressed and critical damage occurred around the 2-m line from the crest. Field tests of Wijmeers 3 consisted of initial experiments after which an average overtopping event with 25 l/s/m was started. During this event, an erosion pit formed after 1 hour of testing. Experiments were stopped after 1 hour and 27 minutes, as can be seen in Figure 2.9. Failure after 2 hour is regarded for this section, as overtopping data from the initial experiments is unavailable. The location of the damage is set around the 1–2 m line from the crest.

Figure 2.9: Grass cover erosion on the slope at test sections (a) Wijmeers 1 and (b) Wijmeers 3 after wave overtopping tests with mean overtopping discharges of 25 l/s/m after 2 h and 1 h and 27 min, respectively (Pleijter et al., 2018).

The profile data of the various dike sections is summarised in Table 2.1. From these data, it can be observed that for a 6-hour event, the profiles collapsed at an average overtopping discharge of q < 10 l/s/m. For a 2-hour event with relatively large wave overtopping volumes, failure occurred at a higher average overtopping rate (q < 30 l/s/m). Moreover, many of the profile sections that collapsed contained a steep slope angle. The profile with the most gradual slope was the section at Kattendijke. This profile proved to be more resistant to overtopping waves and showed no critical failure after the 50 l/s/m event. For Afsluitdijk 2, failure did not occur on the slope.

By including the management forms of the various dike sections as listed in (Van der Meer et al., 2015b), many of the profiles belong to the weakest category, *D*. This is a management category corresponding to weak erosion-resistant covers. It should be noted that the management category for Wijmeers was established by correlating its grassland type to prior experiments in the overtopping database (Van der Meer et al., 2015b). St Philipsland, rated in the best category, A (well-rooted), together with Kattendijke 2, rated in category C (moderately to poorly rooted top layer), demonstrated to be more erosion-resistant for a large number of overtopping waves.

Table 2.1: Profile details with performed overtopping events q*, landward dike slope angle* cot*(α), damage classification after the tests, and the representive management category according to Van der Meer et al.* (2015b)*. Data for the tests at Afsluitdijk, Kattendijke, St Philipsland, Tholen, Tielrodebroek, and Wijmeers is obtained from Bakker et al. (2009), Bakker et al. (2008), Bakker et al. (2011), Peeters et al. (2012), and Pleijter et al. (2018), respectively.*

test section	**q *[l/s/m]***	**cot(α) *[-]***	***damage [-]***	***management category [-]***
Afsluitdijk 2	*6h: 1; 10*	2.3	*bare spots*	*B*
Kattendijke 2	*6h: 30; 50*	3.0	*~ failure*	*C*
St Philiplsland	*6h: 0.1; 1; 10; 30; 50*	2.4	*failure*	*A*
Tholen 3	*6h: 1; 5* ($\frac{2}{3}$)	2.4	*failure*	*D*
Tielrodebroek 1	*2h: 1; 10; 30* ($\frac{2}{6}$)	2.5	*failure*	*D*
Tielrodebroek 2	*2h: 1; 10; 30* ($\frac{1}{6}$)	2.5	*failure*	*D*
Wijmeers 1	*2h: 1; 5; 25*	1.8	*failure*	*D*
Wijmeers 3	*2h: 25*	1.9	*failure*	*D*

Next, locations are investigated where the damage occurred on the dike. A critical flow velocity U_c [m/s] is derived based on experimental data using the COM for many of the profiles. From derived U_c values in Table 2.2 it can be noted that profiles close to the crest collapsed from a lower critical velocity than the profiles at the middle of the dike slope did. However, Tholen 3 is an exception in this respect because for this profile Hoffmans derived a critical velocity of 0 m/s (D = 7,000). A critical failure velocity U_c for Tielrodebriek 1, Tielrodebriek 2, and Wijmeers 1, below 3.5 m/s (Wijmeers) and 3.1 m/s (Tielrodebroek) was derived from the tables listed in Peeters et al. (2012) and Steendam et al. (2013).

Table 2.2: Profile details with failure locations x *measured horizontally as the distance from the start of the landward slope, calibrated critical flow velocities* U_c *relating to the damage category according to Hoffmans* (2015)*, and derived critical flow velocities by interpolation. Data for the tests at Afsluitdijk, Kattendijke, St Philipsland, Tholen, Tielrodebroek and Wijmeers is obtained from Bakker et al. (2009), Bakker et al. (2008), Bakker et al. (2011), Peeters et al. (2012), and Pleijter et al. (2018), respectively.*

test section	***failure location x [m]***	**U_c** ***[m/s]***	***derived*** **U_c** ***[m/s]***
Afsluitdijk 2 (Bakker et al., 2009)	2.8	4.0	4.0
Kattendijke 2 (Bakker et al., 2008)	6.6	6.5	6.5
St Philiplsland (Bakker et al., 2008)	6.5	6.5	6.5
Tholen 3 (Bakker et al., 2011)	6.5	0.0	0.0
Tielrodebroek 1 (Peeters et al., 2012)	1.9	< 3.1	1.2
Tielrodebroek 2 (Peeters et al., 2012)	1.9	< 3.1	1.6
Wijmeers 1 (Pleijter et al., 2018)	1.7	3.5	3.5
Wijmeers 3 (Pleijter et al., 2018)	1.3	< 3.5	3.0

2.5 Probabilistic methods

In this study, probabilistic methods are used to determine the vulnerability of slipped profiles to wave overtopping compared to the vulnerability of normal dike profiles. To achieve this level-III probabilistic calculation, methods are applied for which the dike reliability is directly linked to the probability of failure (Vrijling et al., 1997). Both a common and advanced sampling technique are used to increase the efficiency of computations. For both approaches, stochastic variables X_1 and X_2 are converted to normal variables U_1 and U_2.

Crude Monte Carlo sampling (MCS)

Monte Carlo sampling is a technique that relies on random sampling to approximate failure probabilities (Vrijling et al., 1997). By repeating this procedure numerous times, the probability of failure can be estimated by dividing the number of simulations in which failure occurs by the total number of simulations. An advantage of this method is that results are reliable and accurate. A disadvantage is that failure approximation may take a great deal of computational power, especially for a complex problem or for approximating small failure probabilities. Though it is possible to optimise the sampling procedure, this is often a complicated procedure requiring initial knowledge of the limit state (Z = 0), which is not covered in this research.

Adaptive directional importance sampling (ADIS)

Adaptive directional importance sampling is a technique in which random directions are generated from a standard normal space (directional sampling) consisting of the random variables converted to a normal distribution (Grooteman, 2011; Den Bieman et al., 2014). From here, the limit state is searched randomly to develop an adaptive response surface that replaces the limit state function (LSF). When a sufficiently small difference between the LSF and the adaptive response surface (ARS) is found, the ARS is accepted and used (Figure 2.10). The ARS plane is updated until it sufficiently fits evaluated points, after which a β-sphere is applied for importance sampling. The β-sphere encloses the important domain in which exact evaluations are performed to approximate the limit state. The probability of failure is

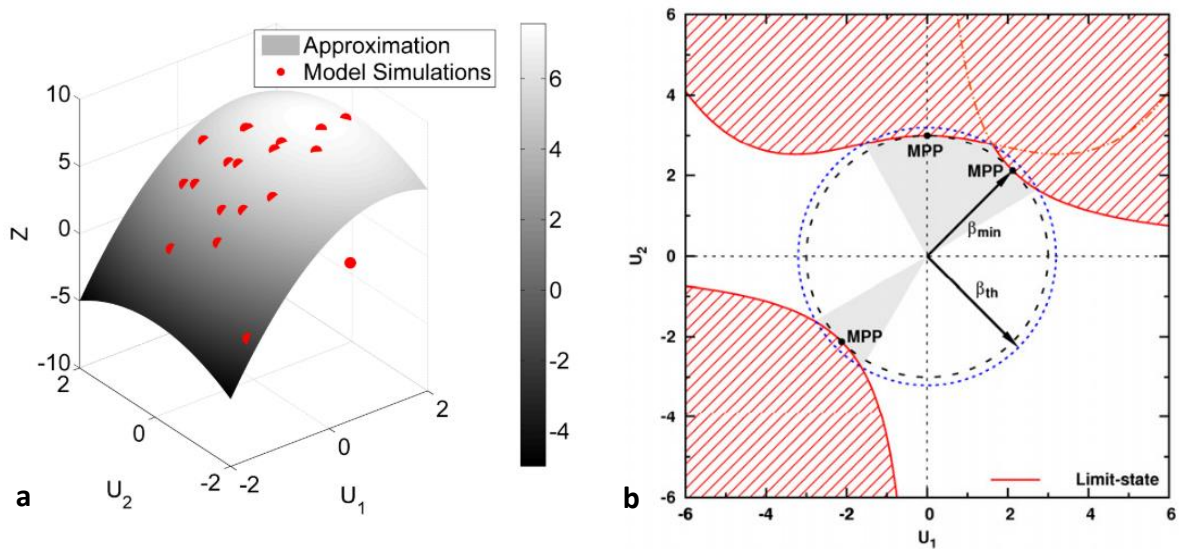

Figure 2.10: ADIS in the standard normal space for two stochastic variables: (a) example of an ARS (grey plane) with LSF evaluations (red points) and (b) importance sampling by a β-sphere. Adopted from Den Bieman et al. (2014) and Grooteman (2011), respectively.

determined by evaluating the limit state function within the β-sphere and on the adaptive response surface outside of it. This can be performed as evaluations outside the sphere have a small impact on the probability of failure. The advantages of this method include applicability for small failure probabilities and suitability when using a larger number of random variables.

Probabilistic techniques are used to derive fragility curves by linking them to erosion models, resulting in erosion failure by wave overtopping. A fragility curve shows the course of the probability of failure as a function of a load parameter, such as the water level. For the construction of fragility curves, the above probabilistic calculation techniques are used to determine the probability of failure.

3 Method

The research structure, as is shown in Figure 1.5, is briefly introduced. First, in Section 3.1 the applied method is described which is used to derive wave properties by using the Brettschneider equations and convert these properties to storm conditions by using a 6-hour storm and the local dike geometry. Second, in Section 3.2, the applied erosion model structures are addressed that are used to evaluate the erosion depths across a dike profile for the Hoffmans model and the Transition model. Moreover, this section covers the identified model runs for evaluation of the model sensitivity. Third, performed calibration for slipped profiles is described using frameworks in Section 3.3 after which a description of the method used to identify failure conditions is defined in terms of an average critical overtopping discharge. Last, in Section 3.4, the method used to derive failure probabilities for varying wind velocities and grass cover strengths is evaluated for which erosion models are converted to a limit state function.

3.1 Hydraulic load on the dike crest

3.1.1 Wind and water level conditions

Varying water levels and wind speeds are used as stochastic variables to generate a hydraulic load distribution. Return frequencies for water levels at Millingen aan de Rijn are obtained from the Hydra-NL WBI 2017 software (Appendix A). Deltares, in collaboration with KNMI, derived the wind statistics for potential wind speeds in the Netherlands (Caires, 2009). This wind speed is the measured wind speed converted to the wind speed u_{10} [m/s] at a standard landscape roughness and a standard height of 10 meters.

Regarding wind characteristics, peaks over threshold (POT) statistics are derived from a series of peaks of wind speeds above a certain threshold (Caires, 2009). These POT series are distributed according to an exponential distribution (generalised Pareto distribution type I) (Chbab, 2017). The cumulative probability distribution for this extreme is defined by F_u in which $\tilde{\sigma}$ is the scale parameter, wind direction specific value λ with u as the threshold wind speed. The value y [m/s] is the wind speed minus the threshold speed u. The formula for the cumulative probability distribution is provided in Equation 14 which can be rewritten into wind speeds for specific return periods z_m as is shown in Equation 15.

$$F_u(y) = 1 - \exp\left(-\frac{y}{\tilde{\sigma}}\right) \tag{14}$$

$$z_m = u + \tilde{\sigma}\ln(\lambda_u m) \tag{15}$$

Following the statistical derivation of Caires, statistics in sectors of 30 degrees have been derived. Both location and wind direction-specific u, $\tilde{\sigma}$ and λ_u parameters used for this research were chosen for Deelden for a m-yr return value, as this is a representative location for extreme wind (Chbab, 2017).

3.1.2. Wave conditions at the outer toe of the dike

The effective fetch length together with the wind speed (wind strength) and the water level determines the size of the waves produced. Local characteristics such as the average riverbed height and the effective fetch length, a measure of the configuration of the water surface in front of the flood defence, are obtained from the Hydra-NL software, using the Hydra-NL database from the WBI2017, for dike ring 42, location 24.

	direction wind [-]	*wind angle [deg]*	*mean bed level height [m+NAP]*	*effective fetch* F *[m]*
	N	360	7.9	2,064
	NNE	30	8.4	2,239
	ENE	60	9.4	2,739
	E	90	6.1	2,509
	ESE	120	12.5	1,326
	WSW	240	13.2	1,736
	W	270	9.4	2,785
	WNW	300	9.9	2,810
a	*NNW*	330	10.0	2,287

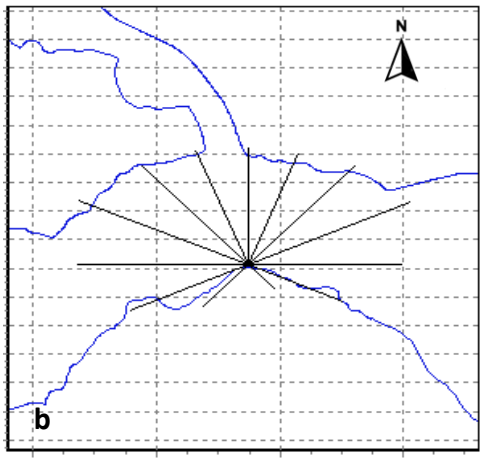

Figure 3.1: (a) Effective fetch lengths and average riverbed heights obtained for 30°-sectors by converting 22.5°-sector characteristics. (b) Figure as obtained from Hydra that show the fetch length directions for 22.5°-sectors.

The Hydra-NL output for 22.5°-sectors needs to be converted as the wind statistics are determined for 30°-sectors. For this purpose the effective fetch and mean bed levels are converted proportionally to the adjacent sectors (Chbab, 2017).

By using the Bretschneider Equations 16 and 17 (Calderon et al., 2016) wind velocity statistics following from Caires (2009) for the potential wind speed u_{10} [m/s] are combined with effective fetch lengths F [m] and water depths d [m]. The water depth was determined by subtracting the average bottom height across the fetch from the water level to derive characteristics for the significant wave height H_s [m] and the significant wave period T_s [s].

$$\frac{gH_s}{u_{10}^2} = 0.283 \tanh\left[0.530\left(\frac{9.81d}{u_{10}^2}\right)^{0.75}\right] \tanh\frac{0.0125\left(\frac{9.81F}{u_{10}^2}\right)^{0.42}}{\tanh\left[0.530\left(\frac{9.81d}{u_{10}^2}\right)^{0.75}\right]} \quad (16)$$

$$\frac{gT_s}{u_{10}^2} = 2.4\pi \tanh\left[0.833\left(\frac{9.81d}{u_{10}^2}\right)^{0.375}\right] \tanh\frac{0.077\left(\frac{9.81F}{u_{10}^2}\right)^{0.25}}{\tanh\left[0.833\left(\frac{9.81d}{u_{10}^2}\right)^{0.375}\right]} \quad (17)$$

3.1.3. Hydraulic load distribution

Next, based on the given boundary conditions for waves and water levels, the overtopping flows are obtained. This process is illustrated in the diagram shown in Figure 3.2.

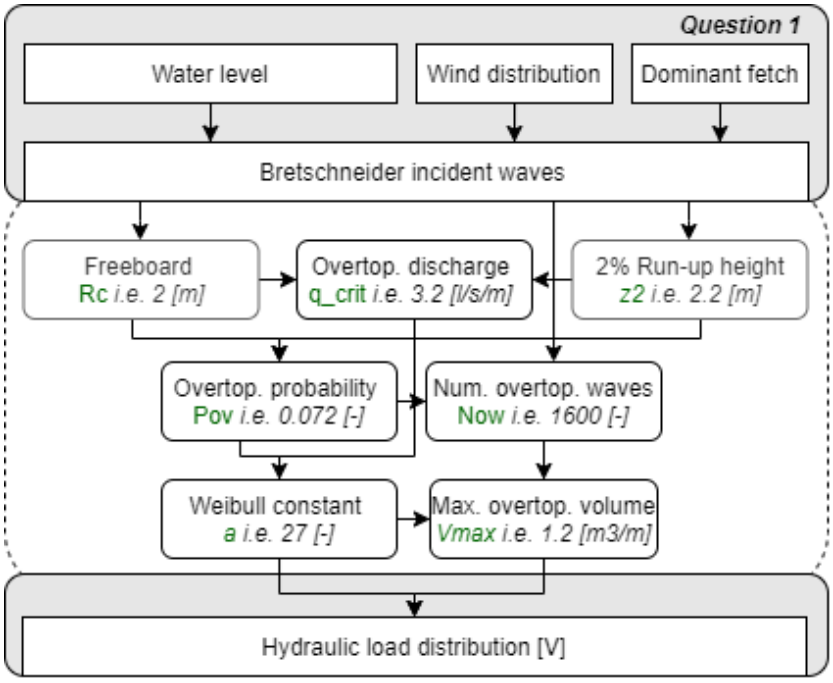

Figure 3.2: Input variables needed to approximate the hydraulic load, green expressions relate to MATLAB variables.

For this approximations the significant wave height $H_{m0} \approx H_s$ and the spectral wave period $T_{m-1.0} \approx 1.08T_s$ are used to determine the relative wave steepness $s_{m-1.0}$ [-] in Equation 18 (Calderon et al., 2016). Subsequently the 2% run-up height $R_{u2\%}$ [m] can be calculated. The relative wave steepness is used to determine the breaker parameter $\xi_{m\text{-}1.0}$ [-] for the outer slope angle of the dike α_{out} [-]. Moreover, the free crest board R_c [m] is determined by subtracting the height of the water level from the crest height of the dike. The formula for the 2%-wave run-up level is given by Equation 20, which is a height that is exceeded by 2% of the surging waves by assuming breaking waves only. Additionally, an influence factor for short crested waves is used for the calculation of this influence factor γ_β. For this purpose, the most perpendicular impact angle to the dike β within each 30° wind direction is used to include the impact angle of waves for wave overtopping (EurOtop, 2018).

$$s_{m-1.0} = \frac{2\pi H_{m0}}{gT_{m-1.0}^2} \tag{18}$$

$$\xi_{m-1.0} = \frac{\tan\alpha_{out}}{\sqrt{s_{m-1.0}}} \tag{19}$$

$$\frac{R_{u2\%}}{H_{m0}} = 1.65\gamma_\beta \xi_{m-1.0} \tag{20}$$

$$\gamma_\beta = 1 - 0.0033|\beta| \quad \text{for} \quad 0° \le |\beta| \le 80°$$
$$\gamma_\beta = 0.736 \quad \text{for} \quad |\beta| > 80° \tag{21}$$

Next, the overtopping probability P_{ov} is determined using Equation 22 after which the number of overtopping waves N_{ow} can be obtained for a fixed storm duration of t_{storm} = 6 hrs with a given number of total waves N_w following recommendations for the overtopping duration (Rijkswaterstaat, 2017a) and former research (Valk, 2009; Van Hoven et al., 2014).

$$P_{ov} = \exp\left(-\left(\sqrt{-\ln 0.02}\frac{R_c}{R_{u2\%}}\right)^2\right) = N_{ow}/N_w \tag{22}$$

To evaluate the average overtopping discharge q during a storm the EurOtop 2007 formulae with average values are used which can be used for probabilistic calculations (EurOtop, 2018). Equation 23 and 24 contain the influence factor for the impact angle.

$$\frac{q}{\sqrt{gH_{m0}^3}} = \frac{0.067}{\sqrt{\tan\alpha_{out}}}\xi_{m-1.0}\exp\left(-4.75\frac{R_c}{H_{m0}\gamma_\beta\xi_{m-1.0}}\right) \tag{23}$$

With the maximum:

$$\frac{q}{\sqrt{gH_{m0}^3}} = 0.2\exp\left(-2.6\frac{R_c}{H_{m0}}\frac{1}{\gamma_\beta}\right) \tag{24}$$

Where:

q	Average overtopping discharge	[m³/s/m]
R_c	Free crest height above still water line	[m]
$R_{u2\%}$	Run-up height exceeded by 2% of the waves	[m]
H_{m0}	Significant wave height at the toe of dike	[m]
α_{out}	Outer slope of the dike	[deg]
γ_β	Reduction factor wave attack angle	[-]

Next it was decided to sample overtopping waves based on volumes instead of on run-up heights due to the relatively simple geometry of river dikes. Following the exceedance sampling approach of Frankena (2019), individual overtopping wave characteristics V_i are derived. According to this approach, volumes are sampled within a maximum range so that the individual overtopping volume cannot exceed the maximum overtopping volume. Wave volumes are randomly generated from the probability exceedance distribution in Equation 25 for the shape parameter *a* from Equation 26.

$$a = 0.84\ q\ (t_{\text{storm}}\ /N_{ow}) \tag{25}$$

$$P(V_i > V) = \exp\left(-\left(\frac{V}{a}\right)^{0.75}\right) \tag{26}$$

The exceedance method of Frankena uses the MATLAB-function *randample* to sample a single overtopping volume from a volume array V_{array} with a wave volume vector interval of 0.001 m^3/s. With an adjustment to this method all overtopping waves are sampled for a single storm. This is performed to increase speed and obtain the set of overtopping waves V_{ow} = {N_{ow} x V_i} with the following MATLAB command: V_{ow} = *randsample*(V_{array}, N_{ow},*true*, $P(V_i=V)$).

3.1.4. Hydraulic load distribution

As both the wave properties and water level causes the overtopping characteristics to vary, both properties are evaluated at a fixed return period. Wave characteristics are first compared from the east-north-eastern (ENE) and west-north-western (WNW) wind directions with an effective fetch of 2739 m and 2810 m. Next, the effect of a varying return period of the water level and the wind speed from *T* = 10 years to *T* = 10,000 years is investigated.

3.2 Erosion across a dike

Erosion is evaluated across the dike profile for the Hoffmans and Transition erosion model. For this purpose, hydraulic loads obtained from the first sub-question are applied to the dike profile of Millingen.

3.2.1. Overtopping flow development

Velocities of overtopping waves across the Millingen aan de Rijn dike profile are required to evaluate the erosion caused by overtopping. The equations of Van Bergeijk et al. (2019b) are used to approximate the depth-averaged maximum flow velocities of individual overtopping waves. Besides parameters related to geometric aspects, the equations require three input parameters: the bottom friction coefficient f, the initial velocity at the start of the crest u_0, and the initial layer thickness at the start of the crest of the overtopping wave h_0. For the bottom friction coefficient, a value of f_{bf} = 0.01 [-] is used (Steendam et al., 2012) which is established for inner dike slopes. For the initial flow velocity and initial layer thickness relations proportional to the wave volume are used: $u_0 = 4.5V^{0.3}$ [m/s] and $h_0 = 0.133V^{0.5}$ [m] (Van der Meer et al., 2015a, 2011; Van Bergeijk et al., 2019a).

3.2.2. Modelling erosion across the dike

For calculation of the erosion across the dike profile, both the Transition model and the erosion model of Hoffmans as described in Section 2.3 are evaluated. Within the erosion models, an overtopping period is applied proportional to the wave volume of $T_0 = 0.39V^{0.46}$ following findings of Hughes (2012). For the Transition model field measurements performed at Millingen aan de Rijn are used with a grass cover strength $\sigma_{roots,0}$ = 7,760N/m^2 and a clay layer strength of $\tau_{clay,0}$ = 11,900N/m^2 (Bomers, 2015).

For the Hoffmans and Transition model, the first objective is to identify which wind direction for a return period of T = 1,000-year results in largest erosion depth across the dike for a water level h of 16.93 m + N.A.P. one meter below the crest of the with an approximated return period of T = 10,000 years. This situation represents an extremely high-water level (> 15.60 m) according to Rijkswaterstaat Waterinfo. The erosion depth following from the Hoffmans model is compared with the following two depth-dependent cases for the Transition model:

- Case TM_A: The default model configuration of the Transition model is used as is specified in Equation 12 with both a depth-dependent relationship for the critical shear stress and a depth-dependent relationship for the strength parameter $CE(d)$.
- Case TM_B: The adjusted Transition model configuration according to Equation 11 is used with a depth-dependent relationship for the critical shear stress with a constant strength parameter CE that can be linked to the critical flow velocity U_c.

To evaluate the erosion depth erosion across the dike profile a depth-averaged turbulence intensity r_0 of 0.1 is used across the dike profile which resembles a turbulence parameter ω of 2.0 [-] following Equation 5 (Van Hoven et al., 2013). For both the Hoffmans model and case TM_B a moderate critical flow velocity of 4 m/s (Aguilar Lopez et al., 2018) is used whereas for the strength parameter CE a value of 10^{-6} s/m is applied for the Hoffmans model corresponding with a good clay cover (Hoffmans, 2012).

3.2.4. The sensitivity of model parameters

Differences between the erosion models are evaluated next from the dominant wind direction for a similar return period for both the Hoffmans model and the Transition model case TM_B from Section 3.2. The sensitivity of the models for varying parameters is examined for a varying clay quality, critical velocity, outer dike slope and water level. This is performed to gain insight into the differences in erosion depths across the dike for both erosion models and between the defined model cases for the Transition Model after which a single case TM case is selected. For the grass cover quality, a moderate critical flow velocity of 4 m/s is applied for both models. For the clay variability, a *CE* value of 10^{-6} s/m within the Hoffmans model is varied between -25 and +25 % (Table 3.1) whereas for the Transition model the parameter sensitivity for the clay cohesion factor *f* of 0.21 is evaluated for similar ranges. Evaluated model runs are listed in Table 3.1.

Table 3.1: Low, standard, and high model runs used to evaluate the erosion depth along the dike section.

		Low	**Standard**	**High**
Cover quality U_c	[m/s]	- 25 %	4	+25 %
Clay cover *CE*	[s/m]	-25 %	10^{-6}	+25 %
Clay cover *f*	[-]	-25 %	0.21	+25 %
Freeboard R_c	[m]	0.75	1.0	1.25
Outer dike slope	[tan(α_{out})]	1/2	1/3	1/4

3.3 Erosion at slipped sections

3.3.1 Characteristics of a damaged dike

As only a small number of slipped profiles is documented, it is unclear how a dike profile evolves as a result of slipping. Particularly for small slipped profiles in which the turf is still largely intact, and the dike core is not yet fully exposed, little is known. To find out which factors could be essential to consider within an erosion model to approximate the residual dike strength, an online meeting was organised with the following experts from the TU Delft affiliated with the All-Risk project:

- *Joost Pol*: PhD researcher in the field of Hydraulic Structures and Flood Risk. With expertise, amongst others, in the field of time-dependent failure mechanisms and interaction between failure mechanisms.
- *Guido Remmerswaal*: PhD researcher in the field of Geo-Engineering. With expertise, amongst others, in the field of dike reliability, sliding failure mechanisms, slope stability and residual dike strength.
- *Mark van der Krogt:* PhD researcher in the field of Hydraulic Structures and Flood Risk. With expertise, amongst others, in the field of geotechnical risk and reliability and deriving semi-probabilistic assessment rules.

Based on expert opinion, the influencing factors that affect the erosion resistance of slipped profiles were explored for a river dike with a clay layer.

The influence of wave overtopping on a slipped profile was found to be particularly interesting for entry points at which failure does not occur immediately. For example, in the case of a sliding entry point close to the outer slope, the probability of flooding would be almost equal to the sliding probability. Moreover, the failure probability in the event of slippage at the bottom of the inner slope is considered small. Failure between these entry points was indicated to be more likely due to the combination with wave overtopping. In this respect, the experts referred to a commonly held rule of thumb that the more the entry point is located towards the landside, the larger the residual strength after sliding will become. To which extent this would still be the case with wave overtopping could not be estimated.

In the case of a slipped profile, the experts stated that a cliff will likely form. The characteristics of the cliff after sliding are, however, unknown because the initial cliff height depends on multiple variables such as the slip circle, the degree of slipping and the dike composition. Many assumptions accompany knowledge regarding the development of a cliff. Given this uncertainty, it was expected that mainly the cliff height in combination with a certain steepness could severely influence the damage development by wave overtopping. Furthermore, the experts also expected that the quality of the soil layer could be affected at the point of entry.

Summarised the three experts expected that three factors have the most influence on the residual strength of wave overtopping which are investigated: (1) location of slipping, (2) impact from a cliff and (3) type of subsoil. The first two aspects are first addressed, after which the modelling approach for slipped profiles is provided, and model runs are presented for slipped profiles.

3.3.2. Location of slipped profile

Three relevant cases have been identified with the experts for which it is expected that wave overtopping in combination with a sliding profile may result in critical erosion. The cases are illustrated in Figure 3.3 and include a slipped profile in the middle of the crest, at the top of the slope and the middle of the slope. The three scenarios were worked out within D-stability using the profile of Millingen aan de Rijn using the soil characteristics listed in the report of Van den Ham et al. (2019). Based on the Uplift Spencer method, a failure probability was obtained by first calculating the slip circle with the lowest safety factor. Next, a failure probability was determined by performing a probabilistic calculation for a water level 1 m below the crest assuming an elevated phreatic line and a saturated dike composition. The slipped profiles are provided in Appendix C. Three slip circles are obtained which as listed in Table 3.2, are used for assessment of critical erosion.

Table 3.2: Entry point location of slipped dike profiles from the crest line along with the modelled of failure probability.

	Crest	**Upper slope**	**Middle slope**
Horizontal position from the start of the landward slope *x* [m]	-2.0	3.0	7.0

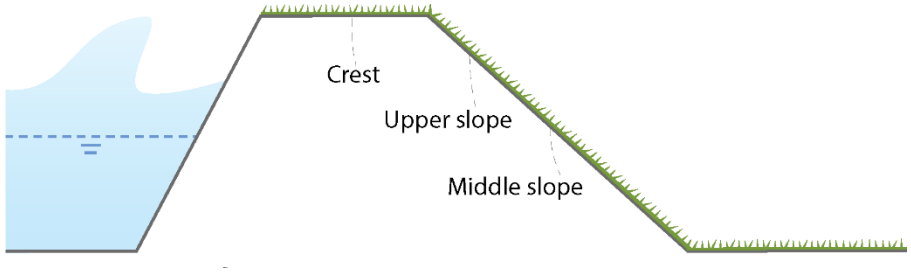

Figure 3.3: Schematic representation of the slipped dike profile scenarios with dashed lines indicating the evaluated slipped entry point locations for the crest, the upper slope section and the middle slope section.

3.3.3. Jet impact relation

Currently, when considering a constant turbulence parameter, the load in the erosion models is determined by the flow velocity leading to most erosion to occur at locations where the velocity is highest, especially at the inner dike toe. However, several experiments have indicated that failure at the cover does not occur solely at the inner toe, but also occurs much higher at the slope. In this case, another mechanism of jet impact is expected to cause cover failure. The jet impact can be approximated within the erosion models by applying a turbulence parameter ω. Yet the value of this factor is unknown and needs to be determined.

To determine a value for the extra load at a slipped profile, dike profiles that showed failure at the slope are investigated to calibrate the value of the turbulence parameter ω. For this purpose, failed dike profiles in Table 2.2 are subdivided into an upper slope section located at 1.3-2.8 m and a middle slope section located 6.5-6.6 m horizontally from the crest, respectively**.** From investigated test sections in Section 2.4, characteristics such as the critical velocities U_c [m/s], performed test conditions q and failure locations x [m] are used. Calibration is performed next as shown in Figure 3.4 for each dike slope to evaluate the turbulence parameter ω for the critical wave impact at the failure locations x [m] by varying the depth-averaged turbulence intensity with an interval value of 0.125 following Equation 5 (r_0 = 0.025). For this, the flow velocities U_i [m/s] of individual overtopping waves along an

evaluated profile are calculated for the performed overtopping events q [l/m/s]. Within the erosion model, flow velocities of overtopping waves at location x are combined with the section-specific threshold value U_c for erosion following COM experiments. Subsequently, a failure value is obtained by varying the turbulence factor until an erosion depth of 20 cm is reached. This process is repeated for the eight identified dike profiles of Section 2.4.

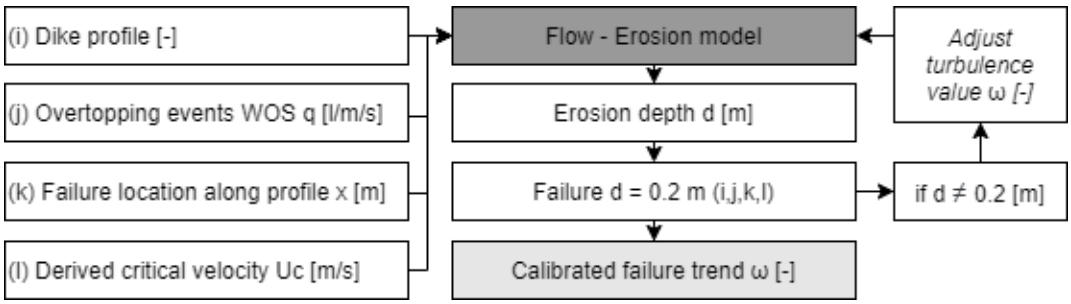

Figure 3.4: Overview with the iterative approach to determine the failure trend by jet impact for which failure is equated to an erosion depth of 20 cm.

Linear polynomial failure trends according to Equation 27 are obtained for the critical velocity and the turbulence parameter for both erosion models for the eight dike sections using the MATLAB Curve Fitting Tool. These relations indicate failure conditions for 20 cm erosion.

$$\omega(U_c) = aU_c + b \tag{27}$$

3.3.4. Modelling slipped profiles

A framework is derived to evaluate the erosion depth near a slipped dike profile. In this framework, an erosion depth is calculated for an increasing average overtopping discharge q for the three locations of slipping for a varying clay quality and grass quality in combination with the calibrated failure trend. This is performed with two erosion models at different entry points of a slipping profile. Failure is defined in cases where an erosion depth of 20 cm for the corresponding average wave overtopping discharge q is reached as shown in Figure 3.5.

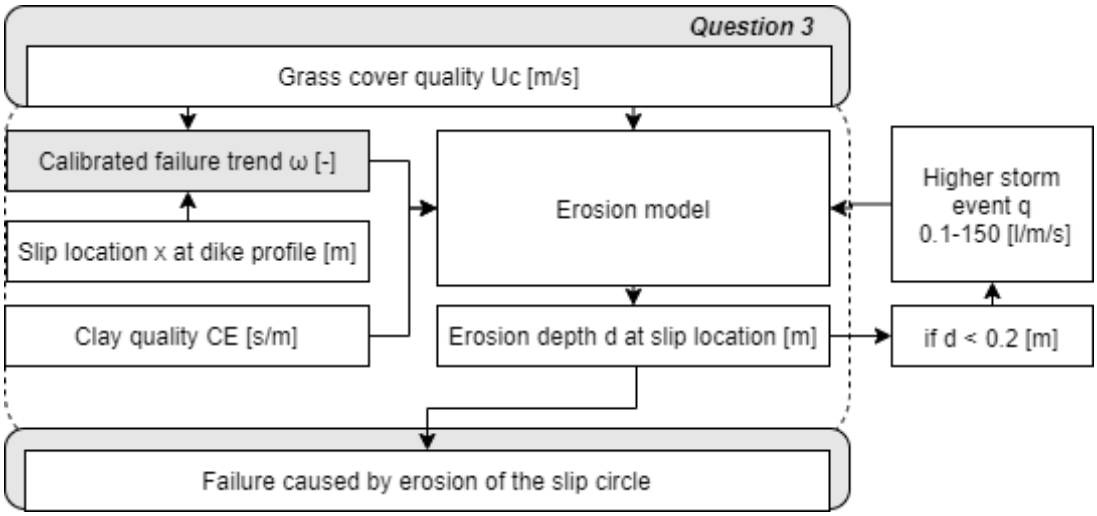

Figure 3.5: Overview with the developed iterative approach to determine failure caused by critical erosion of the slip circle.

3.3.5. Modelling scenarios for a slipped dike

The vulnerability of overtopping on slipped profiles is evaluated according to Figure 3.5, for which model runs are worked out. Parameters included for the model runs are the grass cover layer, clay quality and the wave characteristics. Applied scenarios for these parameters are listed below.

Grass cover quality

The experts expect that in the event of a slipping profile, the quality of the grass quality could locally decrease significantly. As an approximation of the grass quality, a wide range is evaluated based on the eight damaged dike sections. The following characteristic values for the critical velocity U_c are selected.

- Good: The threshold velocity for damage on the slope in Millingen is applied, evaluating the U_c value of 6.5 m/s (Hoffmans, 2015).
- Moderate: Some damage to the cover layer is applied, evaluating a 'moderate' scenario where the U_c value is 4.0 m/s (Aguilar Lopez et al., 2018).
- Poor: Substantial damage to the cover layer is applied, evaluating a 'very poor' cover layer for which the U_c value is 2.5 m/s (Hoffmans et al., 2008).

Clay quality

Regarding the clay quality, it is expected that the damage could be limited since the cover layer remains attached while local sagging occurs as can be seen in Figure 1.4a. It is also possible that the erosion process accelerates, as could be noticed from experiments at Tholen 3. The following scenarios are compared with each other to include an approximation of the turf layer:

- Average: no damage is applied to the clay layer, with an 'average' soil quality with a *CE* value of $2.0 \cdot 10^{-6}$ s/m (Verheij et al., 1995).
- Poor: some damage to the clay layer is applied, assuming a scenario where the *CE* value is $3.3 \cdot 10^{-6}$ s/m classified as 'poor' (Hoffmans et al., 2008).
- Very poor: substantial damage to the clay layer is applied, assuming a scenario where the *CE* value is $6.2 \cdot 10^{-6}$ s/m classified as 'very poor' (Hoffmans et al., 2008)

For the Hoffmans model, the above-listed adjustments to the *CE* parameter are made. The Transition model contains a depth-dependent *CE* value. For this model for the different scenarios as an approximation for poorer clay quality is obtained by modifying the clay cohesion factor (0.21) proportionally to the above-defined scenarios resulting in a cohesion factor of 0.21, 0.13 and 0.07 for average, poor and very poor clay quality, respectively.

Wave characteristics

Wave characteristics are also varied to evaluate how critical erosion could vary for different wave regimes. For each wave regime, a control list has been set up for a storm duration of 6 hours. The control list contains wave characteristics for an overtopping rate with an interval of 0.1 l/s/m for the range of 0.1 to 1 l/m/s and an interval of 1 l/m/s is used up to an overtopping discharge of 150 l/m/s. Wave regimes with three wave heights are compared following Van der Meer et al. (2015b):

- Low: The 'low' wave regime is characteristic of river dikes for which a wave height of 1 m is applied with a mean wave period T_m of 3.3 s.
- Average: The 'average' wave regime is characteristic of dikes along the Dutch coasts and estuaries for which a mean wave height of 2 m is applied with a wave period T_m of 4.7 s.
- High: The 'high' wave regime is characteristic of sea dikes for which a wave height of 3 m can be expected with a mean wave period T_m of 5.8 s.

With the above scenario, several slipped cases are evaluated for the dike profile of Millingen aan de Rijn. For the critical velocities of slipped profiles, values of 2.5, 4.0 and 6.5 m/s are used for a poor, moderate, and good grass cover quality, respectively. The turbulence parameter ω in both models is determined for every scenario for varying critical velocities U_c by using the derived trends. At the crest of the dike a similar turbulence factor is evaluated as for the upper slope section. A total of 18 scenarios are obtained for varying grass quality for a slipped profile. Each of the scenarios for slipped profiles of Table 3.3 is evaluated with a varying clay quality and for a varying wave regime. For the crest and upper slope section, the $-h_x$ scenario are evaluated with the turbulence trend at the upper slope section whereas the middle slope section $-m_x$ scenario are evaluated with the trends derived for this section.

Table 3.3: Slipped section scenarios for investigated erosion scenarios for the Hoffmans (Hoff) and Transition (TM_B) erosion models for a varying critical velocity U_c.

	Grass cover U_c					
Cover quality	**Poor**		**Moderate**		**Good**	
Erosion model	Hoff	TM_B	Hoff	TM_B	Hoff	TM_B
Crest; Upper slope section	Hh_p	TMh_p	Hh_{mod}	TMh_{mod}	Hh_g	TMh_g
Middle slope section	Hm_p	TMm_p	Hm_{mod}	TMm_{mod}	Hm_g	TMm_g

3.4 Probabilistic erosion failure

For the final sub-question, the objective is to gain insight into the failure probability for Millingen as an approximation of the erosion resistance of the (slipped) dike profile. To do so, the full framework, as shown in Figure 1.5 is used. Two proposed probabilistic methods have been identified and are used for approximation of the failure probability. Probabilistic models for ADIS and MCS methods are used from the OpenEarth open-source toolbox.

3.4.1. Probabilistic distributions

As an input to approximate the erosion resistance of the (slipped) dike profile of Millingen, the influence of wind speed during a 6-hour storm for two probabilistic parameters is used. From the dominant western wind direction, the Pareto wind statistics as addressed in Section 3.1.1. a lognormal distribution is applied to describe the uncertainty in the grass quality (Trung, 2014; e.g., Aguilar Lopez et al., 2018). For the critical velocities of slipped profiles, a value of 2.5, 4.0 and 6.5 m/s is used in Table 3.4 for a poor, moderate and good grass cover quality respectively. A coefficient of variation *CoV* of 0.3 is applied following the findings of Aguilar Lopez et al. (2018). Characteristics of these distributions are listed in Table 3.4.

Table 3.4: Stochastic random variables for the grass cover quality U_c (Trung, 2014; e.g., Aguilar Lopez et al., 2018)*, and the wind velocity* u_{10} *from the western wind direction* (Caires, 2009; Chbab, 2017).

		Grass cover U_c			**Wind u_{10}**
		Poor	**Moderate**	**Good**	**West**
Distribution	[-]	Log-norm	Log-norm	Log-norm	Exp-threshold
Mean	[m/s]	2.5	4	6.5	
CoV	[-]	0.3	0.3	0.3	
Mu	[-]	1.83	1.34	0.87	1.97

Distributions are converted to inverse functions to draw a value for the probabilistic analysis randomly. To convert the Pareto distributions of Caires (2009) an exponential distribution was used for which the wind direction-specific threshold value was later added. An impression of both functions is shown in Figure 3.6.

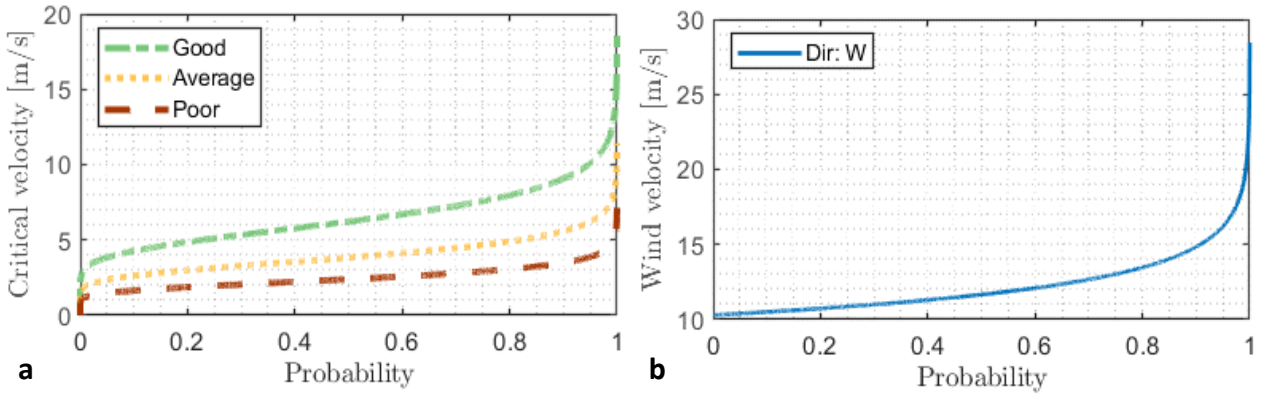

Figure 3.6: (a) Inverse functions obtained for the grass quality for a log normal distribution for a good, moderate and poor grass quality. (b) Inverse functions obtained for the wind speed for the dominant wind direction (west) for an exponential distribution.

3.4.2. Limit state

A limit state can be used to evaluate under which conditions a dike fails. For this evaluation, the limit state function (LSF) is used describing the difference (*Z*) between strength (*R*) and load (*S*): $Z = R - S$. Variables related to the strength and load can be composed of distributed variables. Variables taken into account for this function are the erosion depth of 20 cm (*R*) and the eroded erosion depth (*S*). As failure is regarded for $Z < 0$ conditions that cause an erosion depth of 20 cm result in 'failure'. The following limit state function is used for which d_{max} [m] consists of the maximum erosion depth along the profile given a condition for the water level *h*, the potential wind speed u_{10} and the critical velocity U_c:

$$Z = 0.2 - d_{max}(h, u_{10}, U_c) \tag{28}$$

3.4.3. Modelling scenarios

As the inner slope high up the slope proved to be the most vulnerable for critical erosion from Section 2.4, a slipped profile is evaluated at this location for which obtained turbulence parameters in Table 4.3 are used. Furthermore, a failure scenario is evaluated at the toe of the dike. For the first evaluation, moderate slipped profile scenarios for the Hoffmans model $Hh_{mod,}$ and the Transition model TMh_{mod} are compared. Subsequently, for the Hoffmans model, a poor Hh_p scenario representing failure at the transition is compared with failure by erosion at the dike toe $Htoe_g$. For the dike toe failure scenario $Htoe_g$, the Hoffmans model is compared as turbulence parameters are calibrated for this model at the dike toe. For mild slopes, a value for the turbulence parameter ω of 2.75 is used following Equation 5, corresponding to a depth-averaged turbulence intensity r_0 = 0.25 (Frankena, 2019)**.** For the critical velocity $U_{c,}$ a value of 6.5 m/s is used, which was derived for Millingen aan de Rijn (Hoffmans, 2015). As the calibrated values of Frankena are based on a velocity threshold U_t for the Hoffmans model, the critical flow velocity U_c is replaced by U_t of Equation 29.

$$U_t \approx 2.4 U_c \tag{29}$$

By using a probabilistic method, the probability of failure by overtopping at varying water levels is approximated for different clay qualities as listed in section 3.3.5. A fragility curve is next derived from the results. An overview of the evaluated cases is provided in Table 3.5.

Table 3.5: Scenarios for the Hoffmans (Hoff) and Transition (TM_B) erosion models for which the fragility curve are evaluated at the high slope dike section and for the approximation of erosion at the dike toe.

	Grass cover U_c			
Cover quality	**Poor**	**Moderate**		**Good**
Erosion model	Hoff	Hoff	TM_B	Hoff
Model run	Hh_p	Hh_{mod}	TMh_{mod}	$Htoe_g$

4 Results

This chapter covers the results for which the influence of wind on overtopping wave characteristics is evaluated in Section 4.1. Next, the erosion depth across the dike according to the Transition model and the Hoffmans model is determined in Section 4.2. Subsequently overtopping experiments are analysed from which a turbulence parameter trend is developed for both erosion models in Section 4.3. Based on this trend, critical wave overtopping conditions are derived for slipped profiles in Section 4.4. Critical overtopping conditions are next varied for a probabilistic analysis in Section 4.5.

4.1 Hydraulic load on the dike crest

4.1.1 Analysis of wave characteristics

By applying the wave overtopping approach, the wave period and wave height are examined from two wind directions to identify changes in wave characteristics near the dike. Wave characteristics are compared from the east-north-eastern (ENE) and west-north-western (WNW) wind directions with an effective fetch of 2739 m and 2810 m, respectively. For effectively equal fetch lengths and a riverbed height of 9.4 m + N.A.P. ENE and 9.9 m + N.A.P. WNW, more substantial wave characteristics from the eastern direction could initially be expected. Results in Table 4.1 indicate that the wave characteristics are most extreme from the WNW wind direction. Following the Bretschneider equations differences between significant wave heights from the WNW and ENE can only be caused by the effect of higher wind speeds from the western direction. Increasing wind speeds and water levels thus result in more extreme wave characteristics.

Table 4.1: Significant wave height Hs *and wave period* Ts *from the ENE and WNW direction for fixed return periods* T *of both the wind speed and the water level.*

	ENE		**WNW**	
	H_s [m]	T_s [s]	H_s [m]	T_s [s]
T = 1 yr	0.47	2.5	0.64	2.8
T = 10 yr	0.59	2.7	0.83	3.2
T = 100 yr	0.71	3.0	1.01	3.5
T = 1,000 yr	0.82	3.2	1.20	3.8

4.1.2 Hydraulic load distributions

The impact of varying wave characteristics on the overtopping wave volumes of the dike of Millingen aan de Rijn is shown next by varying the wind velocity for a fixed water level and subsequently by varying the water level at a fixed wind velocity (Figure 4.1).

First, from Figure 4.1 (a), it can be observed that for a low water level with a return period of 10 years, overtopping does not occur. Maximum overtopping volumes of 400 l/m result for a water level corresponding to a return period of 100 years. Secondly, from Figure 4.1 (b), it can be derived that the wind speed influences the wave overtopping considerably, e.g. a wind speed with a return period of 10-year results in a maximum overtopping volume of 200 l/m. Thirdly, what is apparent from both figures is that the number of overtopping waves varies for both evaluated figures. Finally, it is interesting to note that the maximum overtopping volumes illustrated by a dashed line in both Figure 4.1 differ around 500 l/m for similar return

periods while the number of overtopping waves is similar. This difference in the maximum wave volume is caused by the random sampling procedure of wave volumes as is addressed in Section 5.1 and has a relatively limited effect on the erosion depth within erosion models.

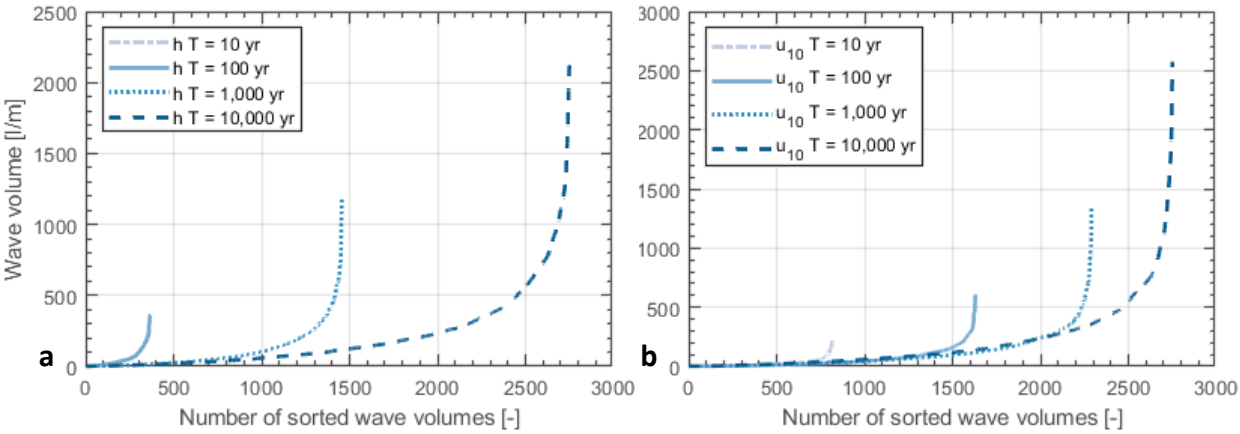

Figure 4.1: Overtopping wave characteristics from the NWN wind direction for (a) a varying water level h *with a fixed wind speed corresponding to a return period* T *of 10,000 year and (b) a varying wind speed* u_{10} *with a fixed water level corresponding to a return period* T *of 10,000 year.*

As can be seen in Table 4.1, extreme wave conditions for Millingen aan de Rijn largely correspond to a wave regime of 1 m in which the extreme wind conditions can result in a wave regime that approaches a wave regime of 2 m. What can be derived from the wave distributions is that the influence of wave conditions can significantly impact the overtopping discharge and the individual wave volume. The number of overtopping wave volumes is found to be larger for extreme fixed water levels than for a fixed extreme potential wind speed. Hydraulic load distributions of storms for which a small number of waves overtopped, as a result of a high freeboard height, included larger overtopping volumes.

4.2 Erosion across the dike

A brief sensitivity study is conducted to evaluate the different erosion depths that occur across the Millingen dike profile. First, this study locally evaluates from which wind direction the most erosion results for a return period of 1,000 years. Next, the development of the erosion depth is investigated by applying the dominant wind direction for a varying grass layer, outside slope gradient, clay layer and water level.

4.2.1 Dominant wind direction

The erosion depths across the Millingen dike profile, according to the Hoffmans erosion model, are presented in Figure 4.2. From Figure 4.2 (a), it can be observed that the erosion depth decreases as the water flows over the crest, which is caused by the deceleration of the overtopping waves. With the acceleration of the overtopping waves along the inner dike slope from a cross distance of 4 m, the erosion depth reaches a maximum erosion depth at the toe at a cross distance of 21.2 m. From this figure, it can be observed that a storm from the W and WNW wind directions induces the largest erosion depth of 28 cm for a T = 1,000-yr event. Figure 24 (b) shows that erosion depends on wind direction and the W and WNW direction are most dominant.

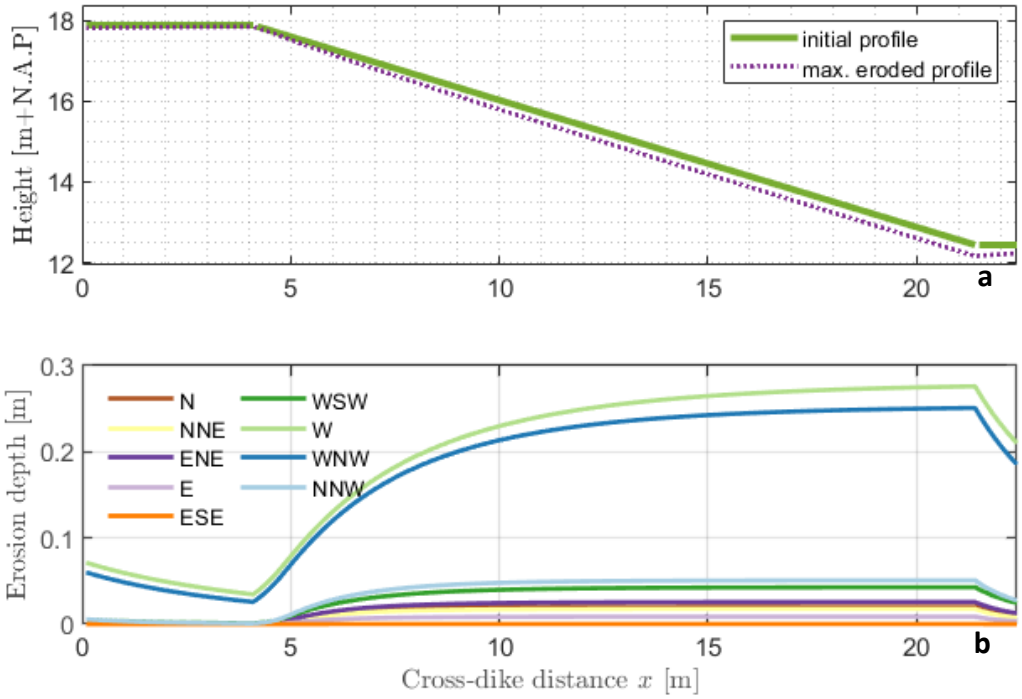

Figure 4.2: (a) The dike profile before and after erosion. (b) Erosion depth along the cross section of the Millingen dike profile, following from the Hoffmans erosion model for varying wind directions.

Additionally, for the Transition model, the westerly wind direction is to be the dominant wind direction from which the largest erosion depth results along the dike. Figure 4.3 (b) shows that significant erosion results only from wind directions of W and WNW. Storms from other directions result in an erosion depth of 0 cm. Erosion development is different for both evaluated cases. For case TM_A the erosion slowly develops onward from the 8 m cross distance whereas for case TM_B, steep erosion occurs from the 7.5 m cross distance.

More erosion occurs for case TM_B than for case TM_A. This is caused by the initial erosion threshold *CE* which is lower for case TM_B, resulting in increased erosion.

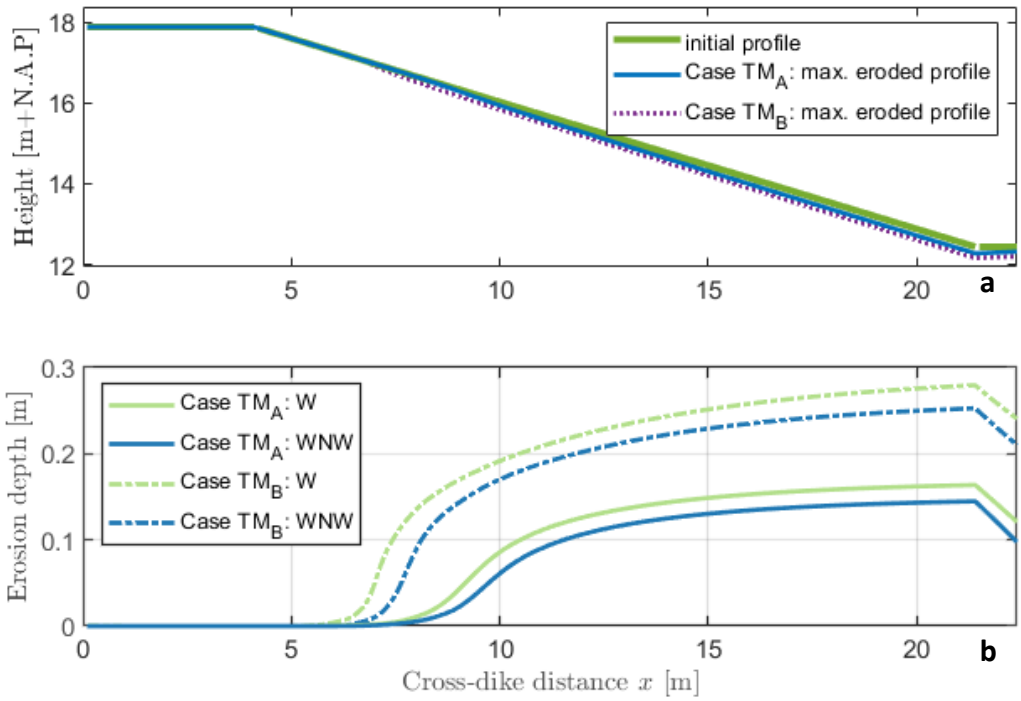

Figure 4.3: (a) The dike profile before and after erosion. (b) Erosion depth along the cross section of the Millingen dike profile, following from the Transition model for case TM_A (solid line) and case TM_B (dash-dotted line) for varying wind directions.

Wind speeds for varying return periods *T* are shown in Table 4.2. What can be observed from this is that the western wind speeds are considerably higher for equal return periods.

Table 4.2: Potential wind speeds u_{10} for a return period T for individual wind directions.

	Potential wind speed u_{10} [m/s]								
	N	**NNE**	**ENE**	**E**	**ESE**	**WSW**	**W**	**WNW**	**NNW**
T = 1,000-yr	17.4	17.4	18.3	17.6	15.8	29.3	28.9	26.1	20.1
T = 100-yr	14.8	14.8	15.6	15.0	15.8	24.6	24.1	21.7	17.1
T = 10-yr	12.3	12.3	12.9	12.4	15.8	20.0	19.2	17.4	14.1

From the above analysis, a significant difference can be observed among the erosion occurrences from various wind directions which were corrected for angle of incident waves. Erosion is thus expected to occur predominantly for storms from the westerly wind direction. From this direction, an erosion depth of 28 cm was obtained at the dike toe for both models for a T = 1,000-yr return period and 1 m freeboard. This is remarkable because, from this direction, the wind is significantly reduced by the angle of attack parameter of Equation 21. The wind speed thus has a much larger influence than the impact angle to the dike *β*, the mean bed level height or the fetch length *F* on the amount of overtopping and subsequent erosion. What can further be noticed is that the Transition model for case TM_A contains a higher threshold for erosion initiation. In terms of the maximum erosion depth, the Transition model for case TM_B shows the most similarity with the Hoffmans model for an equal return period. Moreover, for TM_B the point at which erosion initiates is more similar to results of the Hoffmans model. Because of this similarity, TM_B is evaluated for further analysis.

4.2.2 The sensitivity of the erosion models

This subsection identifies differences in erosion depths for both erosion models for varying parameters for the Hoffmans model (Figure 4.4). Interestingly, for the Hoffmans model, the location of the minimum and maximum erosion is identical for all runs. Also, a less steep outer slope gradient results in a large erosion depth of more than 1 m. The unlikely operation of erosion models to these depths is addressed in Section 5.2. Moreover, a varying clay layer significantly impacts the erosion depth development, whereas grass strength modelled by U_c has little influence for poorer quality. What also can be noted in Figure 4.4 (d) is that the erosion depth is highly dependent on the water level in the river. Presumably, both the outer slope and water level strongly affect the overtopping discharge q, causing parameters on the waterside of the dike to have a great influence on the erosion depth.

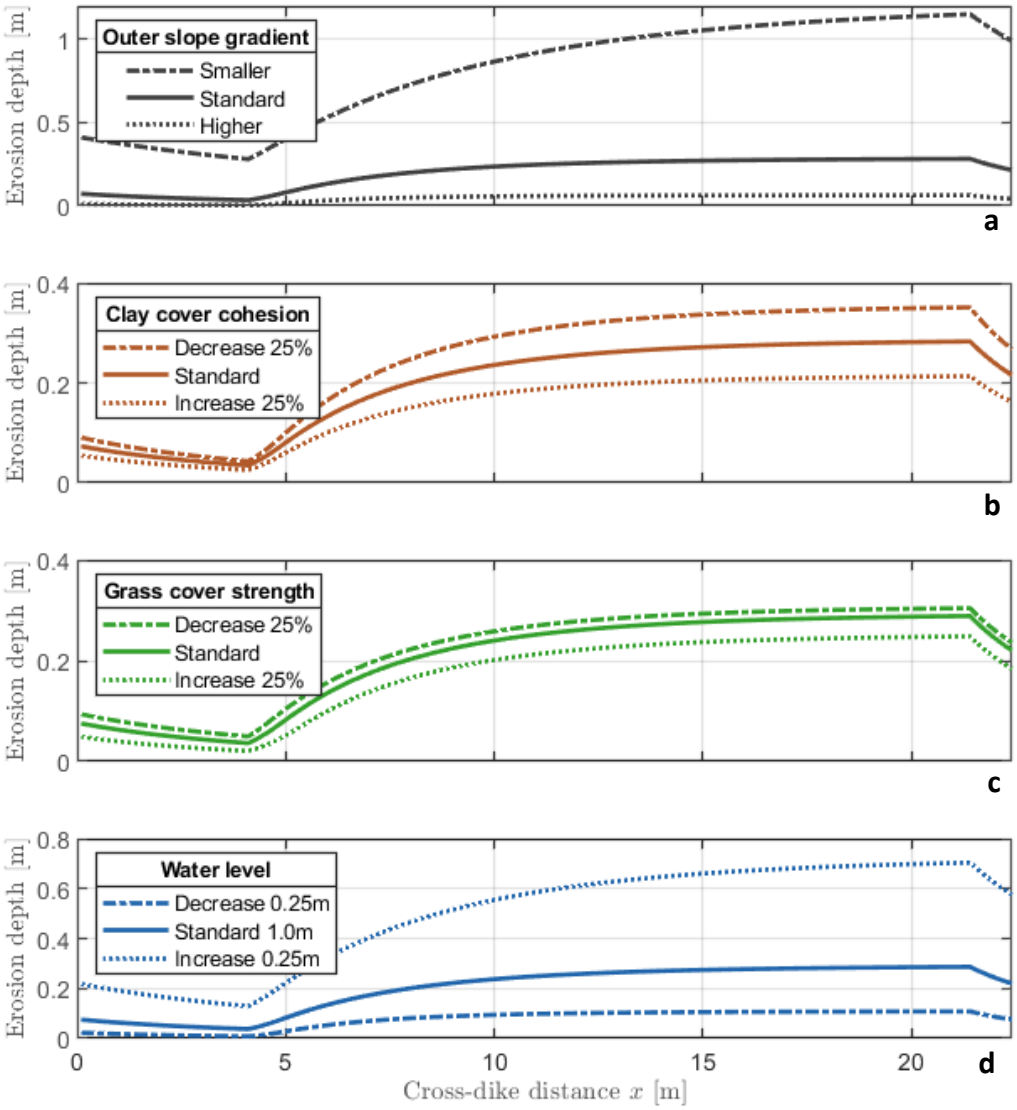

Figure 4.4: Erosion along the dike profile of Millingen aan de Rijn by considering the Hoffmans erosion model for a T = *1,000- yr storm from the westerly wind direction for a varying outer slope gradient, clay cover, grass cover and water level with values according to Table 3.1.*

A similar analysis of results for the Transition model in Figure 4.5 shows that the erosion depth is influenced significantly by a varying outer slope gradient and the water level. In addition, for the Transition model, it appears that the clay quality has the greatest influence on erosion, whereas the depth of erosion with regard to the grass quality mainly changes for a lower U_c

value. The varying model runs for grass strength and clay quality thus result in a similar type of erosive effect compared to the Hoffmans model. Remarkably, the cross-distance position along the profile where erosion occurs varies according to the water level and the outer slope gradient. This location also varies slightly according to changes in grass and clay quality which is caused by the local load that is lower than the strength of the dike profile.

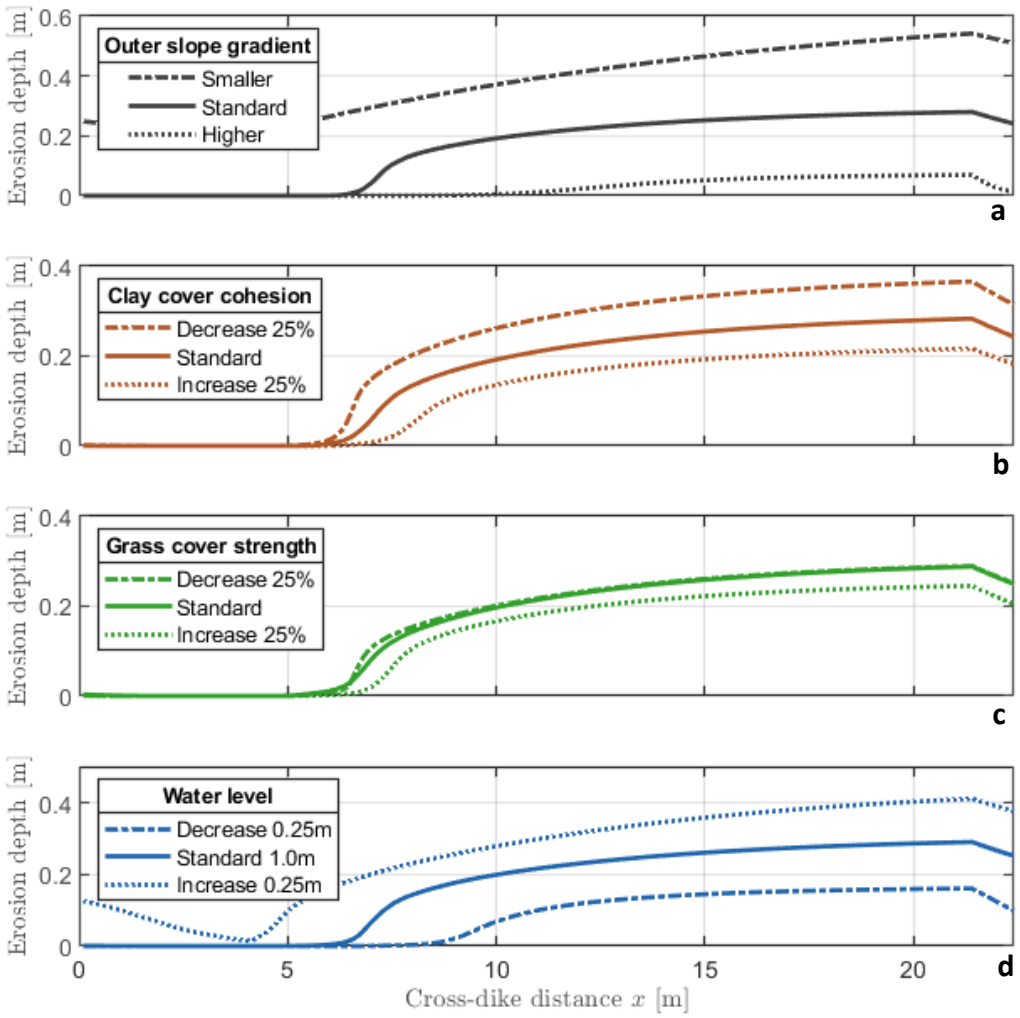

Figure 4.5: Erosion along the dike profile of Millingen aan de Rijn by considering the Transition erosion model for a T *= 1,000-yr storm from the westerly wind direction for a varying outer slope gradient, clay cover, grass cover and water level with values according to Table 3.1.*

Concluding first, this study confirms the findings of Section 4.1.1 regarding the impact of the wind direction. However, by evaluating all wind directions, the W wind direction rather than the WNW appears to result in the most extreme erosion conditions. Second, erosion depths for the Transition model for a constant *CE* as in case TM_B result in a larger erosion depth than the depth-dependent erosion model of case TM_A. Next, it can be observed that both models are most sensitive to dike conditions such as the water level and the outer slope. For calculating the erosion depth, the Transition model distinguishes itself from the Hoffmans model by (1) shifting the location of initial erosion and by (2) altering the contour of the erosion depth across the profile. Furthermore, results indicate that significantly different erosion conditions occur for both models at varying water levels.

4.3 Erosion at slipped sections

Local weaknesses and increased impact from jets are expected at the location of a slipped profile. To approximate the impact from jets trends for the turbulence parameter are derived in this section for failed profiles. In Section 4.4, these trends are used in combination with scenarios for weak profiles scenarios to determine which failure conditions for slipped dike profiles.

4.3.1 Relation between the turbulence and critical velocity

For the two erosion models, overtopping conditions that result in failure were obtained for a varying turbulence parameter ω and the critical flow velocity U_c. Erosion lines in Figure 4.6 and Figure 4.7 represent the critical failure conditions for which stars indicate the derived profile-specific critical velocity. It should be noted that, within the method framework, only the variation of the turbulence parameter was covered. As derived critical velocities may deviate towards slightly higher or lower values, it was also decided to vary the critical velocity to gain further insight into the functioning of both erosion models.

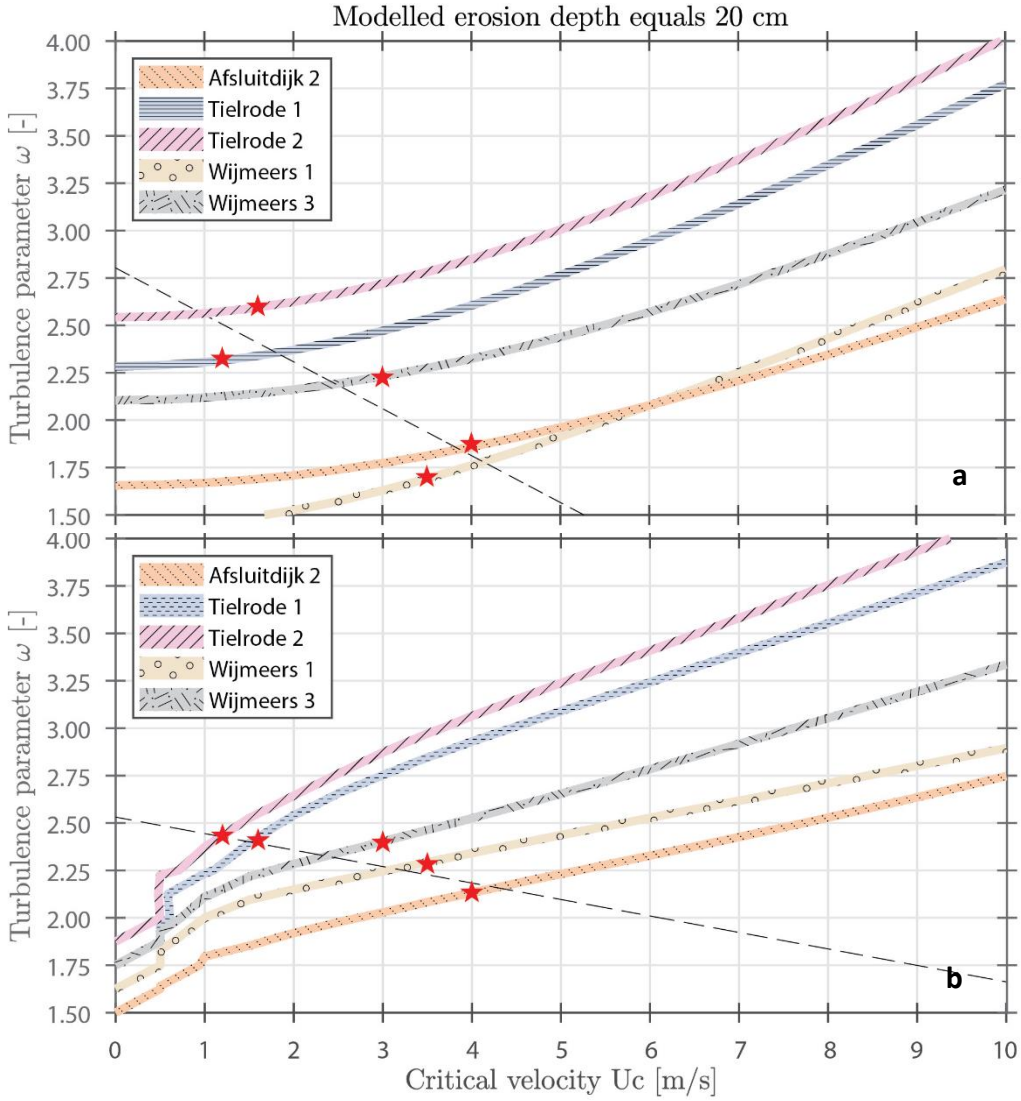

Figure 4.6: The turbulence parameter ω plotted as a function of the critical flow velocity U_c for a modelled erosion depth of 20 cm using the (a) Hoffmans model and (b) Transition model for the five case studies on the upper slope section. The red stars correspond to critical flow velocities of 1.2, 1.6, 3.0, 3.5 and 4.0 m/s. The fits (a): $\omega = -0.25U_c + 2.8$ (RMSE: 0.05) and (b): $\omega = -0.09U_c + 2.5$ (RMSE: 0.01) are indicated by a black dashed line.

4.3.2 Upper slope section

From the previous Figure 4.6, it can be observed that failure at Tielrodebroek occurs for the lowest critical velocities matching a turbulence parameter ω of between 2.3–2.6 for the Hoffmans model and between 2.40–2.45 for the Transition model. For the experiments Afsluitdijk 2 and Wijmeers 1, this value was found to be lower: between 1.7–1.9 for the Hoffmans model in a range of 2.3–2.1 for the Transition model, respectively. Regarding the erosion lines, the evolution for a varying U_c is very similar. This is caused by the similar structure of the erosion models in which a turbulence parameter is multiplied by the flow velocity of individual waves. Variation of the turbulence parameter is found to be lowest for the Hoffmans model in Figure 28 (a) for a varying critical velocity. Figure 28 (b) shows that erosion lines vary greatly for low critical velocities.

4.3.3 Middle slope section

Subsequently, critical erosion conditions for the middle slope section were obtained.

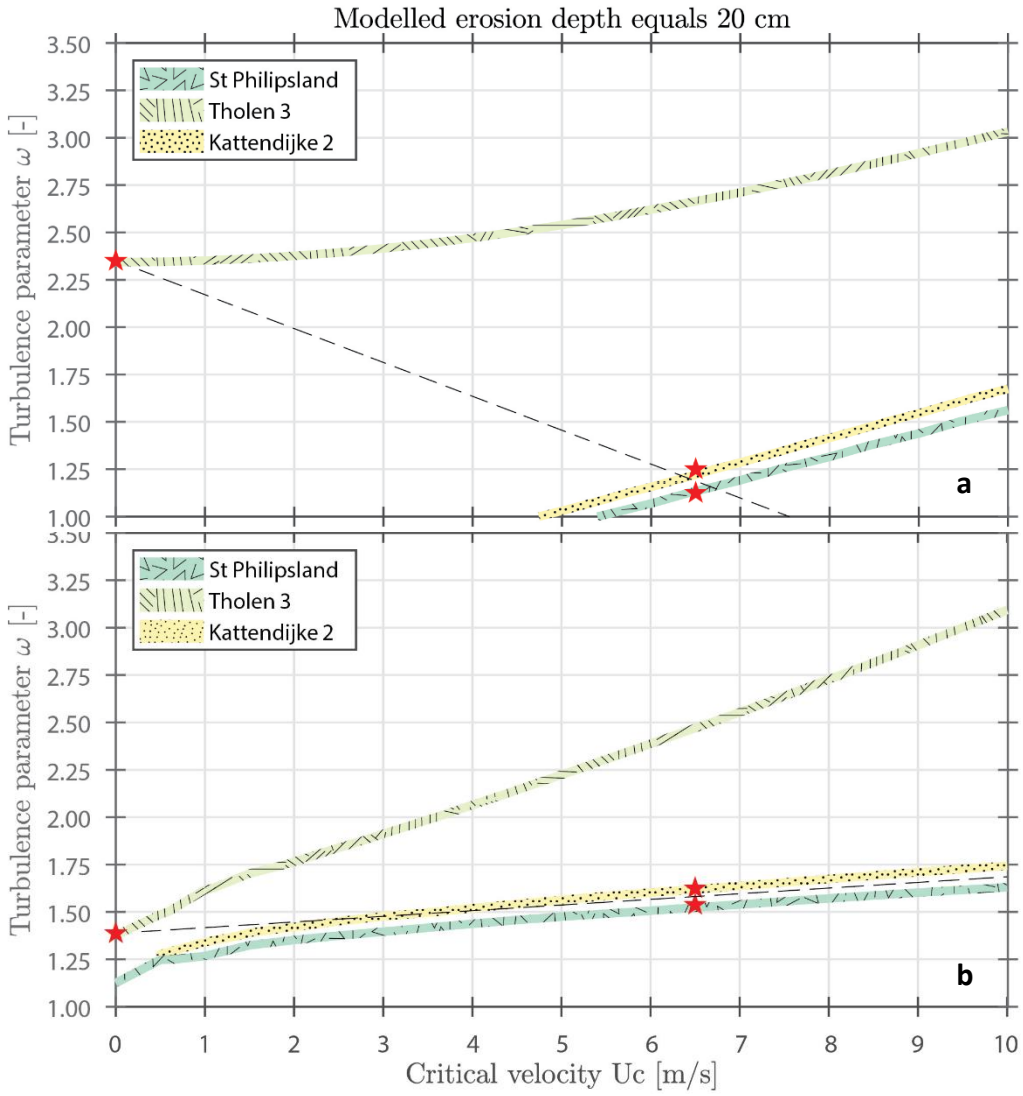

Figure 4.7: The turbulence parameter ω plotted as a function of the critical flow velocity U_c for a modelled erosion depth of 20 cm using the (a) Hoffmans model and (b) Transition model for the three case studies on the middle slope section. The red stars correspond to critical flow velocities of 0 and 6.5 m/s. The fits (a): $\omega = -0.18U_c + 2.35$ (RMSE: 0.02) and (b): $\omega = 0.03U_c + 1.4$ (RMSE: 0.01) are indicated by a black dashed line.

From Figure 4.7, first, a difference between the Hoffmans and Transition models can be noticed for Tholen 3. Here a turbulence parameter of 2.3 was obtained from the Hoffmans model versus a value of 1.4 from the Transition model. Second, a small influence of the turbulence parameter as a calibration parameter was obtained for the dike sections with a higher critical flow velocity: Kattendijke 2 and St Philipsland. For these locations, accelerated flow velocities within the Hoffmans model are expected to result in a turbulence parameter of 1.15–1.25. Interestingly, the erosion lines of Figure 4.7 (a) and (b) are very distinctive. For the Hoffmans model, a trend is observed similar to the upper slope section of Figure 29 (a). For the Transition model, a constant value was found which suggests that because of the highly variable erosion initiation location and varying contour depth across the profile a good approximation of the turbulence parameter ω can be obtained Section 4.2. The extent to which approximation for the Transition model is accurate cannot be assessed from the limited number of experiments.

Trend lines can next be evaluated from the analysed sections. At the upper dike section following Figure 4.6, turbulence conditions for which failure occurs show a low variability for the Hoffmans erosion model around the calibrated critical velocities (except for Wijmeers 1). However, the turbulence values for the Transition model tend to be located near each other and are less dependent on the critical flow velocity. At the middle slope section of Figure 4.7, erosion trends from the Transition model indicate that there is little variation in the turbulence parameter for a varying grass quality. For the Hoffmans model, the trend at the middle slope section is similar with the trend for the upper slope section.

From the analysis performed, differences emerged between the two applied erosion models in combination with the flow equations. The above analysis shows that for values with a low critical flow velocity close to the crest, a high turbulence value is necessary to simulate observed failure with existing erosion models. As the failure location shifts to the middle of a dike slope, this turbulence factor decreases significantly from 2.3 to 1.4 for the Hoffmans model and is close to 1.5 within the Transition model. These findings on collected failure cases demonstrate two points. First, analytical models can be used to describe the erosive load of the inner dike slope. Second, erosion mechanisms such as jet erosion can become the dominant failure mechanism, which one can include in erosion models through a turbulence parameter which can be quantified by a trend in relation to the critical flow velocity.

Derived relationships for the turbulence parameter and the critical velocity are subsequently used to derive turbulence values for the scenarios of Table 3.3. Values for these scenarios are shown in Table 4.3.

Table 4.3: Turbulence parameters ω derived from obtained fits for the Hoffmans (Hoff) and Transition (TM_B) erosion models derived for a varying critical velocity U_c of 2.5, 4 and 6.5 m/s for a poor, moderate and good cover quality respectively.

	Grass cover U_c					
Cover quality	**Poor**		**Moderate**		**Good**	
Erosion model	Hoff	TM_B	Hoff	TM_B	Hoff	TM_B
Crest; Upper slope section	2.2	2.3	1.8	2.2	1.2	2.0
Middle slope section	1.9	1.5	1.6	1.5	1.2	1.5

4.4 Slipped dike scenario

Overtopping conditions that result in >20 cm erosion depth are next calculated across the dike profile of Millingen aan de Rijn. Factors that are considered for this analysis are the slipped profile location, the clay quality, the grass cover quality, and the jet impact approximated with the turbulence parameters of Table 4.3. For each of these factors, a series of scenarios has been created, which is now evaluated. First, overtopping conditions are identified for a wave regime of 2 m. Next, failure conditions are compared with the wave regimes of 1 m and 3 m.

4.4.1 Failure conditions for a slipped section

According to the Hoffmans model in Figure 4.8, the lowest overtopping discharges that result in erosion occur in the inner middle and inner high positions of the dike slope. From these results, it can be noted that a good grass cover quality of Hh_g and Hm_g (with a high critical velocity) in combination with a poor clay layer is more erosion-resistant than a poor grass cover quality Hh_p and Hm_p in combination with the best considered clay layer. This is because for a poor cover layer, failure along the slope occurs for conditions between 3–9 l/m/s. In contrast, for a moderate cover layer Hh_{mod} and Hm_{mod}, failure occurs for conditions between 5–14 l/m/s and 5–16 l/m/s at the inner high and inner middle slipped locations, respectively. The crest appears to be less vulnerable with critical wave overtopping conditions of 6–17 l/m/s for a poor cover layer Hh_p and 13–32 l/m/s for a moderate cover layer Hh_{mod}. Furthermore, it is notable that the resistance of a good grass cover for Hh_g and Hm_g is expected to exceed overtopping conditions of 36 l/m/s.

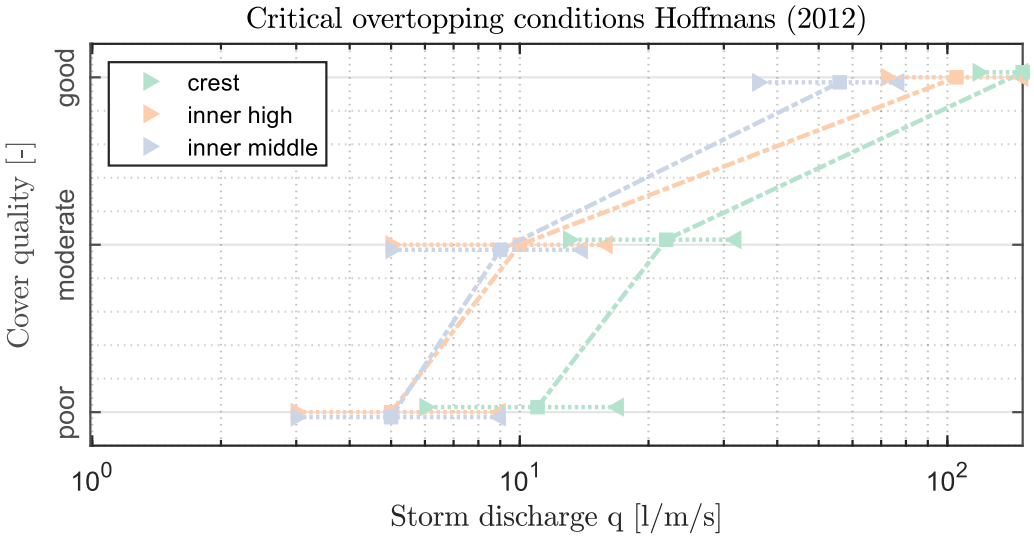

Figure 4.8: Storm discharges for a wave regime of 2 m, following the Hoffmans model, that result in failure for a varying grass quality for three slipped dike profile entry locations for a varying clay quality (on the horizontal range) that indicates a very poor >, poor (square) and average < clay layer.

From the results of the Transition model in Figure 4.9, failure first occurs at the inner high position of the dike. At this location, failure occurs following TMh_p for an overtopping discharge of 2 l/m/s for both a poor and a very poor clay layer and 7 l/m/s for a good clay layer. A moderate grass cover TMh_{mod} collapses at the same location for an overtopping discharge of between 4–13 l/m/s. What is also notable is that, according to the Transition model, the crest which is modelled with $TMh_{p;mod;g}$ is more vulnerable to wave overtopping than the inner middle position of the dike $TMm_{p;mod;g}$. The reason for this may be the turbulence parameter which was relatively high for the Hoffmans model and was found to be constant and lower for the Transition model. Furthermore, a good grass cover fails for an overtopping discharge of >12 l/m/s.

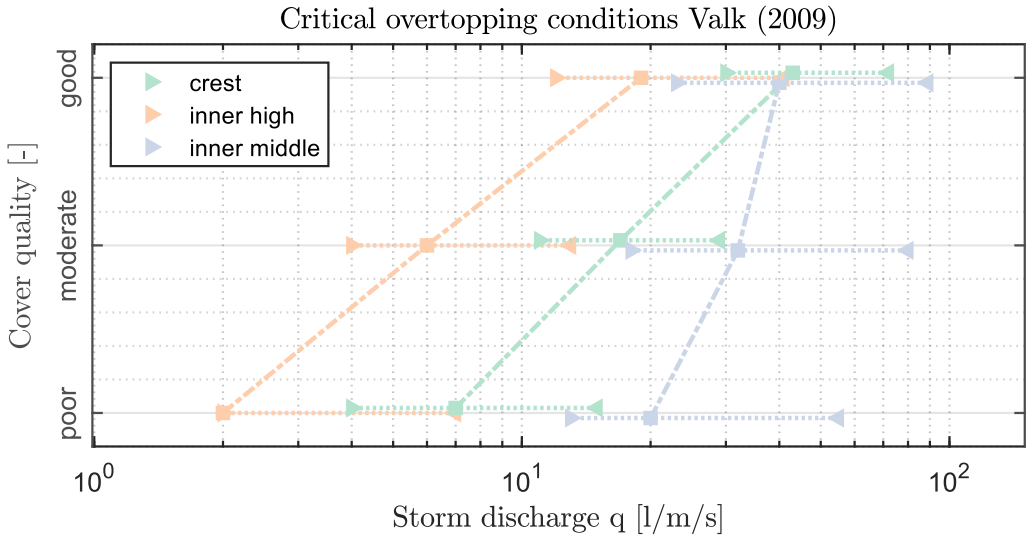

Figure 4.9: Storm discharges for a wave regime of 2 m, following the Transition model, that result in failure for a varying grass quality for three slipped dike profile entry locations for a varying clay quality (on the horizontal range) that indicates a very poor >, poor (square) and average < clay layer.

4.4.2 Varying wave regime for a slipped section

In addition to variability in the clay layer, the variability for different wave heights has been evaluated. Figure 4.10 shows the failure conditions for the Hoffmans model for which larger wave heights of 3 m fail for lower overtopping conditions at the dike crest. Remarkably, no shifts to lower average discharge limits for moderate and poor grass covers of inner high $Hh_{p;mod}$ and inner middle $Hm_{p;mod}$ locations are noticed. Changes in critical overtopping conditions vary, especially for a good grass cover following Hh_g and Hm_g. Results indicate that varying wave heights do not significantly increase the vulnerability of the dike profiles for very poor and moderate grass cover quality.

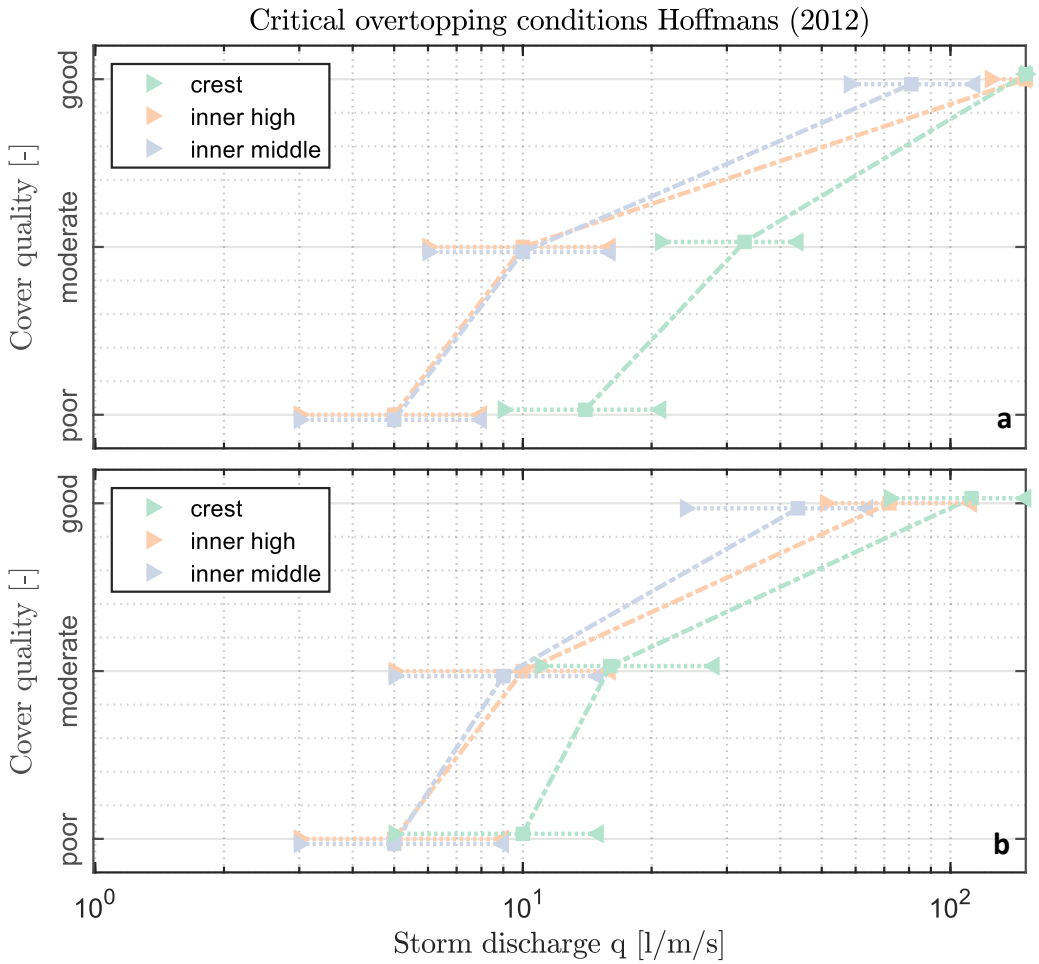

Figure 4.10: Storm discharges for a wave regime of (a) 1 m and (b) 3 m, following the Hoffmans model, that result in failure for a varying grass quality for three slipped dike profile entry locations for a varying clay quality (on the horizontal range) that indicate a very poor >, poor (square) and average < clay layer.

Next, the effect of varying wave heights for the Transition model was evaluated. From Figure 4.11, considerable changes in the lower overtopping limits can be noticed. For a wave height of 3 m, it can be seen that critical discharges for all evaluated scenarios shift to lower overtopping conditions. For this wave height, a poor cover quality of TMh_p fails for an overtopping discharge of between 0.9–3.0 l/m/s, which is considerably lower than for a regime with a 2-m wave height. In general, dike covers become more vulnerable, and failure occurs at lower overtopping discharges. Understandably, lower wave heights of 1 m result in

higher threshold limits for critical overtopping conditions which can be observed in Figure 4.11b.

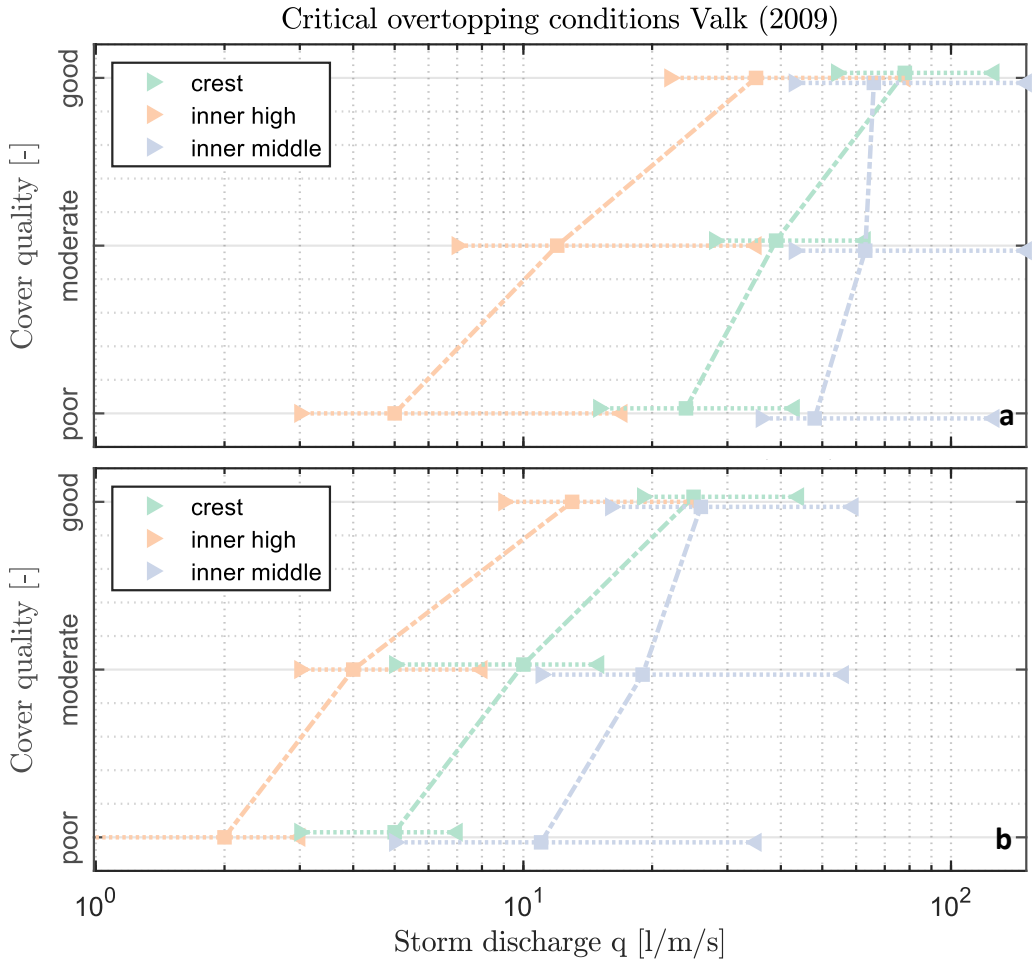

Figure 4.11: Storm discharges for a wave regime of (a) 1 m and (b) 3 m, following the Transition model, that result in failure for a varying grass quality for three slipped dike profile entry locations for a varying clay quality (on the horizontal range) that indicate a very poor >, poor (square) and average < clay layer.

Regarding the results of critical overtopping discharges a semi-logarithmic x-axis has was used to highlight the lower overtopping discharges. This axis does not show well that according to the Hoffmans, a good grass cover does not collapse for high overtopping conditions exceeding 150 l/m/s. Besides, it is notable that the horizontal bandwidths for a varying clay quality within this Transition model are much wider than for the Hoffmans model. Results of this analysis also show that the inner high $TMh_{p;mod;g}$ (Valk) and inner middle $Hh_{p;mod;g}$ (Hoffmans) erosion locations are expected to collapse most quickly because of wave overtopping. The Hoffmans model indicates failure for almost comparable conditions at the inner middle location Hm_x of a slipped profile. Moreover, the above trends for the Hoffmans model indicate that conditions for poor cover qualities remain similar for varying wave regimes. These conditions vary significantly for the Transition model for varying wave regimes.

4.5 Probabilistic analyses

For the probabilistic analysis, a comparison between ADIS and MCS was first carried out in Appendix D. From this analysis it followed that MCS was found to be an applicable method to derive a fragility curve for slipped dike profiles whereas, in comparison to this method ADIS was not able to assess the failure probability at increasing freeboards.

4.5.1 Derivation of fragility curves

Scenarios for Hh_{mod} and TMh_{mod} of Table 3.5 (also listed in Table 3.3) were next evaluated with the MCS method. In Figure 4.12, two fragility curves are obtained for a slipped plane that illustrate critical erosion failure probabilities from the dominant west wind direction. Fragility curves of Figure 4.12 (a) and (b) show that the risk of failure by overtopping, according to the Hoffmans model, is higher than according to the Transition model for a decreasing water level (increasing free crest height). Additionally, the failure probability of critical wave overtopping varies considerably for varying clay quality. From Figure 4.12, it can be noticed that the relative variation between failure probabilities for different types of clay is smaller for the Hoffmans model than for the Transition model. Slipped dike scenarios less frequently fail for the Transition model (TMh_{mod}) than for the Hoffmans model (Hh_{mod}). Moreover, failure ranges between scenarios are wider for the Transition model, which corresponds with the broad ranges observed in Section 4.4.2.

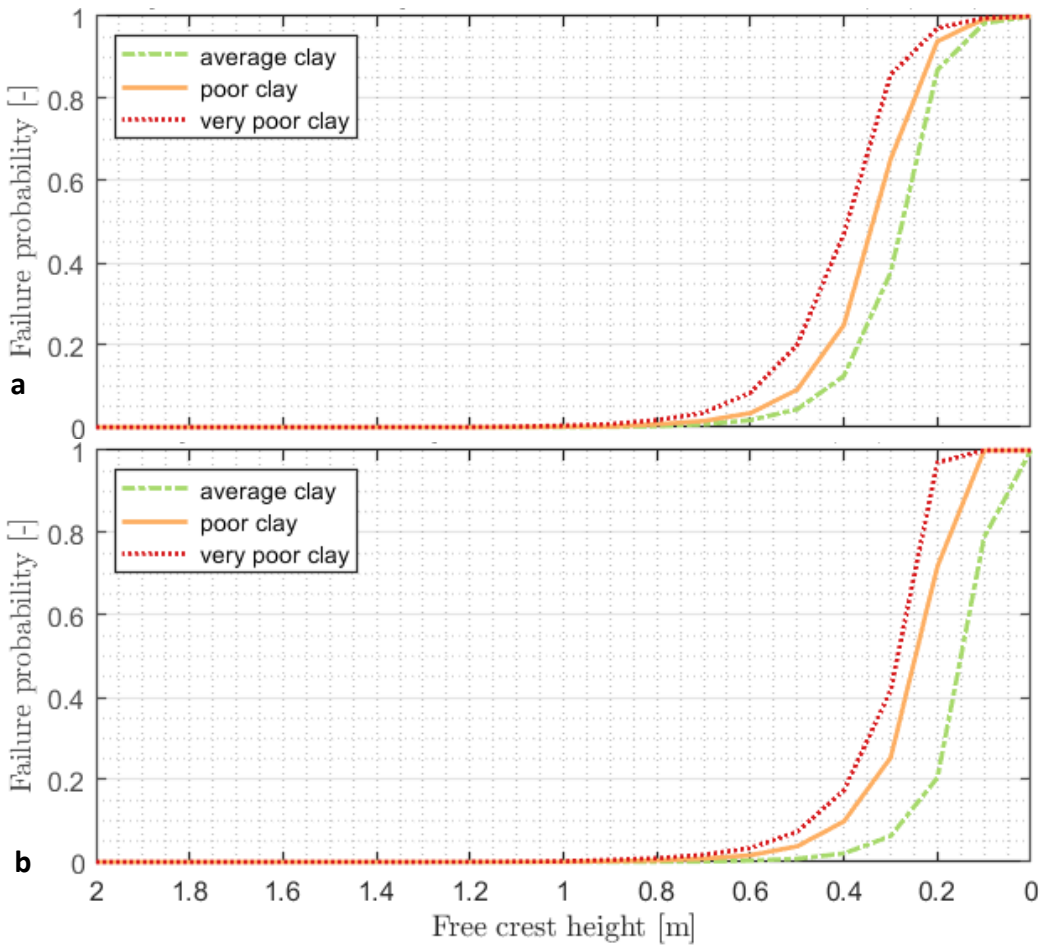

Figure 4.12: Fragility curve for a slipped dike profile at the upper slope near Millingen from (a) the Hoffmans model and (b) the Transition model following a MCS analysis with critical wave overtopping conditions that resulted in 20 cm erosion (failure) for three clay layer types.

4.5.2 Comparing fragility curves

The failure probabilities of critical wave overtopping are now compared for the poor slipped profiles (Hh_p) and for erosion at the dike toe ($Htoe_g$). The four fragility curves are shown in Figure 4.13. From this figure, it is noticeable that erosion for slipped profiles for an average, poor and very poor clay cover occur more quickly than at the dike toe. Additionally, the Hoffmans scenarios for a critical flow velocity of 4.0 m/s in Figure 4.12 show high failure.

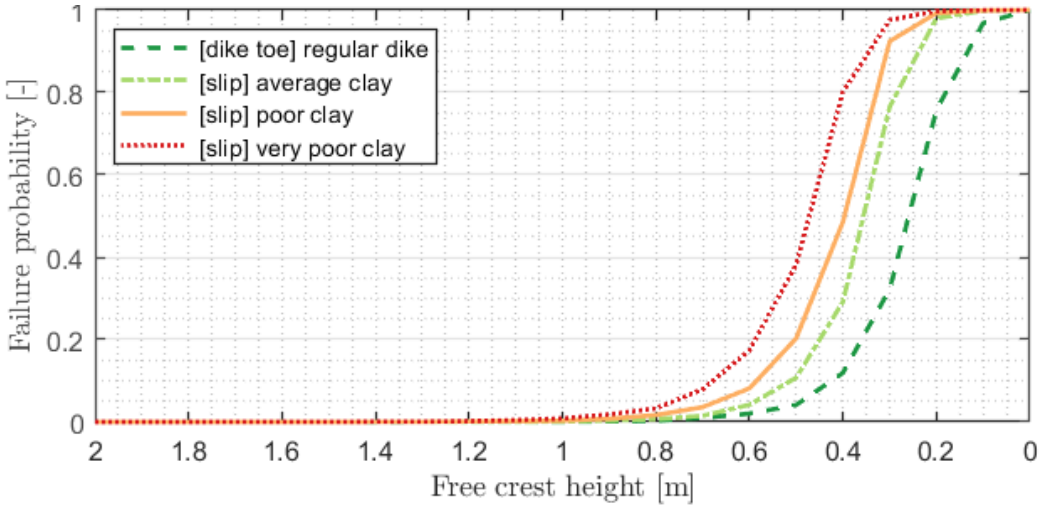

Figure 4.13: Fragility curve from the Hoffmans model for (I) failure by erosion at the dike toe indicated by good clay with a critical velocity U_c of 6.5 m/s and turbulence parameter ω = 2.75 [-] and (II) for a slipped dike profile at the upper slope for three clay layer types with a critical velocity U_c of 2.5 m/s, following wave overtopping conditions that resulted in 20 cm erosion.

By dividing the fragility curves of a slipped profile (Hh_p) of Figure 4.13 by the fragility curve of failure at the dike toe ($Htoe_g$), the extent to which a dike fails more often given a certain water level is obtained (Figure 4.14). Only values are presented up to 0.8 m freeboard as to this height the failure probabilities can be estimated at a 95% confidence interval with a 20% error which was considered acceptable. From this figure, it can be derived that differences between failure frequencies increase gradually for an increasing free crest height. Failure for a slipped profile with an average clay quality is about twice as common as erosion failure at the dike toe, whereas slipped profiles with a poor clay or very poor clay profiles appear to fail five times or ten times as often as erosion failure at the dike toe.

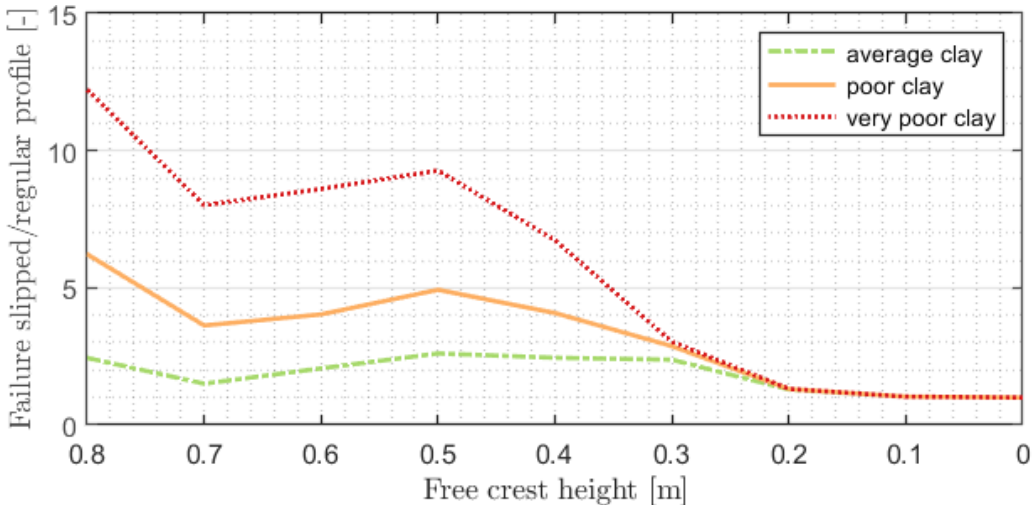

Figure 4.14: Failure occurrence: probability for a slipped profile in relation to the failure probability of critical erosion at the dike toe. Dike toe with a critical velocity U_c of 6.5 m/s and turbulence parameter ω = 2.75 [-] and for a slipped dike profile at the upper slope for three clay layer types with a critical velocity U_c of 2.5 m/s.

5 Discussion

For each sub-question, this chapter discusses the outcomes by reviewing the results and addressing key assumptions after which limitations, implications and suggestions are provided.

5.1 Hydraulic parameters

For the first sub-question, the goal is to identify which wave volumes can be expected to overtop at the Millingen aan de Rijn dike.

Wave formation

The overtopping conditions used in this study were dependent on the wave conditions that were determined by the Bretschneider equations. First, the results of these equations depend on the mean bed level height and the fetch length for which values are conditionally converted from 16 to 12 wind directions, which causes a small transformation error. Second, calculations were performed for the highest load on the dike within each 30° wind direction. Due to this assumption, the reduction factor γ_β of the wind can be overestimated by up to 9.9% following Equation 21, which is considered acceptable for this study. Third, an essential input for Bretschneider is the wind speed based on extreme wind statistics (Caires, 2009). From these statistics, 95% confidence ranges for wind speeds were not considered. Following sigma ranges of Chbab, both increased and decreased wind speeds of 8–10% for T > 1,000-yr return periods can be expected as a result (2017). Moreover, other processes can impact the degree of wave overtopping. These processes include, for example, the local skewness caused within river curves or the influence of longitudinal winds (Ministerie van Verkeer en Waterstaat, 2007). These processes are expected to result in increased overtopping but were not considered within the framework of this thesis. The applied Bretschneider-based approach is considered accurate if the wave conditions at the toe of the dike are dominated by wind growth, as for narrow waters such as rivers (Van Velzen et al., 2007) By these changes this approach is new in comparison to previous research in which erosion calculations were performed at fixed boundary conditions (as performed by Aguilar Lopez et al. 2018).

Storm approximation

An overtopping wave formula for EurOtop 2007 was considered to evaluate the average overtopping discharge. This formula may overestimate the extreme conditions compared to a more recent equation for which a slightly curved line on a log-linear graph is obtained instead of a straight line (EurOtop, 2018). Moreover, to derive the overtopping conditions, a 6-hour storm period is used for derivation of hydraulic conditions which is similar to methods used by Schuttrumpf et al. (2007) and Van der Meer et al. (2010). These studies have demonstrated that a 6-hour overtopping condition with constant for the significant wave height H_s and the spectral wave period $T_{m-1.0}$ can be used to replicate wave overtopping conditions during a storm with varying H_s and $T_{m-1.0}$. Even though this duration period may not be reflective of an actual storm period during a highwater event, the selected 6-hour storm period is regarded as the most accepted approximation for evaluation of the residual strength of a dike.

Moreover, as was summarised in the results from Section 5.1, a variety of maximum wave overtopping volumes may result during the storm for similar conditions because of the random sampling process. Results from Sections 4.2 through 4.4 were not affected significantly by this process because calculations were initiated with a random seed. For the probabilistic analysis in Section 4.5, it is expected that this random sampling process would result in the limit state not following an exact straight line. This is also noticeable in a zoom-in of the MCS analysis in Figure 5.1 (a). From this, it can be noticed that a dike fails one time under certain conditions while this does not happen for a higher wind speed.

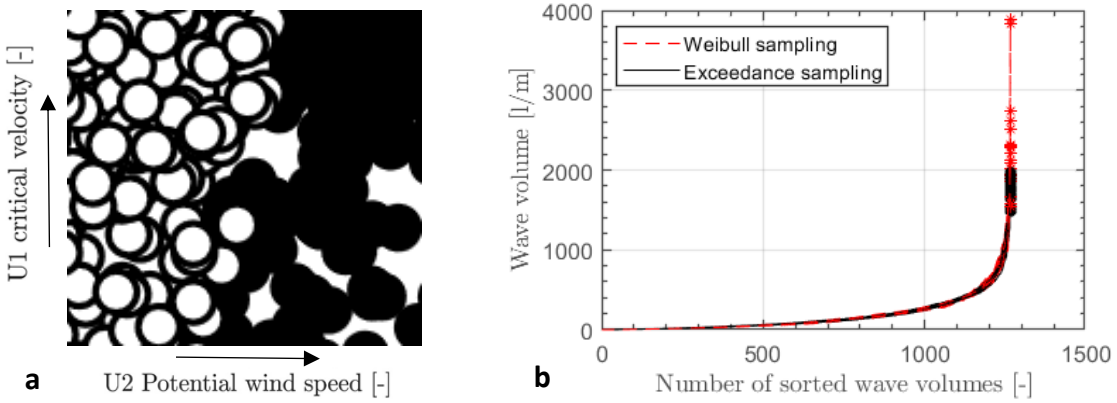

Figure 5.1: (a) Zoom-in of MCS of Appendix D with failure (white) and non-failure (black). (b) Sorted overtopping volumes resulting for Weibull sampling with maximum overtopping (red stars) and for exceedance sampling (black dots).

In addition, the used exceedance volume sampling method developed by Frankena (2019) was compared with the Weibull sampling method included in the report of Valk (2009). In Figure 5.1 (b), it can be observed that the deviations of the maximum wave volume, based on the exceedance sampling method for an evaluation of 20 storms, are limited compared to the deviations that are obtained with the Weibull sampling of storms. This small variation in maximum overtopping waves is expected to correspond with the natural process of wave overtopping in which extreme overtopping volumes will vary. To put this into perspective, differences in maximum erosion depths for a single wave volume of 2,000 l/m compared to 1,500 l/m result in 1.3 mm and 1.0 mm of erosion for the Hoffmans model following the parameters used in Figure 4.2 In comparison, approximately 9.0 mm and 5.9 mm of erosion occurs in the depth-dependent TM_B model following parameters used in Figure 4.3. As a result, the erosion depths, calculated according to the considered exceedance sampling method, result in smaller differences in the modelled erosion depth than the Weibull sampling method; this causes erosion depths to be more similar for identical wave conditions. The adjusted sampling method, as implemented within this study can thus be applied effectively for a model comparison or design study.

5.2 Model assessment

For the second sub-question, the goal is to obtain insight into the functioning of the transition and Hoffmans erosion models for varying parameter values.

Flow approximation

Simulations were performed by using the physics-based analytical acceleration method for overtopping waves across the dike profile (Van Bergeijk et al., 2019b). Flow parameters were assumed to be consistent with those of Van Bergeijk et al. (2019a) in which overflowing wave volumes are linked to initial flow velocities and water depths at the start of the dike crest. Model calculations were performed for a geometric dike interval of 10 cm, which are calculated using analytical formulae and are therefore not sensitive to intervals (Van Bergeijk et al., 2019b). Regarding flow parameters, multiple relationships for wave overtopping exist, and these relationships are expected to vary because of, for example, varying wave regime or dike geometry. Water could also run across the dike from a different angle and take a different course. Moreover, the interaction between flow and erosion was not considered along the dike in this study. On the dike, for example, the current may alter with the formation of a hole or a puddle, causing a thin layer of water to reduce shear stresses (Bomers et al., 2018)**.** Furthermore, cracks and deformations that could occur as a result of slipped profiles were not taken into account (Van Hoven et al., 2014). Advanced models such as the CFD model of Bomers et al. (2018) and Van Bergeijk et al. (2020) are required for such calculations. These models are computationally costly and time-consuming compared to this thesis's approach and are consequently not useful for the derivation of failure probabilities. To offer a solution to this, Aguilar Lopez et al. (2018) showed the advantages of calculating erosion depth and failure probabilities by using an emulator. A disadvantage of this method is that failure probabilities are derived from a black-box approximation. This thesis evaluated the erosion depth by including flow equations and the influence of a turbulence parameter by not considering the evolution of the profile depth in time. As a result, this research positions itself between a COM approach in which the interaction between flow and geometry is excluded and a sophisticated CFD approach which cannot be used to derive failure probabilities.

Erosion Models

The erosion simulations of both the Hoffmans and Transition model are subject to uncertainties. Although as described in Section 2.2, both models are based on scouring erosion mechanisms in which the actual erosion (jet) mechanism is simplified, models based on scouring have demonstrated that there is a similarity between observed erosion depths during experiments (Valk, 2009; Bomers et al., 2018; Frankena, 2019; Van Bergeijk et al., 2019a). An essential assumption in these erosion models is that scouring occurs continuously throughout an overtopping period T_0, which is dependent on the overtopping volume. This linearity during an overtopping wave is expected to slightly overestimate actual critical shear stresses during the period when erosion occurs (Hoffmans, 2012; Aguilar Lopez et al., 2018)**.**

For the Transition model, site-specific measurements of Millingen have been used. Following initial model runs, the TM_B model was used instead of the TM_A model. Maximum erosion depths obtained by the TM_B model (with a single depth dependency) were more consistent with erosion depths obtained for the Hoffmans model. However, as was concluded previously in Section 5.1, the erosive impact of larger wave regimes is greater for TM_B than for the Hoffmans model. As a result, the erosive approximation of the TM_B model is possibly more consistent with the findings of the overtopping experiments of Van der Meer et al. (2011) in which, for similar discharges, large wave heights showed to be more damaging to the cover layer than did smaller wave heights. However, the TM_B model also showed that a shifting erosion contour can occur along the profile which is a feature that is not expected to be valuable for the calibration of trends of, for example, the jet impact. As the effect of the single depth dependency of TM_B is not yet fully evaluated, the Hoffmans model is expected to be a more reliable evaluation method to approximate the erosion depth along a profile. It is recommended to use this model to study erosion across the dike and to derive trends for the turbulence parameter.

Parameter variability

In accordance with Calderon et al. (2016), results showed that wind speed has a large influence on wave characteristics. From the results for the first sub-question, the erosion depth was therefore analysed from a dominant wind direction. By varying other parameter values for grass quality, clay quality, outside slope and water level, the extent to which erosion depths along the profile were different for the two erosion models becomes noticeable. From this, it was noteworthy that for a poorer grass quality, the maximum erosion depth was only reduced to a limited extent at a standard critical velocity U_c of 4 m/s. By conducting an assessment for a higher critical flow velocity of 6 m/s in Figure 5.2, this variation becomes noticeable for both an increasing and decreasing critical velocity. The difference between both model runs is caused by the turbulence parameter within both erosion models for which an increasing U_c value excluded a number of overtopping waves whereas a decreasing U_c value caused the same waves to erode for a slightly lower threshold value. As a result of multiplying the turbulence parameter by the wave velocity, large overtopping waves results in a large erosion depth.

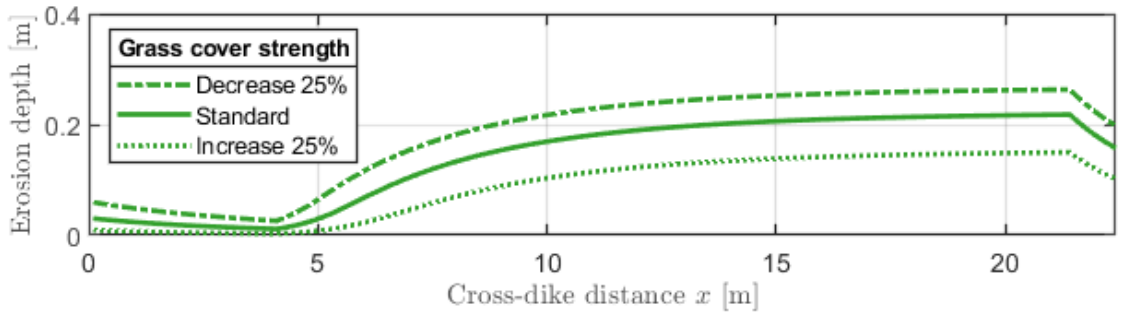

Figure 5.2: Erosion along the dike profile of Millingen aan de Rijn by considering the Hoffmans erosion model for a T = 1,000-yr storm from the westerly wind direction for a varying grass cover with variation of the critical velocity Uc = 6 m/s.

For the sensitivity analysis, it should be noted that only a small variation was applied. Due to this, parameters do not correspond with good average or bad grass and clay cover qualities for the evaluated parameters, which allows only limited conclusions to be drawn in this

respect. Moreover, obtained results with erosion depths exceeding 20 cm did not reflect a realistic erosion depth as erosion models can only be applied up to an erosion depth of 10–20 cm (Bomers et al., 2018). Results did show that the extent to which erosion contours differ for both models for varying characteristics, and results demonstrated that each of the investigated parameter values could be decisive as to whether a dike will or will not fail by overtopping.

5.3 Impact at slipped dikes

To answer the third sub-question, a goal was defined to derive and evaluate the effect of the impact at slipped dikes.

Overtopping storms

For an approximation of overtopping conditions of slipped profiles, storm control lists with a discharge interval of 0.1 and 1 l/m/s were derived for a 6-hour discharge between 0.1–150 l/m/s for the three wave regimes. Hydraulic conditions for three-wave regimes were obtained through linear interpolation of the boundary conditions for standard wave overtopping, as shown in Appendix B (Van der Meer et al., 2015b). Boundary conditions were transformed using Equation 25 and 26 to derive the overtopping events for narrower overtopping intervals. Notably, some uncertainty could be expected for the extreme wave characteristics of a wave overtopping event exceeding 75 l/m/s as overtopping conditions for these overtopping events first required the number of overtopping waves N_{ow} and the freeboard R_c to be extrapolated. Derived conditions exceed WOS experiment tests and are not considered dominant failure conditions. For these large wave overtopping conditions, other parts of the dike, such as the dike toe, are more likely to collapse, as was investigated by Frankena (2019). The above-mentioned technique appears to be an efficient method to identify under what overtopping conditions failure by erosion will occur.

Jet impact intensity

By considering experiments performed at several dike sections, in Section 4.4, a relation was derived between the turbulence parameter and the critical velocity for slipped profiles. To determine the failure condition in the erosion models, the failure depth for all dike profiles was set as equal to 20 cm following the failure definition of the WBI**.** As the failure of the cover layer is ultimately the aspect that needed to be approximated, failure damage states were used from overtopping experiments. For Afsluitdijk 2, this is a conservative definition because less than 20 cm erosion occurred whereas, for other sections, this erosion sometimes exceeded 20 cm before failure was determined. Partly due to the nonlinear erosion that occurred during trials, the exact erosion depth has not been transformed for all evaluated profiles, which could be further investigated in an in-depth study. Consequently, both the transition and Hoffmans models primarily evaluate a failure scenario with calibrated turbulence parameters.

Moreover, critical velocities U_c are determined for each section and are very dependent on local dike characteristics such as the clay cover and geometry. For the experiments Tielrodebriek 1 & 2 and Wijmeers 1, the values for the critical velocity below 3.5 m/s were not specified. For these dikes, values for the critical flow velocities were approximated between the lowest critical flow velocity and 0 m/s. Here the critical velocity for failure was

derived based on a linearity between damage numbers *D* listed in Peeters et al. (2012) and Steendam et al. (2013). As a result, some of the derived critical velocities in Table 2.2 are similar to or lower than the minimum critical velocities derived for a sand dike obtained from experiments performed for the Vechtdijk (U_c = 3.5 m/s, *D* = 4,000) (Van der Meer et al., 2015a). This result shows that some of the dikes collapsed very rapidly for a low critical velocity threshold value. Although critical velocity values are low and are derived with an uncertainty of the exact value, the variability of derived turbulence values for slightly higher or lower values was estimated to be small based on the derivations of the turbulence parameter ω as a function of the critical flow velocity U_c. What can be noted, however, is that derived trends are based on few data points. This is because a limited number of overtopping experiments was performed. As most of the available data was used, it is recommended to perform more measurements to further validate the derived relationships for the turbulence parameter.

Results for the most conservative slipped dike scenarios for both the Hoffmans and Transition models for river dikes indicated that a 6-hour wave overtopping event of at least 3 l/m/s (1 m wave regime) is required for critical erosion to develop and evolve into headcut erosion. As headcut erosion was considered to develop an overtopping discharge of 1 l/m/s for a dike (Van Hoven et al., 2014), a larger residual strength is therefore expected to be present due to the presence of a grass cover, based on the worst-case scenario for both the clay and grass layer and the entry location of a slipped profile on the inner slope. From the current results, it can be concluded that failure is highly dependent on the critical flow velocity U_c as derived from COM. In addition, little is known about low critical flow velocities U_c for grass covers below 3.5 m/s, which are highly dependent on local conditions. It would therefore be of great interest to examine the process of erosion for poor profiles more closely to improve model assessment methods for slipped dikes.

For this research, an assumption is made that, with the derived trends of the turbulence parameter and the critical flow velocity, the impact of wave overtopping can be simulated for a variety of slipped profiles. For this purpose, new relationships have been derived to include the increase in load at a slipped dike. Following the approach of Valk (2009), a jet impact load factor of 0.016 [-] at the dike toe was derived following the findings of Beltaos (1976). These relations for the dike toe with turbulence parameter ω = 2.5 [-] can be compared with the jet impact for a slipped profile across the dike slope with a turbulence parameter of ω = 2.0 [-] (Van Hoven et al., 2013). By converting the turbulence relations in Figure 4.6 (b) into a constant value and a jet impact load for a slipped profile, a similar impact load value of 0.0156 is obtained for a poor cover layer and a value of 0.0110 for a moderate cover layer. The impact factor at slipped sections at the upper slope, thus correspond with the impact factor at the dike toe according to Valk. However, this does not apply to the relations in Figure 4.7 (b) for which jet impact load values below 0.010 are obtained. Such a low value would imply that, according to the Transition model, no damage by jet impact is expected to have occurred at the middle of the dike slope. It is currently estimated that derived relations apply for small slipped profiles for which it is recommended to consider the most conservative scenarios as a starting point for both erosion models. The current framework does not consider the influence of different cliff heights on the turbulence parameter as it was not possible to

incorporate the jet height for this study. Although this was initially attempted within this study by assuming a circular rotation of the slipped plane, relationships for the turbulence parameter appeared unknown. However, the more detailed CFD models of Bomers et al. (2018) and Van Bergeijk et al. (2020) could be used to investigate this effect of changing geometry on velocity and force. The outcomes could subsequently be added to simpler models, as considered in this thesis, by adjusting the turbulence parameter. For follow-up research, it is thus advised to evaluate the effect of different cliff heights by using more complex types of models to approximate the influence of varying cliff heights.

5.4 Failure probabilities

To answer the fourth sub-question, failure probabilities of a slipped dike were obtained and compared with failure occurrence by erosion at the dike toe.

Probabilistic parameters

Parameters for the wind speed and critical velocity of the cover layer were used to obtain failure probabilities of overtopping by erosion across the dike. Wind statistics that were used to approximate actual wind speed contain extreme wind speeds, which, at lower probabilities, are expected to overestimate wind speed (Chbab, 2017). As a result, the failure probability is expected to be slightly smaller, especially for dike profiles with a freeboard of 10 or 20 cm, as shown in Figure 4.13. For the entire fragility curves, the effect of these low return periods for wind velocity is assumed to be small, as, at larger freeboards, higher wind speeds are required before erosion failure occurs. Another assumption is related to Equation 29 that was used to approximate the critical velocity at the dike toe. This equation was introduced by Frankena (2019) and is based on a threshold velocity for which no erosion occurred at the dike slope. As calibrated values derived by Frankena rely on this threshold velocity concept, Equation 29 was also used to determine the erosion depth at the dike toe. The concept has however not been used for the derivation of critical erosion relations at a slipped profile because (1) the threshold value is expected to be low for the dike slope at a slipped profile and (2) such a threshold underestimates the erosion damage to the dike that is not visible (e.g. fatigue), as shown by Bijlard (2015) and Wegman (2020).

Probabilistic methods

A probabilistic method was designed, extending existing erosion and overtopping models with both a distribution for wind speed to derive hydraulic loads and a distribution for the strength of the grass cover layer. To the best of my knowledge, combining this kind of wave overtopping approach has not been performed before. This approach enabled the calculation of the failure probability of overtopping by erosion for the cover of the inner dike slope. Moreover, the defined framework determined the failure probability of erosion for a slipped profile by applying derived relationships for the increase in load for sheared profiles.

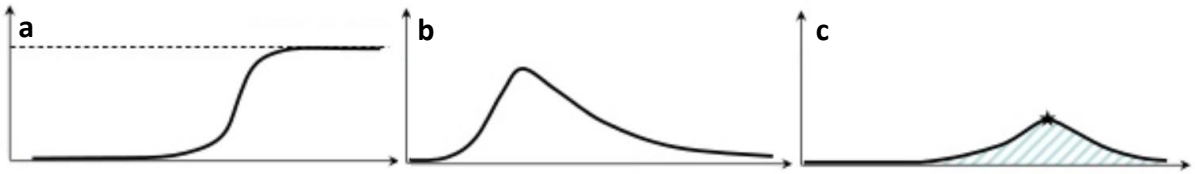

Figure 5.3: Fragility curve, water level probability, and failure probability; (a) Fragility curve of critical erosion due to wave overtopping, (b) probability density function of the water level, and (c) distribution of the total probability of failure for the water level as a product of graphs a and b.

Implementation of the designed framework and the optimization of current calculation methods allowed for extensive MCS analysis to be performed within a limited time.

ADIS was also evaluated, for which the relative error for the approximated failure probability was not expected to exceed an error of approximately 20% (Grooteman, 2011). Findings presented in Appendix D indicate that these values agree with the permitted error margin; however, the extent to which the error range could be improved was not identified. Accuracy of ADIS appeared to decrease as a result of (1) the random wave volume sampling process discussed in Section 5.1 which complicated the derivation of the adaptive response surface and (2) the model structure was unable to approximate large failure probabilities. This second point was caused by the beta importance plane, which, for low freeboards, reverted to the default values. Although ADIS was found to be inaccurate in determining large failure probabilities, it can be a more efficient method to determine the lower range of failure probabilities. ADIS may, however, be useful for the derivation of the lower end of the failure probability distribution, as Figure 5.3, showed that MCS requires many calculations to determine low failure probabilities accurately.

Failure probabilities in perspective

Fragility curves can be derived by applying the proposed framework. Failure probabilities are currently derived for the most conservative wind direction. From these fragility curves, the return period *T* for evaluated failure conditions can be determined by multiplying the failure probability by the lambda λ value of 6.99 (western wind direction), as shown in Equation 30 (Caires, 2009). From Appendix D, a failure probability *Pf* value of $1.3 \cdot 10^{-3}$ was obtained from the MC analysis for a 1-meter freeboard. This failure probability thus corresponds to a *T* = 110-yr wind speed. These are substantial return periods, especially on larger freeboards, which can significantly affect the failure probability of the dike.

$$T = \frac{\lambda}{(1 - Pf)} \tag{30}$$

By combining the probability of failure with block hours that occur from any wind direction during a year, the probability of failure by overtopping causing erosion for all wind directions can be estimated (Chbab, 2017). This failure probability is generally smaller, as less strong wind directions are also considered. It is thus interesting to examine the difference between failure probability from a single wind direction and failure probability from all wind directions.

Moreover, by combining water level statistics in Figure 5.3b with the derived fragility curves, the probability of failure can be obtained across the entire range of the fragility curve, as is shown in Figure 5.3c. The probability of failure by erosion can subsequently be related to the probability of occurrence of a slipped profile, as demonstrated by Van der Krogt et al. (2019). For this purpose, Van der Krogt et al.'s (2019) framework can be extended to evaluate both the probability of the next shearing event and the probability of dike failure by overtopping. One possible way to do this is to link the erosion model with a slipped dike section. A simplified method can also be implemented in which the increased likelihood of failure by overtopping is incorporated for a slipped dike. Accordingly, failure probabilities can be

determined and compared with current standards to evaluate the degree to which the dike strength is currently expected to be overestimated.

Overtopping discharge and overtopping erosion

The developed framework enables varying storms to cause failure by erosion both at a slipped dike and at the dike toe. Because storm volumes are known, the average wave overtopping discharge *q* can also be determined for each of the 10,000 evaluated storms at each freeboard level. This enables the wave overtopping approach for failure by erosion to be compared to a wave overtopping discharge approach. By rewriting the limit state function, it can be determined for which conditions the Millingen dike is expected to fail, given an average overtopping discharge *q* [l/m/s] criterion. For this purpose, storms with average overtopping discharges of 1, 5, and 10 l/m/s were compared to model evaluations for both the very poor clay slipped dike section Hh_p and erosion at the dike toe $Htoe_g$ of Figure 4.13.

As can be observed in Figure 5.4, fragility curves for wave overtopping discharges appear to advance roughly similar at varying freeboards to fragility curves for critical erosion by wave overtopping. Fragility curves for critical erosion were expected to be similar to the results in Section 4.4.2 where the critical wave overtopping conditions for the Hoffmans model were found to be identical at a varying wave regime of 1–3 m. These results with overtopping conditions for failure were confirmed in Figure 5.4 in which overtopping conditions for the slipped profiles are situated between 1–5 l/m/s.

Notably, the failure probability of the dike toe $Htoe_g$ is smaller than the failure probability for a wave overtopping discharge above q = 10 l/m/s. This value of 10 l/m/s may appear high because it is also the permitted average overtopping discharge that is set for overtopping resistant dikes. The overtopping experiments described in Section 2.4 already demonstrated that dikes can often withstand a higher discharge. Furthermore, the current evaluation of erosion at the dike toe does not take into account the effect of transitions or the distribution of grass quality at the dike toe caused by bare spots.

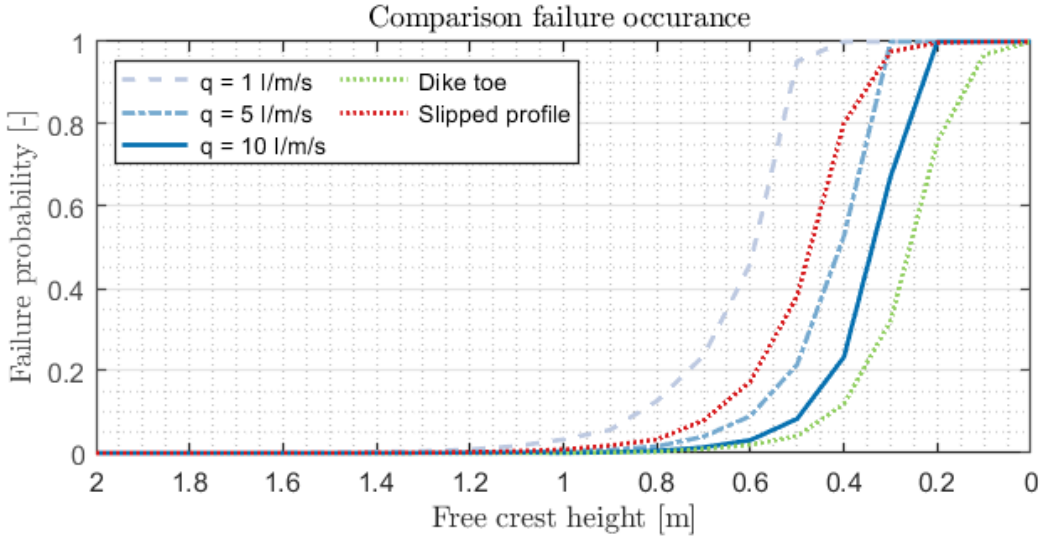

Figure 5.4: A slipped dike profile with a very poor cover and a critical velocity of U_c = 2.5 m/s at the upper slope and failure by erosion at the dike toe for good clay cover with a critical velocity U_c of 6.5 m/s for the Hoffmans model, following a MCS analysis with overtopping conditions that resulted in 20 cm erosion (failure). Shown together with three fragility curves for average overtopping discharge of q = 1 l/m/s, q = 5 l/m/s, and q = 10 l/m/s.

6 Conclusions and Recommendations

In the following chapter, the conclusions are provided in Section 6.1, and recommendations with respect to the developed framework are presented in Section 6.2.

This study analysed the influence of critical wave overtopping for regular dike profiles and slipped profiles with erosion models. A framework was constructed to calculate cover erosion by overtopping waves based on extreme wave characteristics at a dike caused by high wind speeds and was applied to a case study of a grass-covered dike near Millingen aan de Rijn using the Hoffmans and Transition models. Erosion depths caused by overtopping wave volumes along the dike profile of Millingen aan de Rijn were calculated for the Hoffmans model and the Transition model to investigate the sensitivity of the erosion models to changes in parameters. Moreover, the relationship between the turbulence parameter and the grass cover strength was derived to model the increase in the turbulence at slipped profiles through overtopping experiments on real grass-covered dikes for which approximate failure occurred and depended on the location of the slip circle. By both identifying and taking into account three factors from experts, model runs as an approximation of three slipped profile locations were performed, based on which the critical wave overtopping conditions were determined. Model runs were subsequently conducted to derive the probability of failure with the Monte Carlo method. Following this, fragility curves that described the failure probability of erosion at slipped and regular dike profiles for varying water levels were obtained. Based on the findings of the comparison, it was expected that a slipped dike would fail significantly faster than a regular profile at the dike toe.

6.1 Conclusions

1. What are the wave volumes that can overtop a dike crest for varying return periods?

In this study, wind speeds at large return periods were found to have a significant influence on both the wave height and the wave period. High wind speeds showed that hydraulic wave volumes that flow over the dike of Millingen aan de Rijn could be generally be characterized with a wave overtopping regime corresponding to a wave height of 1 m. In contrast, return periods for wind speeds far exceeding T = 10,000-year matched a wave overtopping regime with a wave height of 2 m. Consequently, the overtopping approach of this thesis framework varies substantially from conventional approximation methods in which only a wave regime with a wave height of 1 m is considered for river dikes. The findings of the present research, which reveal that overtopping wave volumes vary for different wind directions, demonstrate the importance of evaluating erosion conditions at varying wave heights and water levels. As critical erosion occurs primarily because of the largest overtopping waves during a storm, dikes can collapse for a lower average wave overtopping discharge.

2. How is the erosion depth in erosion models along the crest and landward slope affected by the outer dike slope, cover type, hydraulic load and grass cover characteristics?

The simulation results of the Hoffmans and Transition models revealed that the wind speed significantly impacted on the depth of erosion. In addition, the erosion depth was shown to be dependent on the outer dike slope, and a substantial change in erosion development occurred for varying water levels. The erosion depth increased with decreasing clay quality for both models, but the increase was slightly smaller for the Transition model compared with

the Hoffmans model. For the critical velocity of the grass cover, a positive variation of this parameter for both models was found to result in a smaller erosion depth. A low value for the critical velocity resulted in a limited increase in erosion depth; however, this was not the case for higher values, as discussed in section 5.2. The results also showed that the Hoffmans model evaluated erosion across the entire profile, whereas erosion initiated near the middle of the crest for the Transition model. Differences in the erosion depth for the Transition model were caused by the conversion to shear stresses in this model approach. This conversion resulted in more substantial differences between the flow velocity and the critical flow velocity for varying wave velocities. The Transition model did not approximate erosion at the start of the inner slope, which was an erosion-prone spot based on overtopping experiments; therefore, it is thought that the model underestimated the actual erosion depth considerably compared with the Hoffmans model.

3. *For which overtopping conditions are the critical erosion depth reached for different slip locations and characteristics?*

The failure characteristics for a slipped dike that result in failure by overtopping, according to consulted researchers, are dependent on the location of the slipping, cliff properties and the type of subsoil. Turbulence intensity trends have been developed based on overtopping experiments to approximate the jet impact from a cliff. This has resulted in the formulation of a relationship for the turbulence parameter at varying critical velocity U_c for slipped profiles. This has revealed a maximum turbulence parameter ω = 2.8, corresponding to a turbulence intensity r_0 = 0.26 from Equation 5. The conservative turbulence relationships for the Hoffmans model (on the upper slope) depend on the critical flow velocity according to the relation $\omega = -0.25U_c + 2.8$, while for the Transition model (on the middle slope), they depend on the relation $\omega = 0.03U_c + 1.4$. Model runs were subsequently evaluated for Millingen aan de Rijn with different slipped circle locations, clay qualities and cover qualities, with derived jet relationships for a wave regime with varying wave heights. Conservative model results from the performed runs indicated that slipped dikes could be expected to collapse for the Hoffmans model for a minimum overtopping discharge of q = 3 l/m/s for wave regimes with wave heights of 1, 2 and 3 m. For the Transition model, the critical overtopping discharge was found to be q = 3 l/m/s for a wave regime with a wave height of 1 m. In contrast, the critical wave overtopping discharge decreased for wave regimes with larger wave heights. The results of the present study indicate that the lower limit for the residual strength by overtopping is larger than the safety limit of 1 l/m/s as defined for headcut erosion for clay dikes. Current turbulence relations for erosion models are based on a limited number of wave overtopping experiments 1.3–6.5 m from the crest. For this reason, it is advisable that the derived relationships are validated by performing additional overtopping experiments. Moreover, approximating the erosion process of slipped profiles more accurately would enable more definite conclusions to be drawn.

4. *What are the failure probabilities of wave overtopping of a dike with and without slope instability?*

The findings of the present study suggest that failure probabilities can be computed accurately with the Monte Carlo method. This method is utilised to derive fragility curves that describe the failure probability for critical erosion by wave overtopping as a function of the

water level. Fragility curves for overtopping by critical erosion are very steep; this can also be observed for fragility curves with an average overtopping discharge. The results of this study showed that fragility curves for an average cover layer (U_c = 4.0 m/s) with a slipped profile high upon the inner slope failed more quickly than was the case for the dike toe. For a poor cover layer (U_c = 2.5 m/s), a slipped dike can be expected to fail, two, five and 10 times more rapidly than a regular dike toe for average, poor and very poor cover layers, respectively. This suggests that the results of the residual strength by wave overtopping for erosion could be incorporated in a simple manner in the case of a slipped profile by (1) using the proportions for which a cover layer collapses more quickly by wave overtopping, or more extensively, (2) by implementing model connection using the method presented in this thesis. For the latter suggestion, some further translations are useful to extend on the current framework.

6.2 Recommendations

Findings of the combined framework and impact relationships at a slipped profile can be used to approximate the residual dike strength by overtopping after damage because of slipping. This developed approach can be tailored to assess the failure probability of other river dikes by using local dike characteristics and extreme wind statistics. It is recommended that this method is used for multiple dike sections to extend understanding of the ranges that could occur for residual dike strength. Moreover, it is recommended for follow-up studies into residual dike strength to use fragility curves for failure by overtopping as derived in this research to evaluate the potential residual dike strength of a slipped dike.

It is also advised to investigate the effect of the turbulence parameter at different cliff heights of a slipped section as this could not be evaluated within this study. For this purpose, it is first essential to obtain insight into which different cliff heights occur. For follow-up research, it is recommended to use slipped geometries from more complex RFEM simulations and examine the turbulence at different heights. By assuming a circular rotation along the slip circle to the desired height of a cliff, CFD models can next be used to approximate the jet load impact. Findings in this field may contribute to the validation and extension of derived trends for the turbulence parameter of this research.

Because current relationships for the turbulence parameter are based on only a few experiments, it is advised to perform additional overtopping experiments. Moreover, it would be relevant to perform overtopping tests at slipped dikes. For experiments at a slipped dike, a dike profile could be pre-loaded for up to different cliff heights. Measurements for the jet impact for varying cliff heights from these tests could indicate the residual strength that occurs after slipping. Experiments are needed to evaluate for which conditions alternative overtopping failure mechanisms (e.g. washing out) occur and if the residual strength approach for wave overtopping based on the grass cover strength (COM) can be validated.

Lastly, model improvements could be made to extend the current framework. It is recommended to use both high and low range wind statistics for the different wind sectors to perform calculations with probabilistic models. It is recommended to compose functions for the wind statistics of both the low (Weibull) and high (POT) wind range. In addition, it is necessary to obtain an understanding of the storm periods and their dependencies so that they can be incorporated into probabilistic methods.

7 References

't Hart, R., de Bruijn, H., & de Vries, G. (2016). *Fenomenologische beschrijving*. Technical report, Deltares, 1220078-000

Aguilar Lopez, J. P., Warmink, J., Bomers, A., Schielen, R., & Hulscher, S. J. M. H. (2018). Failure of Grass Covered Flood Defences with Roads on Top Due to Wave Overtopping: A Probabilistic Assessment Method. *Journal of Marine Science and Engineering*, *6*(3), 74. https://doi.org/10.3390/jmse6030074

Bakker, J. J., Mom, R. J. C., & Steendam, G. J. (2008). *Factual Report Golfoverslagproeven Zeeuwse zeedijken*. Technical report, Infram, 09i002

Bakker, J. J., Mom, R. J. C., & Steendam, G. J. (2009). *Factual Report Overslagproeven en afschuifproef Afsluitdijk*. Technical report, Infram, 08i011

Bakker, J. J., Mom, R. J. C., Steendam, G. J., & van der Meer, J. W. (2011). *Factual Report Overslagproeven en oploopproef Tholen*. Technical report, Infram, 10i092

Beltaos, S. (1976). Oblique impingement of plane turbulent jets. *Journal of the Hydraulics Division*, *102*(9), 1177–1192.

Bijlard, R. W. (2015). Strength of the grass sod on dikes during wave overtopping. In *Master Thesis, TU Delft.* http://resolver.tudelft.nl/uuid:bd2c6618-3143-45d3-8bd9-f24c76e7d8ae

Bomers, A. (2015). Road Impact on Erosion Development During Overtopping Flood Events. *Master Thesis, University of Twente, Water Engineering and Management*. https://essay.utwente.nl/67530/1/thesis Anouk Bomers.pdf

Bomers, A., Aguilar Lopez, J. P., Warmink, J. J., & Hulscher, S. J. M. H. (2018). Modelling effects of an asphalt road at a dike crest on dike cover erosion onset during wave overtopping. *Natural Hazards*, *93*(1), 1–30. https://doi.org/10.1007/s11069-018-3287-y

Caires, S. (2009). *Extreme wind statistics for the Hydraulic Boundary Conditions for the Dutch primary water defences. SBW-Belastingen: Phase 2 of subproject "Wind Modelling."* Technical report, Deltares, 1200264-005

Calderon, A. C., Smale, A., Nieuwkoop, J., & Morris, J. (2016). *Input database for the Bretschneider wave calculations for narrow river areas*. Technical report, Deltares, 1209433-000

Chbab, H. (2017). *Basisstochasten WBI-2017*. Technical report, Deltares, 1209433-012-HYE-0007

De Visser, M., Jongejan, R., & Tigchelaar, J. (2018). *Factsheet: Afweging ter bepaling glijvlak voor faalmechanisme Macrostabiliteit Binnenwaarts*.

Den Bieman, J. P., Stuparu, D. E., Hoonhout, B. M., Diermanse, F. L. M., Boers, M., & Van Geer, P. F. C. (2014). Fully probabilistic dune safety assessment using an advanced probabilistic method. *Proceedings of the Coastal Engineering Conference*, *January*. https://doi.org/10.9753/icce.v34.management.9

EurOtop. (2018). *Manual on wave overtopping of sea defences and related structures. An overtopping manual largely based on European research, but for worldwide application.* Van der Meer, J.W., Allsop, N.W.H., Bruce, T., Rouck, J., De Kortenhaus, A., Pullen, T., Schüttrumpf, H., Troch, P. & Zanuttigh, B. www.overtopping-manual.com

Frankena, M. (2019). Modelling the influence of transitions in dikes on grass cover erosion by wave overtopping. *Master Thesis, University of Twente, Water Engineering and Management*, *July*. https://essay.utwente.nl/79017/1/Frankena%2C M. 1570234 _openbaar.pdf

Grooteman, F. (2011). An adaptive directional importance sampling method for structural reliability. *Probabilistic Engineering Mechanics*, *26*(2), 134–141. https://doi.org/10.1016/j.probengmech.2010.11.002

Hoffmans, G. (2012). *The influence of turbulence on soil erosion* (Vol. 10). Eburon Uitgeverij BV.

Hoffmans, G. (2015). *WTI 2017 Onderzoek en ontwikkeling landelijk toetsinstrumentarium*. Technical report, Deltares, 1209437-003

Hoffmans, G., Akkerman, G. J., Verheij, H. J., Van Hoven, A., & van der Meer, J. W. (2008). *The erodibility of grassed inner dike slopes against wave overtopping*. 1–13.

Hoffmans, G., Van Hoven, A., Steendam, G. J., & van der Meer, J. W. (2018). Summary of research work about erodibility of grass revetments on dikes. *Proc. Protections 2018 3th International Conference against Overtopping, Grange-over-Sands, UK*, *June*.

Hoogwaterbeschermingsprogramma. (2019). *Feitenanalyse veranderende kostenramingen HWBP*.

Hughes, S., Thornton, C., van der Meer, J. W., & Scholl, B. (2012). Improvements in describing wave overtopping processes. *Proceedings of the Coastal Engineering Conference*, 1–15. https://doi.org/10.9753/icce.v33.waves.35

Ministerie van Verkeer en Waterstaat. (2007). *Voorschrift Toetsen op Veiligheid Primaire Waterkeringen*. 476.

Peeters, P., De Vos, L., Vandevoorde, B., Taverniers, E., & Mostaert, F. (2012). *Erosiebestendigheid van de grasmat bij golfoverslag: Golfoverslagproeven Tielrodebroek*. Technical report, Waterbouwkundig Laboratorium, Versie 2_0. WL Rapporten, 713_15b

Pleijter, G., van Steeg, P., ter Horst, W., van Hoek, M., & Pol, J. (2018). *Data analyse golfoverslag en overloop*. Technical report, Waterloopkundig Laboratorium, PR3517

Pollen, N. L., & Simon, A. (2003). A new Approach for Quantifying Root-Reinforcement of Streambanks: the RipRoot. *American Geophysical Union, Fall Meeting 2003, Abstract*.

Ponsioen, L., van Damme, M., Hofland, B., & Peeters, P. (2019). Relating grass failure on the landside slope to wave overtopping induced excess normal stresses. *Coastal Engineering*, *148*. https://doi.org/10.1016/j.coastaleng.2018.12.009

Rijkswaterstaat. (2017a). *Regeling veiligheid primaire waterkeringen 2017: Bijlage II Voorschriften bepaling hydraulische belasting primaire waterkeringen*.

Rijkswaterstaat. (2017b). *Regeling veiligheid primaire waterkeringen 2017: Bijlage III Sterkte en veiligheid*.

Schüttrumpf, H. (2001). Wellenüberlaufströmung bei Seedeichen - Experimentelle und theoretische Untersuchungen. In *Bautechnik* (Vol. 78, Issue 8). https://doi.org/10.1002/bate.200104190

Schuttrumpf, H., Kortenhaus, A., Pullen, T., Allsop, N., Bruce, T., & van der Meer, J. W. (2007). *Tolerable discharges*. in: Die Küste 73. Heide, Holstein: Boyens. S. 29-39.

Sprangers, J. (1999). Vegetation dynamics and erosion resistance of sea dyke grassland. *Proefschrift Wageningen*. Proefschrift Wageningen

Steendam, G. J., Hoffmans, G., Bakker, J., van der Meer, J. W., Frissel, J., Paulissen, M., & Verheij, H. (2012). *SBW Wave overtopping and grass cover strength*. *January*. Technical report, Deltares, 1206016-007

Steendam, G. J., Peeters, P., van der Meer, J. W., Van Doorslaer, K., & Trouw, K. (2013). Destructive wave overtopping tests on Flemish dikes. *4th Specialty Conference on*

Coastal, Estuary and Offshore Engineering, *September*, 1249–1260. https://doi.org/10.1142/9789814412216

Steendam, G. J., van der Meer, J. W., Hardeman, B., & Van Hoven, A. (2010). Destructive wave overtopping tests on grass covered landward slopes of dikes and transitions to berms. *Proceedings of the Coastal Engineering Conference*, 1–14. https://doi.org/10.9753/icce.v32.structures.8

Steendam, G. J., Van Hoven, A., van der Meer, J. W., & Hoffmans, G. (2014). Wave Overtopping Simulator tests on transitions and obstacles at grass covered slopes of DIKES. *Proceedings of the Coastal Engineering Conference*, *2014-Janua*. https://doi.org/10.9753/icce.v34.structures.79

Temple, D. M., Hanson, G., Neilsen, M., & Others. (2007). *SITES 2005 Water Resource Site Analysis Computer Program-User Guide* (Issue October). TR No. 210-728.5, USDA

Trung, L. H. (2014). Overtopping on grass covered dikes. *Doctoral Thesis, TU Delft*. https://doi.org/10.4233/uuid:8b33536e-fd2b-4d65-b493- 410694b46131

Valk, A. (2009). *Wave overtopping impact of water jets on grassed inner slope transitions*. *February*, 149. http://repository.tudelft.nl/view/ir/uuid:5ca03ac7-0296-4ccd-b7b0-e9485cfc934f/

Van Bergeijk, V. M., Warmink, J. J., Frankena, M., & Hulscher, S. J. M. H. (2019a). Modelling Dike Cover Erosion by Overtopping Waves: The Effects of Transitions. *Hydraulic Engineering Repository*, 1097–1106. https://doi.org/https://doi.org/10.18451/978-3-939230-64-9_110

Van Bergeijk, V. M., Warmink, J. J., & Hulscher, S. J. M. H. (2020). Modelling the Wave Overtopping Flow over the Crest and the Landward Slope of Grass-Covered Flood Defences. *Journal of Marine Science and Engineering 2020, Vol. 8, Page 489*, *8*(7), 489. https://doi.org/10.3390/jmse8070489

Van Bergeijk, V. M., Warmink, J. J., Van Gent, M. R. A., & Hulscher, S. J. M. H. (2019b). An analytical model of wave overtopping flow velocities on dike crests and landward slopes. *Coastal Engineering*, *149*(March), 28–38. https://doi.org/10.1016/j.coastaleng.2019.03.001

Van den Ham, G., Van Hoven, A., & Van der Meer, A. (2019). *Faalpadenanalyse macrostabiliteit binnenwaarts*. Technical report, Deltares, 11203719-027

Van Der Krogt, M. G., Schweckendiek, T., & Kok, M. (2019). Do all dike instabilities cause flooding? *13th International Conference on Applications of Statistics and Probability in Civil Engineering, ICASP 2019*.

Van der Meer, J. W. (2011). Design aspects of breakwaters and sea defences. *5th International Short Conference on Applied Coastal Research*, 1–32.

Van der Meer, J. W., Hardeman, B., Steendam, G. J., Schüttrumpf, H., & Verheij, H. (2011). Flow depths and velocities at crest and landward slope of a dike, in theory and with the wave overtopping simulator. *Proceedings of the Coastal Engineering Conference*, *February 2016*. https://doi.org/10.9753/icce.v32.structures.10

Van der Meer, J. W., Hoffmans, G., & van Hoven, A. (2015a). *WTI Onderzoek en ontwikkeling landelijk toetsinstrumentarium*. Technical report, Deltares, 1209437-005

van der Meer, J. W., Schrijver, R., Hardeman, B., Van Hoven, A., Verheij, H., & Steendam, G. J. (2010). Guidance on erosion resistance of inner slopes of dikes from three years of testing with the Wave Overtopping Simulator. *Coasts, Marine Structures and Breakwaters: Adapting to Change - Proceedings of the 9th International Conference*, *2*,

460–473. https://doi.org/10.1680/cmsb.41318.0044

Van der Meer, J. W., Van Hoven, A., Paulissen, M., Steendam, G. J., Verheij, H. J., Hoffmans, G., & Kruse, G. (2015b). *Handreiking Dijkbekledingen Deel 5: Grasbekledingen*. Technical guide, Deltares

Van Hoven, A., Den Haan, E. J., & Rozing, A. P. C. (2014). *Residual dike strength after macro-instability, WTI2017*. Technical report, Deltares, 1207811-013

Van Hoven, A., Verheij, H., Hoffmans, G., & Van der Meer, J. W. (2013). *Evaluation and model development: grass erosion test at the Rhine dike*. *1207811–002*. Technical report, Deltares, 1207811-002

Van Velzen, E., Beyer, D., Berger, H., Geerse, C., & Schelfhout, H. (2007). *Technisch Rapport Ontwerpbelastingen voor het rivierengebied*.

Verheij, H. J., Meijer, D. G., Kruse, G. A. M., Smith, G. M., & Vesseur, M. (1995). *Investigation of the strength of a grass cover upon river dikes*. https://doi.org/Q1878

Vrijling, J. K., Roos, A., Ale, B. J. M., Van der Brand, D., De Bruyn, L., Bueno de Mesquita, K. G., Van gelder, P. H. A. J. M., Van hengel, W., Janssen, J. P. F. M., De jong, G. C., Van der meer, M. T., Meermans, W., Nederend, J. M., Van otterloo, R. W., Redeker, F. R., De ridder, H. A. J., Van de velde, A. A., & Vrouwenvelder, A. C. W. M. (1997). *Kansen in de civiele techniek Deel 1 : probabilistisch ontwerpen in theorie*.

Wegman, R. J. (2020). Strength of Grass Covers on Dikes. *Master Thesis, TU Delft.* http://resolver.tudelft.nl/uuid:9af2efca-90e7-4006-95a7-8d87180b0709

Zwanenburg, S., Steeg, P. van, & Hoven, A. van. (2018). Integrale benadering toegestaan golfoverslagdebiet. In *Povmacrostabiliteit.Nl* (Vol. 3, Issue 3). http://www.povmacrostabiliteit.nl/wp-content/uploads/2015/03/Consequentie-golfoverslagdebiet_v3_definitief.pdf

8 Appendix

Appendix A Return period of water levels

Return periods for water levels at the dike profile in Millingen were obtained by performing calculations with Hydra-NL. Return periods for different water levels are illustrated with the following water level frequency line.

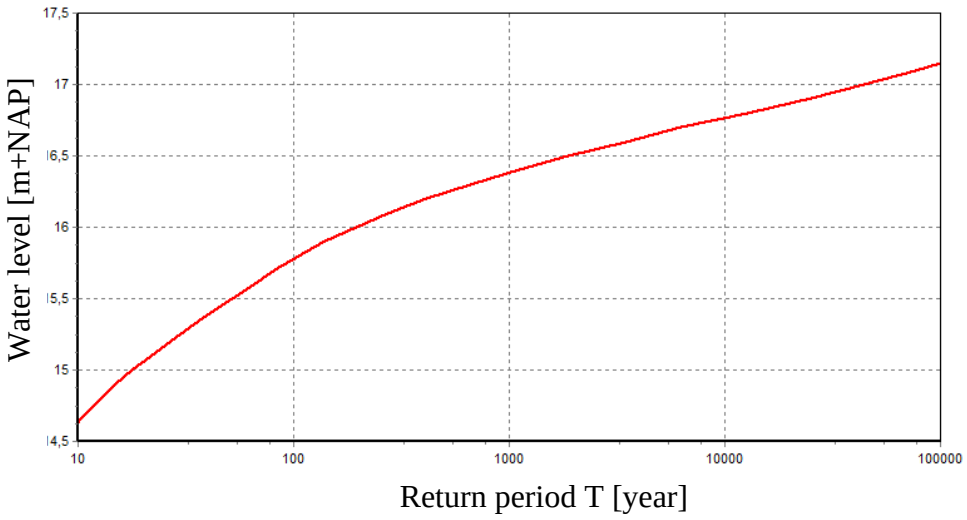

Appendix B Wave volumes

Replicated wave volumes from the technical reports in Table 2.1 are shown within this chapter. These overtopping volumes have been used to perform calibration for the trend line analysis in Section 4.3.1 for the overtopping experiments that are listed in Table 2.1.

Standard wave overtopping – 2m wave regime

Regular overtopping volumes for a 6-hour storm were been simulated based on the boundary conditions for a wave height of 2 m (Van der Meer et al., 2015b).

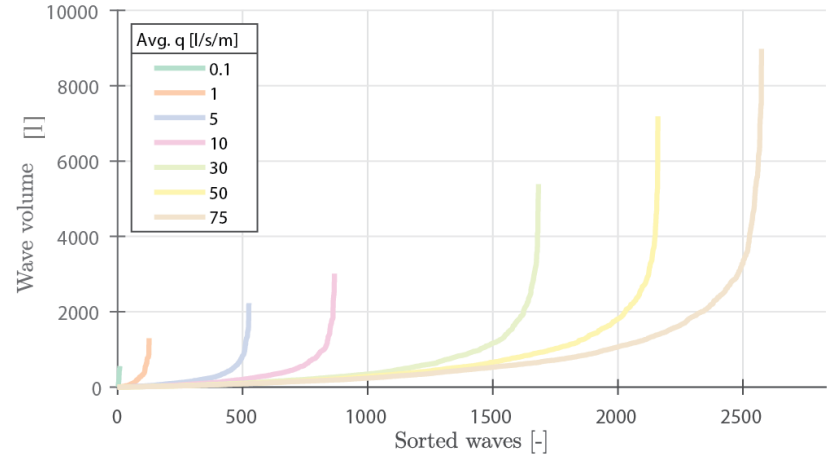

	Mean overtopping discharge q [l/s/m]						
	0.1	**1**	**5**	**10**	**30**	**50**	**75**
R_c [m]	5.06	3.84	2.98	2.61	2.03	1.76	1.54
P_{ow} [%]	0.2	2.7	11.4	18.9	36.6	47	56
N_{ow} [-]	9	126	525	867	1,683	2,160	2,574
V_{max} [l/m]	769	1,222	2,018	2,697	4,707	6,387	8,278

Wijmeers wave overtopping

For the overtopping tests of Wijmeers, special overtopping volumes were derived for a 2-hour storm period.

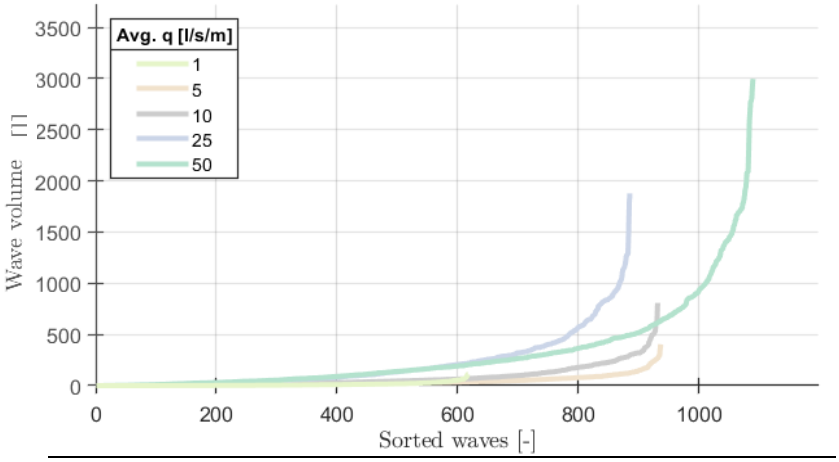

	Mean overtopping discharge q [l/s/m]				
	1	**5**	**10**	**25**	**50**
R_c [m]	0.76	0.91	1.13	1.55	1.4
P_{ow} [%]	18,1	33,6	38,6	44,9	57,5
N_{ow} [−]	617	936	931	885	1089
V_{max} [l/m]	113	349	672	1,162	2,230

Tielrodebroek wave overtopping

For the overtopping tests of Tielrodebroek, special overtopping volumes were derived for a 2-hour storm period.

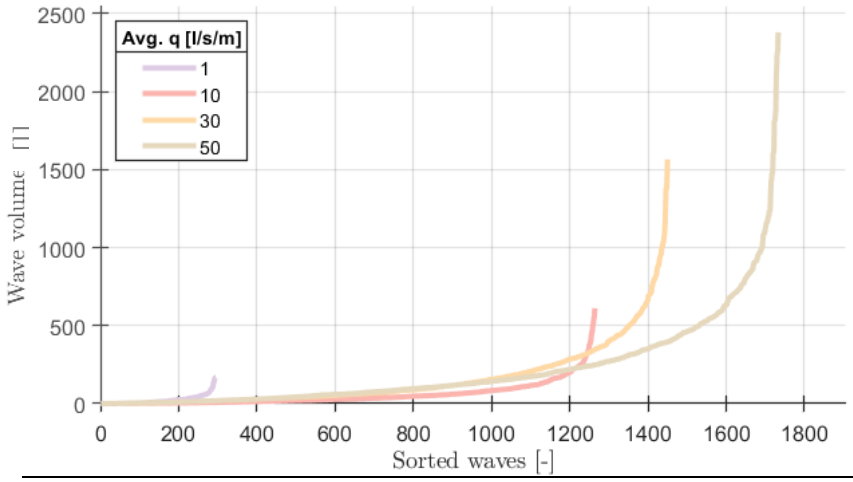

	Mean overtopping discharge *q* [l/s/m]			
	1	**10**	**30**	**50**
H_s [m] – T_s [s]	0.75 – 3.1	0.75 – 3.1	1.0 – 3.6	1.0 – 3.6
P_{ow} [%]	10.2	43.5	58	69.3
N_{ow} [−]	295	1,264	1,450	1,733
V_{max} [l/m]	209	659	1,766	2,544

Appendix C Evaluated dike shear cases

Three slipped cases are shown for the dike profile of Millingen aan de Rijn for which slipped profiles were obtained. In this study, the occurrence of individual cases has not been further calculated further probabilistically. Displayed cases serve as a demonstration of slip circles that evolve following D-Stability at different locations across the dike. For evaluated cases an elevated phreatic line was included and a water level one meter below the crest height. Dots show predominant radiuses of shear circles that followed from an initial particle swarm analysis.

1. *Slippage at the dike crest*

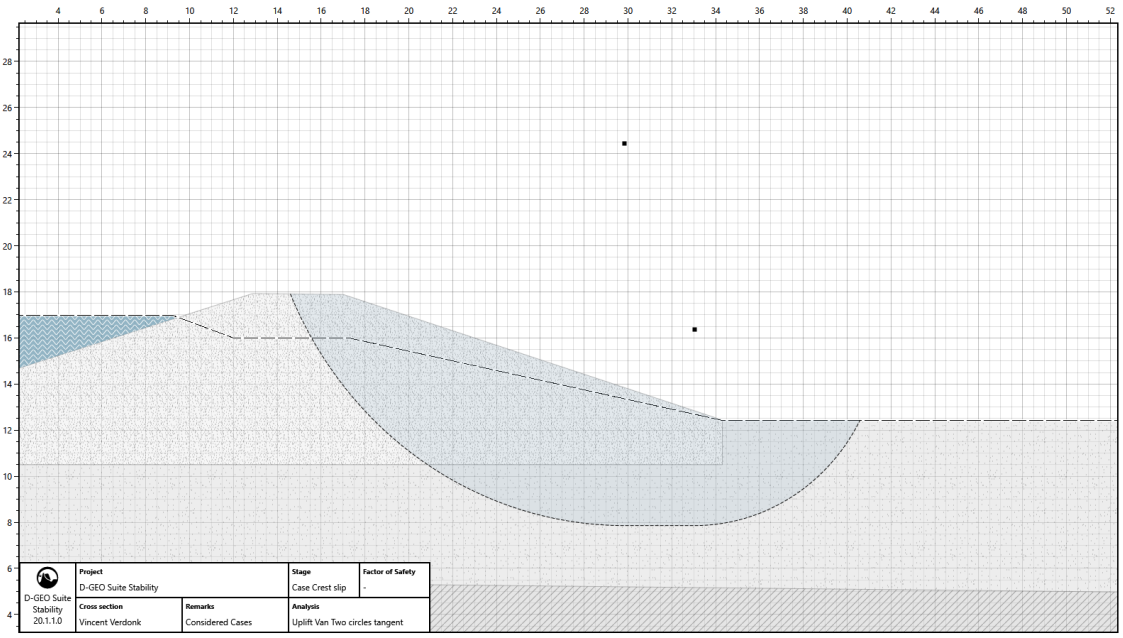

2. *Slippage at the dike slope (up)*

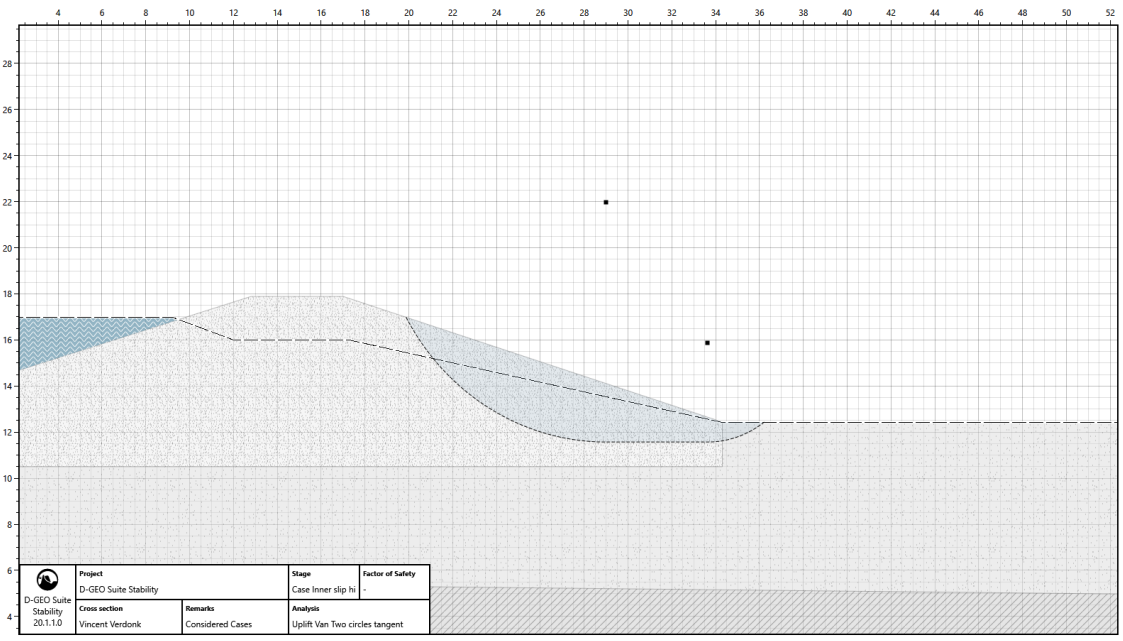

3. Slippage at the dike crest (middle)

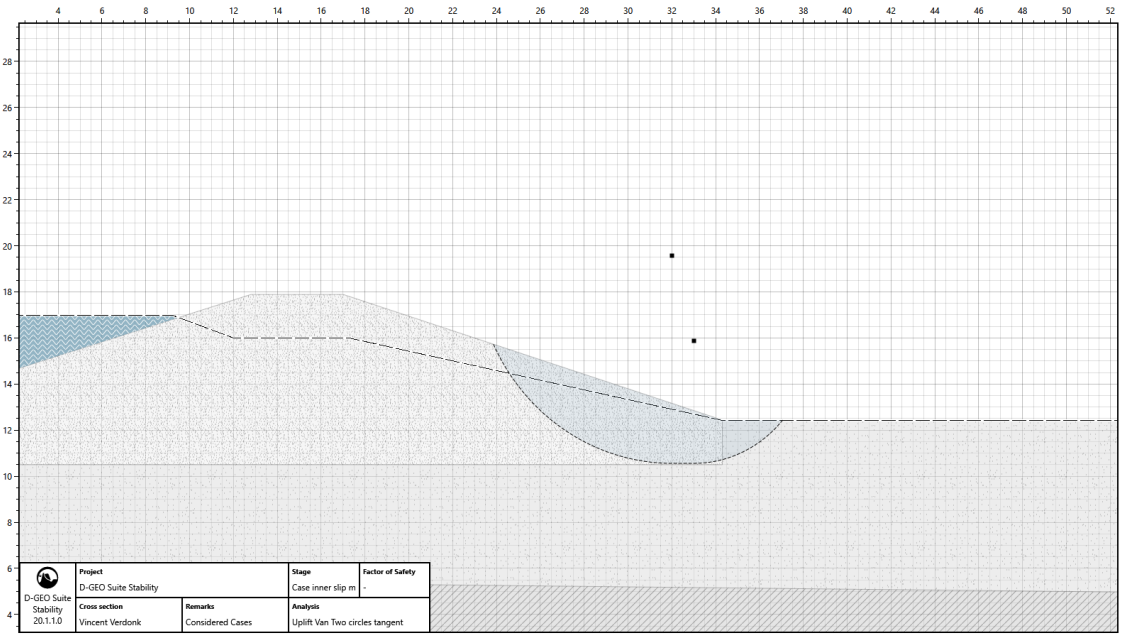

Appendix D Probabilistic analyses

For the two probabilistic methods, the applicability of a fragility curve is investigated. This is performed by comparing the two methods at a fixed water level. Subsequently, the failure probabilities *Pf* [%] of these models are analysed at varying water levels, after which the most convenient method is selected to compute fragility curves for slipped dike profiles.

Assessment of failure probabilities

Failure conditions are first evaluated with a MCS analysis for a fixed water level. A failure approximation with n = 10.000 samples is performed for a poor clay cover, $CE = 3.3 \cdot 10^{-6}$s/m with grass cover U_c of 4.0 m/s and a 50-cm freeboard representing a slipped profile at the upper part of the slope. From the figure on the left, it can be noted that for a 50-cm freeboard condition, it is rather simple to identify the limit state in the normal space. The figure below on the left shows 915 'failure' cases (in black) that are separated from the 'non-failure' cases (in white). These failure cases correspond with *Pf* = 9.15% for which a high accuracy is obtained of 6.2% as is shown on the right figure.

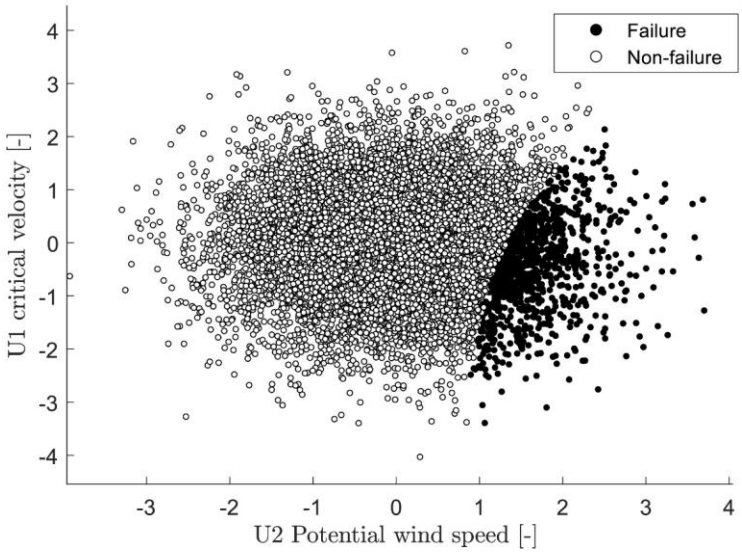

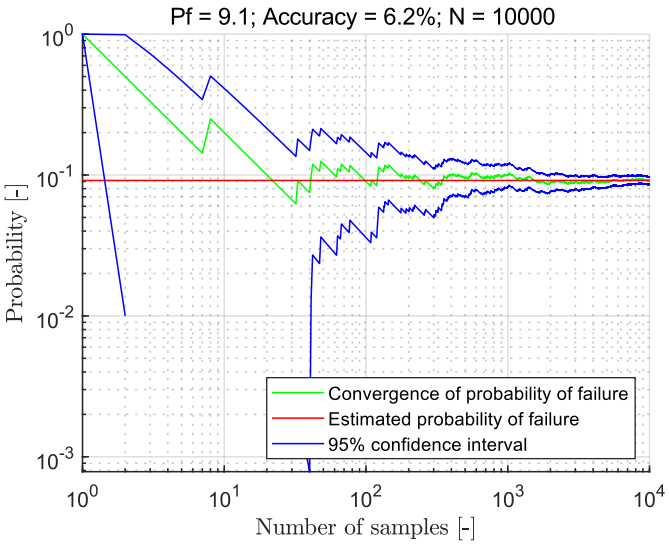

Next, for identical conditions for a slipped profile at the upper slope section, the ADIS method is demonstrated. For this evaluation, a good fit for the adaptive response surface could not be initially identified. This was resolved by increasing the minimum number of random directions to be evaluated from 100 to 600. The figure on the next page shows the two-parameter combinations in the normal space. Here the β-plane (importance plane) is visualised in red within which the evaluated points contribute most to the failure probability. The tangent of this plane similarly crosses the normal space, as can be seen for the MCS analysis. This method is substantially faster for which 68 exact calculated failure cases (green) and 159 non-exact failure cases (cyan) are evaluated. The adaptive response surface (ARS) obtained from the logarithmic limit state function is indicated by the dark plane.

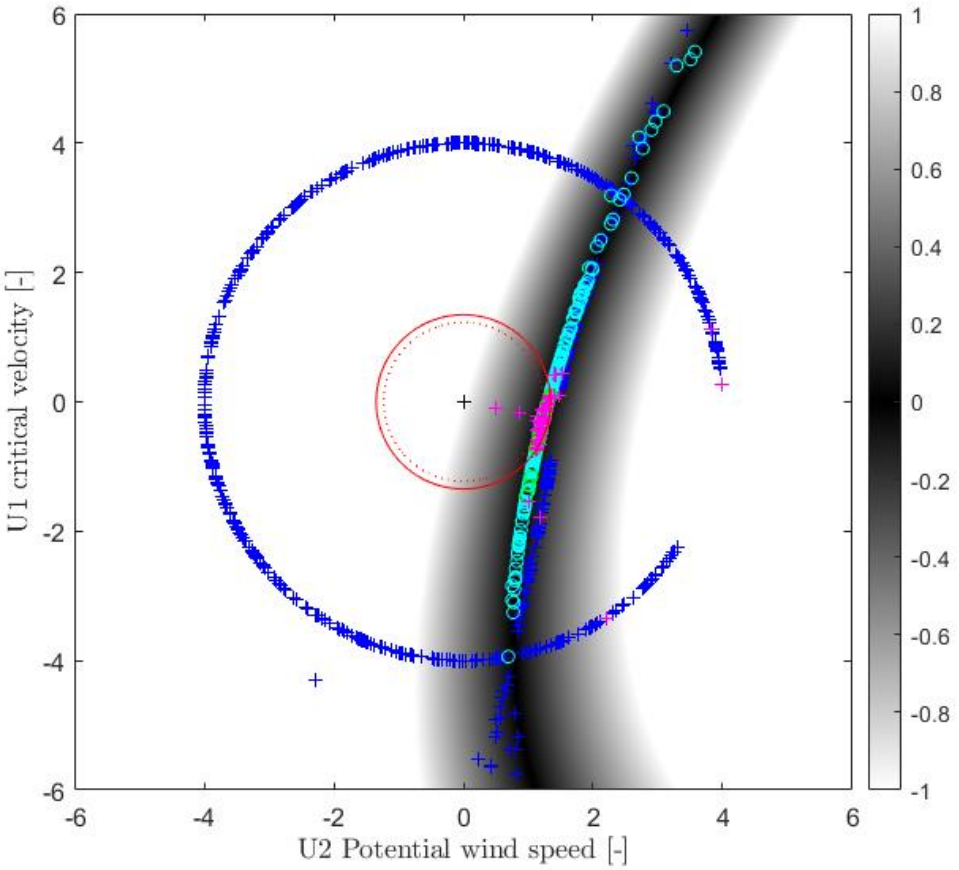

	Values
Pf_total	0.0979
Pf_exact	0.0491
Pf_approximated	0.0489
Nr. evaluations (exact and approach zero)	68
Nr. evaluations (NOT exact and approach zero)	159
Nr. evaluations exact	179
Nr. directions	600
Nr. directions Z~0	234

Failure probabilities for a varying water level

Next, failure probabilities are examined at a varying water level for which a freeboard is considered of 1.5 m with a 10-cm interval up to the dike crest. Results of this analysis are presented in the table on the next page. In this respect, it is important to note that an ADIS calculation (with uncertainties) is compared to an MCS calculation (with a provided 95% CI accuracy bandwidth). From these results, two essential aspects can be observed. First, the ADIS analysis quickly obtains low failure rates (60–200 exact evaluations) with acceptable deviations from available MCS evaluations given the predefined maximum deviation of 20% for low failure probabilities of 23% and 12% for a freeboard of 1.3 m, 1.1 m, respectively. Second, for a decreasing freeboard, the failure probability estimation of the MCS analysis becomes more accurate whereas for a $Pf > 0.23$, the ADIS analysis starts to show significant inconsistencies causing the failure probability to suddenly decreases for a small freeboard (0.1–0.3 m), which indicates that ADIS cannot be used at these freeboards.

This table shows the results of the probabilistic analysis at varying water levels with associated freeboard, failure probabilities (*Pf*) according to ADIS and MCS (*n* = 10.000) with the respective 95% confidence interval and probability deviations of ADIS from MCS. Increased comparative efficiency of both methods is indicated by the green arrows.

Freeboard [m]	**ADIS *Pf* [%]**	**MCS *Pf* [%] (accuracy of 95% CI [%])**	**Deviation *Pf* ADIS/MCS [%]**
1.5	$1.1 \cdot 10^{-4}$	-	-
1.4	$1.2 \cdot 10^{-4}$	-	-
1.3	$1.2 \cdot 10^{-4}$	$1.0 \cdot 10^{-4}$ (195.6)	23
1.2	$2.1 \cdot 10^{-4}$	-	-
1.1	$5.3 \cdot 10^{-4}$	$6.0 \cdot 10^{-4}$ (80.0)	12
1.0	$1.2 \cdot 10^{-3}$	$1.3 \cdot 10^{-3}$ (54.3)	7
0.9	$3.0 \cdot 10^{-3}$	$1.4 \cdot 10^{-3}$ (52.3)	111
0.8	$7.3 \cdot 10^{-3}$	$7.2 \cdot 10^{-3}$ (23.0)	1
0.7	$1.8 \cdot 10^{-2}$	$1.5 \cdot 10^{-2}$ (15.8)	17
0.6	$4.2 \cdot 10^{-2}$	$3.5 \cdot 10^{-2}$ (10.4)	21
0.5	$1.0 \cdot 10^{-1}$	$9.2 \cdot 10^{-2}$ (6.2)	14
0.4	$2.3 \cdot 10^{-1}$	$2.5 \cdot 10^{-1}$ (3.4)	7
0.3	$1.7 \cdot 10^{-1}$	$6.5 \cdot 10^{-1}$ (1.4)	74
0.2	$4.9 \cdot 10^{-2}$	$9.4 \cdot 10^{-1}$ (0.5)	95
0.1	$8.4 \cdot 10^{-4}$	$9.9 \cdot 10^{-1}$ (0.2)	100